

Accuracy and Simplicity in One-Equation Turbulence Models

by

Kiera Kean

B.S. in Mathematics, University of Pittsburgh, 2018

Submitted to the Graduate Faculty of
the Kenneth P. Dietrich School of Arts and Sciences in partial fulfillment

of the requirements for the degree of

Doctor of Philosophy

University of Pittsburgh

2022

UNIVERSITY OF PITTSBURGH
KENNETH P. DIETRICH SCHOOL OF ARTS AND SCIENCES

This dissertation was presented

by

Kiera Kean

It was defended on

July 22, 2022

and approved by

William Layton, Professor of Mathematics, University of Pittsburgh

Michael Neilan, Professor of Mathematics, University of Pittsburgh

Ivan Yotov, Professor of Mathematics, University of Pittsburgh

Gautam Iyer, Professor of Mathematics, Carnegie Mellon University

Accuracy and Simplicity in One-Equation Turbulence Models

Kiera Kean, PhD

University of Pittsburgh, 2022

Human life faces challenges including climate change and energy transformation that require predictive accuracy in numerical simulations of fluid motion. However, the complex structure and dynamics of turbulence combined with computational limitations create a fundamental barrier. Turbulence is both rich in scale and chaotic in time, thus time accurate predictions of turbulent flows are out of reach for many important applications. If direct numerical simulations are not feasible, we turn to turbulence modeling. Unfortunately, many inexpensive popular models lack a strong theoretical backbone. They rely on data fitting and calibration, and have limited generality. Higher accuracy models, e.g., large eddy simulation models, are more expensive and remain infeasible for many large applications.

We seek models that efficiently and accurately capture important flow characteristics. Eddy viscosity models, which model the effect of unresolved scales with enhanced dissipation, are the most commonly used today. In particular, we consider the one-equation model of Kolmogorov and Prandtl, where turbulent kinetic energy is modeled with the k -equation.

The scaling of the time averaged energy dissipation rate as $\frac{U^3}{L}$ is fundamental, and has been proved mathematically and supported experimentally. Nonetheless, this law is violated in numerical tests of popular models. Numerical dissipation introduced by commonly used multistep methods is a potential cause or contributing factor. We explore the effects of numerical dissipation in multistep methods applied to the Navier-Stokes equations on this scaling, showing the treatment of the convective

term may greatly effect the scaling of the total energy dissipation rate even for low Reynolds number flows.

Additionally, any eddy viscosity models themselves may overdissipate, particularly in the presence of boundary layers. We address this problem by changing the framework through which we view the development of turbulence models. Rather than calibrating a model with data, which can lead to needless complexity and a lack of generality, we look to create models that fit the true behavior of the underlying equations. By enforcing correct near wall behavior of the turbulent viscosity through a new turbulence length scale, we prevent overdissipation in the long time average while minimizing computational complexity.

Motivated by enforcing model accuracy in the near wall area, the inclusion or exclusion of viscous diffusion in the k -equation is debated. By examining the derivation of the k -equation, we show that inclusion leads to incorrect near wall asymptotics. However, the exclusion of the term may be ill posed in the continuous case, leading solver failures and ill conditioning. We address this by proposing alternate regularization strategies that are not based on physical parameters.

Table of Contents

Preface	xi
1.0 Introduction	1
2.0 Preliminaries	5
2.1 Mathematical Preliminaries	5
2.1.1 Fluid Dynamics Preliminaries	8
2.2 Navier-Stokes Equations	8
2.3 Turbulence Modeling	10
2.3.1 Eddy Viscosity Turbulence models	10
2.3.2 The k-equation	12
3.0 Numerical Dissipation in Multistep Methods	15
3.1 Notation and Preliminaries	16
3.2 Fully Implicit Timestepping Methods	18
3.2.1 Backward Euler	18
3.2.2 General Two Step Methods	23
3.2.2.1 A-stability	23
3.2.2.2 G-Stability	24
3.2.3 Long Time Energy Dissipation	26
3.3 Nonconstant Forcing Term	30
3.4 Treatment of Nonlinear Term	35
3.5 Numerical Experiments	41
3.5.1 Problem Setting	41
3.5.2 Total Dissipation versus Reynolds Number	43

3.5.2.1	Backward Euler	43
3.5.2.2	Second Order A-stable Method	45
3.5.3	Higher Order Extrapolation in Nonlinear Term	47
3.6	Conclusions	50
4.0	A New Turbulence Length Scale	52
4.1	Introduction	52
4.1.1	Justification of New Length Scale	54
4.1.2	Related work	55
4.2	Shear Flow	56
4.2.1	Notation and preliminaries	57
4.3	Energy dissipation in shear flows	61
4.4	Application to a 1-equation URANS model	66
4.5	A Numerical Illustration	69
4.5.1	Problem Setting	69
4.5.2	Energy Dissipation Rate	72
4.6	Conclusions and open problems	73
5.0	Conditioning of Super-Muckenhoupt Degenerate Elliptic Bound- ary Value Problems	75
5.1	Introduction	75
5.2	The k-Equation	76
5.3	General Degenerate Elliptic Boundary Value Problems	78
5.4	Notation and Preliminaries	80
5.5	Condition Number Estimates	81
5.5.1	Muckenhoupt Case	82
5.5.2	Non-Muckenhoupt weights	83
5.5.3	Condition Number	86

5.5.4 Numerical Tests	88
5.5.4.1 Effects of Degeneracy at the Boundary	88
5.5.4.2 Effects of lower order terms	88
5.6 Regularization	89
5.6.1 Regularization for General Ill-Posed Problems	91
5.6.2 Regularization for Degenerate Elliptic Boundary Value Problems	95
5.7 Conclusion	96
6.0 Conclusions and Open Problems	98
Bibliography	102

List of Tables

1	Large numerical dissipation in BDF2 drives the flow to a lower Reynolds number state. The effect is amplified for small values of ν	49
---	---	----

List of Figures

1	We consider flow between offset cylinders. The domain and a top view of the mesh are pictured.	41
2	Q-criterion for $\nu = \frac{1}{250}$ using LIBE.	42
3	Using LIBE with $k = .05$, at high Reynolds numbers, the numerical dissipation rate is similar in size to the rate of viscous dissipation.	44
4	Using LIBE, the kinetic energy increases as ν decreases despite increased numerical dissipation.	44
5	Using LIBE with $k = .05$, we see correct scaling of the average total dissipation rate despite the large timestep.	45
6	Using BDF2 with $k = .05$, at high Reynolds numbers, the numerical dissipation rate is much larger than the viscous dissipation rate.	46
7	Using BDF2 with $k = .05$, $U \approx U^*$. Large numerical dissipation leads to decreased kinetic energy as ν decreases.	46
8	Numerical Dissipation in BDF2 is proportional to $(\ u^{n+1}\ ^2 - \ 2u^n - u^{n-1}\ ^2)$	47
9	Using BDF2 with $k = .05$, we do not see the correct scaling of the average total dissipation rate due to the large timestep.	48
10	Average Dissipation vs k , $\nu = \frac{1}{250}$. Total dissipation is near constant for LIBE, in contrast to LIBE2 and BE.	49
11	Re versus k , $\nu = \frac{1}{250}$. The Reynolds number is near constant for LIBE, even for large timesteps. A small timestep is required for LIBE2 and BDF2 to see the correct Reynolds number.	50
12	The unstructured mesh used in the numerical experiments.	70

13	Q-criterion at $T = 30$	71
14	The energy dissipation rate over time.	72
15	The energy dissipation rate over time.	73
16	Minimum eigenvalue scales like $h^{N-1+\alpha}$ for $\alpha \geq 1$, h^{N-1} for $\alpha < 1$. Maximum eigenvalue scales like h^{N-2}	89
17	Minimum and maximum eigenvalues varying a_0, a_1 agree with theory: lower order terms alleviate ill conditioning	90

Preface

First, I cannot thank my advisor, William Layton, enough. I would not have gone to graduate school without his encouragement, and I can not imagine making it through without him. Thanks as well to Michael Neilan for setting me on the right path as my first college math professor eight years ago, and thanks to Michael Schneier for his mentorship throughout graduate school. I also would like to thank Ivan Yotov and Gautam Iyer for their support and for serving on my committee.

I want to thank my mother, my siblings, and the rest of my family and friends for their patience, love, and good humor these years, with a special acknowledgement to my loyal cat Minnie. And finally to my fiancé Mitchell, you got me through this. I couldn't ask for anyone better.

1.0 Introduction

Difficulties in predictions arise as turbulence is both chaotic in time and rich in scale. Deterministic chaos occurs when a small perturbation in initial condition leads to exponential separation of bounded trajectories, Lorenz's butterfly effect. The separation of trajectories leads to a finite predictability horizon, as initial conditions are not perfectly known. Analytic upper bounds give a $\mathcal{O}(\mathcal{Re}^{-3})$ window of accurate prediction. Next, turbulent flows contain large and small eddies, each with a characteristic time and length scale that must be resolved. The time scale of small eddies is proportional to $\mathcal{O}(\mathcal{Re}^{-1/2})$, and the length scale is proportional to $\mathcal{O}(\mathcal{Re}^{-3/4})$. This renders direct numerical simulations of flows impossible in many technologically important applications within time and resource constraints. Though turbulence in a pipe flow begins around $\mathcal{Re} \sim 3 \times 10^3$ and may be fully resolved, a model airplane has $\mathcal{Re} \sim 2.5 \times 10^6$, and a typical commercial jet has $\mathcal{Re} \sim 1.1 \times 10^8$, where full resolution cannot be expected.

There is still no one approach that can solve this problem, there are more than can be contained in this work. To offer context for other current thrusts in the pursuit of time accurate fluid flows, we will briefly discuss some methods not considered in this dissertation. This is with the understanding that these ideas can and should be explored in tandem with the work in this dissertation in the future as we build towards a more complete understanding of fluid modeling. Ideas for such work will be discussed Chapter 6 where we present open problems and future works.

The richness of scales seen in fluid flows require fine meshes and thus solving large linear systems. As the Reynolds number increases, storage requirements and solve time may quickly exceed computational resources. Reduced order models (see

[38], [18], [57]) decrease computational expense by using problem data or offline pre-computation to dramatically lower the degrees of freedom. Additionally, methods such as artificial compression and penalty methods perturb the incompressibility constraint and allow us to decouple velocity and pressure. Artificial compressibility models allow for a lagged pressure term, leading to a velocity only system and an algebraic update of the pressure. For example, [55] shows a 3-8 times speed increase in artificial compressibility tests. Penalty methods result in a velocity only system, which further decreases storage costs and solve times, extending the boundary of what is computable. These methods may be sensitive to the choice of penalty parameter; this is addressed in recent work by adaptive, algorithmic selection of the penalty parameter [46], [82].

Adaptive timestepping methods increase accuracy and efficiency particularly in flows that vary dramatically over time. Selecting the largest timestep that keeps error below a preset tolerance increases efficiency. However, these methods do not necessarily inherit the stability properties of the constant timestep analogues. [48], [49] presents a timestepping method that is unconditionally G -stable under variable timesteps. Other timestepping advancements include variable step, variable order algorithms [16], [17]. These select the order that allows for the largest timestep while keeping error below a set tolerance and may further decrease computation time and expense by minimizing total timesteps without sacrificing accuracy.

The chaotic dynamics of fluid flow are best addressed by ensemble simulations. Perturbing initial conditions, calculating multiple trajectories, and averaging this collection of trajectories results in an increased predictability horizon. However, this process may be computationally expensive and require large amounts of storage. Recent ensemble algorithms allow for a single coefficient matrix and a block linear solve. Further, the kinetic energy in the ensemble fluctuations can be used in eddy

viscosity turbulence models.

At low Reynolds numbers, we may use direct numerical simulations (see [64], [60]). For extremely high Reynolds number flows, direct numerical simulation becomes impossible. We turn here to turbulence models, which truncate the scales that are directly calculated and model the effect of what is not directly calculated. These models vary in complexity and accuracy. More accurate models, e.g., large eddy simulations (LES), directly calculate large scales and model only small scales (see [43], [81]). However, for high Reynolds number flows, they remain out of reach. For example, it is predicted that full LES for simulation of airplane wings will be computationally infeasible until 2045 [71]. Reynolds Averaged Navier-Stokes (RANS) models model flow averages over finite or infinite time windows. Due to their simplicity and comparative lack of computational expense, RANS models are the most popular choice for many current applications. In particular, one equation eddy viscosity models are commonly used.

This dissertation addresses practical aspects of turbulence models. First, the goal of such models is to accurately capture important flow behavior for use in application. This goal may be hard to quantify, particularly when the true behavior is not known. In light of this, we focus on the energy dissipation rate. It is a physical fact, proven through experiment and backed by theory that the time averaged energy dissipation rate will scale uniformly in the Reynolds number as $\frac{U^3}{L}$. Still, many turbulence models violate this, and we see growth in the energy dissipation rate as the Reynolds number increases. This also manifests as incorrect flow behavior in the simulation, e.g., driving a time dependent flow to steady state. For example, the Smagorinski model, an algebraic eddy viscosity turbulence model, is known to overdissipate in the presence of boundary layers, requiring ad hoc solutions such as Von Driest damping [61]. Additionally, time discretization schemes may add numerical dissipation to the

viscous and model dissipation, potentially contributing to or causing overdissipation.

Chapter 2 presents mathematical and fluid dynamical preliminaries that are used throughout the dissertation, and ensures notational consistency. Chapter 3 presents analysis of numerical dissipation for multistep methods. In this chapter, we analyze the Navier-Stokes equations without turbulent viscosity to isolate the effects of the numerical dissipation caused by the timestepping method. We briefly discuss the extension to turbulence models.

Chapter 4 presents a method for analyzing eddy viscosity turbulence models in shear flow applications. We also present new turbulence length scale for use in the k -equation of Kolmogorov and Prandtl, which is designed to enforce correct near wall behavior of the turbulent viscosity. Chapter 5 further investigates the k -equation, demonstrating that the exclusion of viscous dissipation is the correct choice for model accuracy. We explore the effect of this on conditioning of the numerical system, and we suggest regularization strategies. Finally, chapter 6 presents conclusions and open problems.

2.0 Preliminaries

We will begin with consideration of the Navier-Stokes equations. Beyond mathematical mysteries and analytic interest, accurate simulation of fluid flow is vital for a variety of applications. However, in practice, with current computational capacity, time accurate simulations of high Reynolds number turbulent flows remain out of reach. This chapter will introduce notation and present basic results that will be used throughout the remainder of this work. Additionally, we will present some basic energy results from the Navier-Stokes equations, and present the derivation of Prandtl and Kolmogorov's k -equation.

2.1 Mathematical Preliminaries

Here, we present mathematical and notational preliminaries that will be used throughout this document. It is difficult to present these preliminaries absent motivation; it is similarly difficult to present the motivating equations without this notation and basic results. The motivation for these preliminaries will follow immediately in this introductory chapter.

The $L^p(\Omega)$ norm will be denoted as $\|\cdot\|_{L^p(\Omega)}$. The $L^2(\Omega)$ norm as $\|\cdot\|_{L^2(\Omega)} = \|\cdot\|$. In cases where the domain may be unclear, the subscript may be used. The standard L^2 inner product is denoted (\cdot, \cdot) .

We will use Cauchy-Schwarz inequality,

$$(x, y) \leq \|x\| \|y\| \tag{2.1.1}$$

the polarization identity,

$$(x, y) = \frac{1}{2} (\|x\|^2 + \|y\|^2 - \|x - y\|^2) \quad (2.1.2)$$

and Young's inequality:

$$ab \leq \frac{1}{2\varepsilon} a^2 + \frac{\varepsilon}{2} b^2 \text{ for } a, b \geq 0, \varepsilon > 0. \quad (2.1.3)$$

In general, we will consider the velocity space X and pressure space Q .

$$X := H_0^1(\Omega)^d = \{v \in H^1(\Omega)^d : v|_{\partial\Omega} = 0\}$$

$$Q := L_0^2(\Omega) = \left\{ q \in L^2 : \int_{\Omega} q \, dx = 0 \right\}.$$

The velocity space will be altered in situations where no slip boundary conditions are not used. For example, in the case of periodic boundary conditions, we will consider velocity functions that satisfy the periodic boundary conditions and have zero mean. If at any point, the changes affect the results in this preliminary section, it will be noted.

For both periodic and no slip boundary conditions, for $v \in X$ we have the Poincaré-Friedrich's inequality

$$\|v\| \leq C_{PF} \|\nabla v\|. \quad (2.1.4)$$

We define the space H^{-1} as the dual space of X . The associated dual norm is given

$$\|f\|_{-1} := \sup_{0 \neq v \in X} \frac{(f, v)}{\|\nabla v\|}.$$

Clearly, we have $(f, v) \leq \|f\|_{-1} \|\nabla v\| \, \forall v \in X$. We also define

$$V := \{v \in X : \nabla \cdot v = 0\}.$$

We define the trilinear form

$$b(u, v, w) := (u \cdot \nabla v, w) \quad \forall u, v, w \in H^1(\Omega)^2$$

and the explicitly skew-symmetric trilinear form

$$b^*(u, v, w) := \frac{1}{2} (b(u, v, w) - b(u, w, v)) \quad \forall u, v, w \in H^1(\Omega)^2.$$

It is sometimes convenient to consider equivalent notions for the trilinear form.

Lemma 2.1.1. *Let $u, v, w \in X$. Then*

$$(u \cdot \nabla v, w) = (\nabla \cdot (v \otimes u), w) - ((\nabla \cdot u)v, w)$$

and

$$(u \cdot \nabla v, w) = -(u \cdot \nabla w, v) - ((\nabla \cdot u)v, w).$$

Proof. The first is immediate by the definition of divergence and tensor product.

The second follows from applying integration by parts. \square

Corollary 2.1.1. *We may rewrite the explicitly skew symmetric trilinear form in two forms*

1. $b^*(u, v, w) = (u \cdot \nabla v + \frac{1}{2}(\nabla \cdot u)v, w)$
2. $b^*(u, v, w) = (\nabla \cdot (v \otimes u) - \frac{1}{2}(\nabla \cdot u)v, w)$

Additionally, if $u \in V$, $b(\cdot, \cdot, \cdot)$ is skew symmetric, and we have the following equalities.

1. $b(u, v, w) = -b(u, w, v)$
2. $b(u, v, w) = b^*(u, v, w)$
3. $b(u, v, w) = (\nabla \cdot (v \otimes u), w)$

2.1.1 Fluid Dynamics Preliminaries

2.2 Navier-Stokes Equations

A thorough and insightful derivation of the Navier-Stokes equations can be found in [9]. Many useful results, historical notes, and other details may be found in [45]. Here, we will present a basic overview to allow for unified notation in future sections.

Here, we consider Ω to be a connected, open, bounded domain in \mathbb{R}^d , with $d = 2, 3$ as the spacial dimension. The incompressible Navier-Stokes equations with no slip boundary conditions are given:

$$\begin{aligned} \frac{\partial u}{\partial t} + u \cdot \nabla u - \nu \Delta u + \nabla p &= f, \nabla \cdot u = 0 \\ u(x, 0) &= u_0(x), u|_{\partial\Omega} = 0. \end{aligned} \tag{2.2.1}$$

Here, u is the fluid velocity, p is the pressure, f is a body force, and ν is the kinematic viscosity.

It can be useful to rescale the Navier-Stokes. Let U be a reference velocity, L a reference length, $T = \frac{L}{U}$, $u^* = \frac{u}{U}$, $x^* = \frac{x}{L}$ and $t^* = \frac{t}{T}$. Then, (2.2.1) is equivalent to the following nondimensionalized system (see pg 100 of [45]).

$$\frac{\partial u^*}{\partial t^*} + u^* \cdot \nabla^* u^* - \frac{\nu}{LU} \Delta^* u^* + \nabla^* p = f, \nabla^* \cdot u^* = 0. \tag{2.2.2}$$

The Reynolds number, $\mathcal{Re} = \frac{LU}{\nu}$ determines the flow characteristics.

The following results are useful, and the proofs are simple and illuminating, and are thus included.

Theorem 2.2.1. *Let u be a solution to 2.2.1. Then the kinetic energy in u is bounded uniformly in time. The time averaged average energy dissipation rate is also uniformly bounded in time.*

Proof. Multiply (2.2.1) by u and integrate over Ω . By skew symmetry of the non-linear term, we have:

$$\frac{1}{2} \frac{d}{dt} \|u\|^2 + \nu \|\nabla u\|^2 = (f, u).$$

Integrating this term from 0 to T results in the energy equality: current kinetic energy plus the total energy dissipated over time is equal to the energy input through the body force plus the initial kinetic energy.

Using the definition of the inverse norm and Young's inequality, we have

$$\frac{1}{2} \frac{d}{dt} \|u\|^2 + \frac{\nu}{2} \|\nabla u\|^2 \leq \frac{1}{2\nu} \|f\|_{-1}^2. \quad (2.2.3)$$

By Poincaré's inequality

$$\frac{1}{2} \frac{d}{dt} \|u\|^2 + \frac{\nu}{2C_P^2} \|u\|^2 = \frac{1}{2\nu} \|f\|_{-1}^2.$$

Then, by use of an integrating factor or Gronwall's inequality, we have

$$\|u(t)\|^2 \leq \|u(0)\|^2 + \int_0^t \frac{1}{\nu} \|f\|_{-1}^2 \exp \left\{ \frac{\nu}{C_P^2} (s-t) \right\} ds < C(\nu, f, u(0)).$$

That is, the kinetic energy $\|u\|^2$ is bounded independent of time.

Time averaging (2.2.3), we get

$$\frac{1}{T} \|u(T)\|^2 + \frac{1}{T} \int_0^T \nu \|\nabla u\|^2 dt \leq \frac{1}{\nu} \|f\|_{-1}^2 + \frac{1}{T} \|u(0)\|^2 < C(\nu, f, u(0)). \quad (2.2.4)$$

□

2.3 Turbulence Modeling

It is impossible to sum up the theory of turbulence briefly, we seek to touch on the relevant background to this dissertation. More details are found in [65],[45]. The richness of scales spatially of turbulence leads directly to the necessity of turbulence modeling. The action of the nonlinearity is to break down large eddies, and is the dominant effect in all but the smallest scales. At the smallest scales, the viscous effects dominate, and energy is dissipated. The problem then is the scales at which this dissipation occurs; the smallest relevant scales are $\mathcal{O}(\mathcal{R}e^{-3/4})$ for three dimensional flow. Thus, failing to resolve these scales will result in underdissipation, and nonphysical checkerboard oscillations on the mesh.

We will focus herein on eddy viscosity models. Eddy viscosity models, the most common turbulence models used today, model the overall dissipative effects of turbulent fluctuations on the mean with an enhanced viscosity. In this section, we will examine the derivation of RANS eddy viscosity models. We will also consider briefly the derivation of the k -equation, used to model turbulent kinetic energy for use in calculations of eddy viscosity.

2.3.1 Eddy Viscosity Turbulence models

In practice, we consider turbulence models to predict averages to the Navier-Stokes equations (e.g. spatial averages, infinite time averages, small time averages, or ensemble averages). Consider a general averaging operator with the properties that $\overline{\bar{u}} = \bar{u}$ and $\overline{u\bar{v}} = \bar{u}\bar{v}$. We can then decompose the velocity u into the mean and fluctuations, $u = \bar{u} + u'$, with the property that $\overline{u'} = 0$.

We may average (2.2.1). Derivatives will commute with averaging:

$$\bar{u}_t + \overline{u \cdot \nabla u} - \nu \Delta \bar{u} + \nabla \bar{p} = \bar{f}. \quad (2.3.1)$$

As u is divergence free, we have

$$\overline{u \cdot \nabla u} = \nabla \cdot (\overline{u \otimes u}).$$

Properties of the averaging operator gives us

$$\nabla \cdot (\overline{u \otimes u}) = \nabla \cdot (\bar{u} \otimes \bar{u}) + \nabla \cdot (\overline{u' \otimes u'}).$$

Then, we have the Reynolds averaged Navier-Stokes equations

$$\bar{u}_t + \bar{u} \cdot \nabla \bar{u} + \nabla \cdot (\overline{u' \otimes u'}) - \nu \Delta \bar{u} + \nabla \bar{p} = \bar{f}, \quad (2.3.2)$$

where $\overline{u' \otimes u'}$ are the Reynolds stresses, or the effect of the fluctuations on the mean flow. It was conjectured by Boussinesq in 1877 [2] that this effect is overall dissipative. In practice, unresolved eddies in these fluctuations may combine to larger eddies, adding energy to the mean flow, a phenomenon known as backscatter (corrected eddy viscosity models, which add terms to model backscatter, are explored in [35]). It was proved by Layton in [51] that in the long time average, the effect is indeed dissipative (see also [36]). Thus, modeling the Reynolds stresses with an enhanced viscosity and modification to the pressure term is simple and computationally inexpensive method to model turbulent flows. Let $v \approx \bar{u}$. Then, we have

$$v_t + v \cdot \nabla v - \nu \Delta v - \nabla \cdot (\nu_T \nabla^s v) + \nabla p = f, \quad \nabla \cdot v = 0. \quad (2.3.3)$$

Where ν_T is the turbulent viscosity. Dimensional arguments set $\nu_T = \mu \ell \sqrt{k}$. Here, μ is a calibration constant, typically 0.2 to 0.6, and often 0.55, p. 114,[65]. ℓ is the turbulent length scale, and k models the kinetic energy in turbulent fluctuations,

$\frac{1}{2}|\overline{u'}|^2$. The specific model depends the choice of ℓ and how k , an unknowable quantity, is modeled. They are determined ad hoc either by an algebraic formula (0-equation model), or auxiliary equations (e.g., k -equation, ε -equation, etc.). We will consider the 1-equation model of Prandtl [67] and Kolmogorov [41], where k is the solution to the k equation and ℓ is a prescribed length scale.

2.3.2 The k -equation

Here, we briefly derive the k -equation. Detailed derivations are found, for example, in [8] p.99, Section 4.4, [56] p.60, Section 5.3 or [65] p.369, Section 10.3. Here, we seek more to clarify the origin of the various terms in the k -equation to shed light on the question of the inclusion or exclusion of the $\nu\Delta k$ term, which we explore more fully in Chapter 5.

To derive an equation for the energy in the turbulent fluctuations, $\frac{1}{2}|u'|^2$ we begin by taking the dot product of (2.2.1) and u and averaging, and subtracting the dot product of (2.3.2) and \bar{u} :

$$\begin{aligned} \overline{u_t u} - \bar{u}_t \bar{u} + \overline{u \cdot \nabla u u} - (\bar{u} \cdot \nabla \bar{u} \bar{u} + \nabla \cdot (\bar{u} \otimes u) \bar{u}) \\ - \nu \overline{\Delta u u} + \nu \Delta \bar{u} \bar{u} + \overline{(\nabla p) u} - \nabla \bar{p} \bar{u} = 0. \end{aligned} \quad (2.3.4)$$

We use the following properties of the averaging operator:

$$\begin{aligned} \overline{uv} &= \bar{u}\bar{v} + \overline{u'v'} \\ \overline{uvw} &= \overline{u'v'w'} + \overline{u'v'}\bar{w} + \overline{u'w'}\bar{v} + \overline{v'w'}\bar{u} + \bar{u}\bar{v}\bar{w}. \end{aligned}$$

Then, (2.3.4) simplifies to

$$\overline{u'_t u'} + \overline{u \cdot \nabla u u} - (\bar{u} \cdot \nabla \bar{u} \bar{u} + \nabla \cdot (\bar{u} \otimes u) \bar{u}) - \nu \overline{\Delta u' u'} + \overline{\nabla p' u'} = 0. \quad (2.3.5)$$

Addressing the nonlinear terms, we have

$$\overline{u \cdot \nabla u u} - \bar{u} \cdot \nabla \bar{u} \bar{u} = \bar{u} \cdot \overline{\nabla u' u'} + \overline{u' \cdot \nabla u' \bar{u}} + \overline{u' \cdot \nabla \bar{u} u'} + \overline{u' \cdot \nabla u' u'}. \quad (2.3.6)$$

Derivative rules can be applied to each term:

$$\begin{aligned} \bar{u} \cdot \overline{\nabla u' u'} &= \frac{1}{2} \bar{u} \cdot \nabla (|u'|^2) \\ \overline{u' \cdot \nabla u' \bar{u}} &= \nabla \cdot (\overline{u' \otimes u'}) \bar{u} \\ \overline{u' \cdot \nabla \bar{u} u'} &= (\overline{u' \otimes u'}) : \nabla \bar{u} \\ \overline{u' \cdot \nabla u' u'} &= \frac{1}{2} \nabla \cdot (\overline{|u'|^2 u'}) \end{aligned}$$

Note the second term will cancel with the Reynolds stresses in (2.3.5). Further:

$$\begin{aligned} \overline{u'_t u'} &= \frac{1}{2} |u'|^2_t \\ \overline{\Delta u' u'} &= \frac{1}{2} \overline{\Delta (|u'|^2)} - \overline{|\nabla u'|^2} \end{aligned}$$

Then, we may substitute in $k = \frac{1}{2} |u'|^2$ in (2.3.5)

$$k_t + \bar{u} \cdot \nabla k + (\overline{u' \otimes u'}) : \nabla \bar{u} + \frac{1}{2} \nabla \cdot (\overline{|u'|^2 u'}) + \nabla \overline{p' u'} - \nu \Delta k + \nu \overline{|\nabla u'|^2}. \quad (2.3.7)$$

Following (2.3.3), the energy lost to the mean flow by turbulent fluctuations is input in our equation for the energy in these turbulent fluctuations:

$$\overline{u' \otimes u'} : \nabla \bar{u} \approx -\nu_T |\nabla^s v|^2$$

by the gradient-diffusion hypothesis [26], we have:

$$\frac{1}{2} \nabla \cdot (\overline{|u'|^2 u'}) + \nabla \overline{p' u'} \approx -\nabla \cdot \nu_T \nabla k.$$

Finally, $\varepsilon' = \nu \overline{|\nabla u'|}$ is the dissipation rate. The expected scaling is $\frac{u^3}{\ell}$, which leads to the term being independently modeled by Kolmogorov and Prandtl as

$$\nu \overline{|\nabla u'|^2} \approx \frac{k^{3/2}}{\ell}.$$

The material derivative of k is exact. We recall \bar{u} is approximated with v in (2.3.3) We then have the k -equation as

$$k_t + v \cdot \nabla k - \nabla \cdot (\nu_T \nabla k) - \nu \Delta k + \frac{k^{3/2}}{\ell} = \nu_T |\nabla^s v|^2. \quad (2.3.8)$$

It may seem natural to leave the term $\nu \Delta k$ for the reason that it appears directly in the derivation. When we consider the near wall asymptotics of this term in conjuncture with the near wall asymptotics of the modeled terms, exclusion is more accurate.

3.0 Numerical Dissipation in Multistep Methods

The richness of scales found in fluid flows requires A -stable time stepping methods. Full analysis of one and two step A -stable linear multistep methods applied to the incompressible Navier-Stokes equations is found in Girault and Raviart [28]. Limitations of computational resources inherent in fluid flow simulations have frequently led to the choice of the backward Euler time discretization. This method, however, is known to introduce numerical dissipation, which can push flow to lower Reynolds number states. Second order A -stable methods in almost all cases add numerical dissipation as well, though they are less dissipative than the backward Euler method. Higher order A -stable multistep methods do not exist [12]; we will not address second order methods k -step multistep methods with $k > 2$, however the extension to higher order G -stable multistep methods is clear.

In the continuous time, it holds that the time averaged energy dissipation rate is bounded above by $\frac{U^3}{L} (c_1 + c_2 \mathcal{R}e^{-1})$. The question then arises if a similar bound can be found for the combined viscous and numerical dissipation, uniform in the Reynolds number and independent of the timestep size.

Herein, we will consider this for a number of perturbed problems. Section 3.1 presents preliminary results and notation for the consideration of discrete time problems. Section 3.2 considers the fully implicit time discretization for both the one step method backward Euler and a general, A -stable two step method. We show that this result is analogous to the continuous time setting. Section 3.3 extends results to a nonconstant forcing term.

Section 3.4 discusses linearly implicit treatment of the nonlinear term, commonly implemented due to computational limitations. Here, we show that a first order

extrapolation in the nonlinear term is analogous to continuous results independent of timestep size, but that this result does not hold for higher order extrapolations. Numerical tests to confirm theoretical results are given in section 3.5. Finally, we discuss the extension to turbulence models and other conclusions in 3.6.

3.1 Notation and Preliminaries

In addition to notation and preliminaries introduced in 2.1, we introduce notation specific to this chapter. We will consider herein body force driven flow with no slip boundary conditions, where f is assumed to be zero at the boundary. The analysis will extend immediately to body force driven flow in a periodic box. In particular, we will see no additional terms from boundary contributions when performing integration by parts.

We define a generic k -step linear multistep method (LMM) applied to the problem $y' = f(t, y)$ and normalized by enforcing $\sum_{j=0}^k \beta_j = 1$ as

$$\sum_{i=0}^k \alpha_i y^{n+i} = h \sum_{j=0}^k \beta_j f(t^{n+j}, y^{n+j}) \quad (3.1.1)$$

and define the corresponding one leg method (OLM)

$$\sum_{i=0}^k \alpha_i y^{n+i} = h f\left(\sum_{j=0}^k \beta_j t^{n+j}, \sum_{j=0}^k \beta_j y^{n+j}\right). \quad (3.1.2)$$

If f is linear, these methods are identical, hence if a LMM is A -stable, the corresponding OLM is A -stable as well. We will analyze herein OLM methods, as they are considered better choices for stiff nonlinear problems [13], and the implementation, requiring a single function evaluation per timestep, is more efficient. We will also

focus on 1 and 2-step methods that are A -stable, though there exist k -step second order A -stable methods for $k > 2$.

Definition 3.1.1. *The finite and infinite time average of a sequence is given by*

$$\langle \phi \rangle_N := \frac{1}{N} \sum_{n=0}^{N-1} \phi^{n+1}, \quad \langle \phi \rangle_\infty = \limsup_{N \rightarrow \infty} \langle \phi \rangle_N,$$

In both cases, it holds

$$\langle |\phi\psi| \rangle \leq \langle |\phi|^2 \rangle^{1/2} \langle |\psi|^2 \rangle^{1/2}.$$

Definition 3.1.2. *The large force scale and the large length scale. The length scale is used to define the Reynolds number*

$$F = \sqrt{\frac{1}{|\Omega|} \|f\|^2}$$

$$L = \min \left\{ |\Omega|^{1/3}, \frac{F}{\left(\frac{1}{|\Omega|} \|\nabla f\|^2\right)^{1/2}}, \frac{F}{\|\nabla f\|_{L^\infty(\Omega)}} \right\}$$

It can be easily verified that L has units of length, moreover $\frac{1}{|\Omega|} \|\nabla f\|^2 \leq \frac{F^2}{L^2}$ and $\|\nabla f\|_{L^\infty(\Omega)} \leq \frac{F}{L}$.

The definition of the large scale velocity, U , will depend on the time stepping scheme and will be specified later. As we consider body force driven flow, it is natural to consider U to be a discrete analogue to the infinite time and space average of the velocity:

$$U \approx \left(\limsup_{T \rightarrow \infty} \frac{1}{T} \int_0^T \frac{1}{|\Omega|} \|u\|^2 dt \right)^{1/2}.$$

3.2 Fully Implicit Timestepping Methods

3.2.1 Backward Euler

The backward Euler (BE) time discretization is given by

$$y^{n+1} - y^n = hf(t^{n+1}, y^{n+1}). \quad (3.2.1)$$

We consider fully implicit BE applied to the Navier-Stokes equations. We assume that f is constant and divergence free. Let $k > 0$ be the fixed timestep, let $t_n = kn$ be the n^{th} timestep and $T = kN$ be the final time. Set $u^0 = u_0(x)$. We then seek u^{n+1} that solves

$$\begin{aligned} \frac{u^{n+1} - u^n}{k} + u^{n+1} \cdot \nabla u^{n+1} - \nu \Delta u^{n+1} + \nabla p^{n+1} &= f \\ \nabla \cdot u^{n+1} &= 0. \end{aligned} \quad (3.2.2)$$

Or we seek $u^{n+1} \in V$ such that for all $v \in X$

$$\left(\frac{u^{n+1} - u^n}{k}, v \right) + b(u^{n+1}, u^{n+1}, v) + \nu (\nabla u^{n+1}, \nabla v) - (p^{n+1}, \nabla \cdot v) = (f, v) \quad (3.2.3)$$

Take $v = u^{n+1}$, take the spacial average, use skew symmetry of the nonlinear term and apply the polarization identity 2.1.2:

$$\frac{1}{2|\Omega|k} (\|u^{n+1}\|^2 - \|u^n\|^2 + \|u^{n+1} - u^n\|^2) + \frac{\nu}{|\Omega|} \|\nabla u^{n+1}\|^2 = \frac{1}{|\Omega|} (f, u^{n+1}). \quad (3.2.4)$$

This equation is directly analogous to (2.2.3), with the addition of numerical dissipation.

Definition 3.2.1. *The viscous dissipation rate (per unit volume), ε_0 , and numerical dissipation rate (per unit volume), ε_N , are*

$$\varepsilon_0^{n+1} := \frac{\nu}{|\Omega|} \|\nabla u^{n+1}\|^2$$

$$\varepsilon_N^{n+1} := \frac{1}{|\Omega|k} \|u^{n+1} - u^n\|^2.$$

Definition 3.2.2. *For the BE time discretization, we have the following definition for U*

$$U_N = \left(\frac{1}{N} \sum_{n=0}^{N-1} \frac{1}{|\Omega|} \|u^{n+1}\|^2 \right)^{1/2}$$

$$U = \left(\limsup_{N \rightarrow \infty} \frac{1}{N} \sum_{n=0}^{N-1} \frac{1}{|\Omega|} \|u^{n+1}\|^2 \right)^{1/2}.$$

Theorem 3.2.1. *Let $\{u^n\}_{n \in \mathbb{N}} \subset X = H_0^1(\Omega)$ be the sequence of functions defined by (3.2.3). Let f be constant in time, divergence free, and zero on the boundary. Then,*

$$\langle \varepsilon_0 + \varepsilon_N \rangle_\infty \leq \frac{U^3}{L} (2 + \mathcal{R}e^{-1}).$$

Proof. Apply Cauchy-Schwarz inequality (2.1.1) to the right hand side of (3.2.4):

$$\frac{1}{2k} (\|u^{n+1}\|^2 - \|u^n\|^2 + \|u^{n+1} - u^n\|^2) + \nu \|\nabla u^{n+1}\|^2 = \|f\| \|u^{n+1}\|. \quad (3.2.5)$$

Take the finite time average:

$$\begin{aligned} & \frac{1}{2T|\Omega|} \|u^N\|^2 - \frac{1}{2T|\Omega|} \|u^0\|^2 + \frac{1}{N} \sum_{n=0}^{N-1} \left(\frac{1}{2} \varepsilon_N^{n+1} + \varepsilon_0^{n+1} \right) \\ & \leq \left(\frac{1}{N} \sum_{n=0}^{N-1} \frac{1}{|\Omega|} \|f\|^2 \right)^{1/2} \left(\frac{1}{N} \sum_{n=0}^{N-1} \frac{1}{|\Omega|} \|u^{n+1}\|^2 \right)^{1/2}. \end{aligned} \quad (3.2.6)$$

Equivalently

$$\frac{1}{2T|\Omega|}\|u^N\|^2 - \frac{1}{2T|\Omega|}\|u^0\|^2 + \left\langle \frac{1}{2}\varepsilon_N + \varepsilon_0 \right\rangle_N \leq FU_N. \quad (3.2.7)$$

In the long time average, initial and final kinetic energy will disappear, as both terms are $\mathcal{O}(\frac{1}{T})$. We now look to bound F in terms of flow variables. Take $v = f$ in (3.2.3)

$$F^2 = \left(\frac{u^{n+1} - u^n}{k}, f \right) + b(u^{n+1}, u^{n+1}, f) + \nu(\nabla u^{n+1}, \nabla f). \quad (3.2.8)$$

We note pressure terms drop out as f is divergence free. As u^{n+1} is divergence free, we may use an alternate form of the trilinear form b , (2.1.1), and then apply integration by parts:

$$\begin{aligned} F^2 &= \frac{1}{|\Omega|} \left(\frac{u^{n+1} - u^n}{k}, f \right) + \frac{1}{|\Omega|} (\nabla \cdot (u^{n+1} \otimes u^{n+1}), f) + \frac{\nu}{|\Omega|} (\nabla u^{n+1}, \nabla f) \\ &= \frac{1}{|\Omega|} \left(\frac{u^{n+1} - u^n}{k}, f \right) - \frac{1}{|\Omega|} (u^{n+1} \otimes u^{n+1}, \nabla f) + \frac{\nu}{|\Omega|} (\nabla u^{n+1}, \nabla f). \end{aligned} \quad (3.2.9)$$

We now take the time average:

$$\begin{aligned} F^2 &= \frac{1}{|\Omega|} \frac{1}{N} \sum_{n=0}^{N-1} \left(\frac{u^{n+1} - u^n}{k}, f \right) + \frac{1}{N} \sum_{n=0}^{N-1} \frac{1}{|\Omega|} (u^{n+1} \otimes u^{n+1}, \nabla f) \\ &\quad + \frac{1}{|\Omega|} \frac{1}{N} \sum_{n=0}^{N-1} \frac{\nu}{|\Omega|} (\nabla u^{n+1}, \nabla f) \\ &= I. + II. + III. \end{aligned} \quad (3.2.10)$$

We will address these terms successively.

Term I. is a simple telescoping sum:

$$\begin{aligned}
I. &= \frac{1}{|\Omega|} \frac{1}{N} \sum_{n=0}^{N-1} \left(\frac{u^{n+1} - u^n}{k}, f \right) \\
&= \frac{1}{N|\Omega|} \left(\frac{u^N - u^0}{k}, f \right) \\
&= \frac{1}{T|\Omega|} (u^N - u^0, f).
\end{aligned} \tag{3.2.11}$$

Addressing term II., we use Hölder's inequality, Cauchy Schwarz, and definitions 3.1.2, 3.2.2

$$\begin{aligned}
II. &= \frac{1}{N} \sum_{n=0}^{N-1} \frac{1}{|\Omega|} (u^{n+1} \otimes u^{n+1}, \nabla f) \\
&\leq \|\nabla f\|_{L^\infty(\Omega)} \frac{1}{N} \sum_{n=0}^{N-1} \frac{1}{|\Omega|} \|u^{n+1}\|^2 \\
&\leq \frac{F}{L} \frac{1}{N} \sum_{n=0}^{N-1} \frac{1}{|\Omega|} \|u^{n+1}\|^2 \\
&\leq \frac{F}{L} U_N^2 \\
&= \frac{F}{U_N} \frac{U_N^3}{L}.
\end{aligned} \tag{3.2.12}$$

Addressing term III., we use the Cauchy Schwarz inequality in space and time and Young's inequality, and definition 3.1.2. This results in the following string of

inequalities:

$$\begin{aligned}
III. &= \left\langle \frac{\nu}{|\Omega|} (\nabla u, \nabla f) \right\rangle_N \\
&\leq \left\langle \frac{F}{U_N} \frac{\nu}{|\Omega|} \|\nabla u\|^2 \right\rangle_N^{1/2} \left\langle \frac{U_N}{F} \frac{\nu}{|\Omega|} \|\nabla f\|^2 \right\rangle_N^{1/2} \\
&\leq \frac{1}{2} \frac{F}{U_N} \left\langle \frac{\nu}{|\Omega|} \|\nabla u\|^2 \right\rangle_N + \frac{1}{2} \frac{U_N}{F} \left\langle \frac{\nu}{|\Omega|} \|\nabla f\|^2 \right\rangle_N \\
&\leq \frac{1}{2} \frac{F}{U_N} \langle \varepsilon_0 \rangle_N + \frac{1}{2} \frac{U_N}{F} \frac{\nu F^2}{L^2} \\
&\leq \frac{1}{2} \frac{F}{U_N} \left(\langle \varepsilon_0 \rangle_N + \frac{U U_N^2}{L} \frac{\nu}{LU} \right).
\end{aligned} \tag{3.2.13}$$

Combining all terms in our estimate (3.2.10), we have

$$F^2 \leq \frac{1}{T|\Omega|} (u^N - u^0, f) + \frac{F}{U_N} \left(\frac{1}{2} \langle \varepsilon_0 \rangle_N + \frac{1}{2} \frac{\nu}{LU} \frac{U U_N^2}{L} + \frac{U_N^3}{L} \right). \tag{3.2.14}$$

Immediately, from (3.2.7), we have

$$\begin{aligned}
&\mathcal{O} \left(\frac{1}{T} \right) + \left\langle \frac{1}{2} \varepsilon_N + \varepsilon_0 \right\rangle_N \\
&\leq F U_N \leq \mathcal{O} \left(\frac{1}{T} \right) + \left(\frac{1}{2} \langle \varepsilon_0 \rangle_N + \frac{1}{2} \frac{\nu}{LU} \frac{U U_N^2}{L} + \frac{U_N^3}{L} \right).
\end{aligned} \tag{3.2.15}$$

Then, by rearranging and taking $T \rightarrow \infty$ we may conclude

$$\langle \varepsilon_N + \varepsilon_0 \rangle_\infty \leq \left(\frac{\nu}{LU} + 2 \right) \frac{U^3}{L}. \tag{3.2.16}$$

□

3.2.2 General Two Step Methods

When analyzing the numerical dissipation of a multistep method, it is useful to consider the framework of G -stability. For one step methods and second order two step methods, this is equivalent to the notion of A stability [1] but allows for a more convenient framework for which to discuss the numerical dissipation of these methods.

3.2.2.1 A-stability

We recall a linear multistep method is A -stable if the stability region includes the entire left half of the complex plane.

Definition 3.2.3. *A multistep method is A -stable if applied to the problem*

$$y'(t) = e^{\lambda t}$$

$$y(0) = 1$$

we have $y(t) \rightarrow 0$ as $t \rightarrow \infty$ when $\operatorname{Re}(\lambda) < 0$.

Common A -stable methods are backward Euler, the trapezoid method, and second order backwards differentiation method.

Theorem 3.2.2. *All second order, two-step methods in form (3.1.1) or (3.1.2) have the following conditions on the coefficients:*

- $\alpha_0 = -1 + \alpha_2, \alpha_1 = 1 - 2\alpha_2$
- $\beta_0 = \frac{1}{2} - \alpha_2 + \beta_2, \beta_1 = \frac{1}{2} + \alpha_2 - 2\beta_2$

These methods are A -stable for $\alpha_2 \geq \frac{1}{2}, \beta_2 > \frac{\alpha_2}{2}$ and strongly A -stable for $\alpha_2 > \frac{1}{2}, \beta_2 > \frac{\alpha_2}{2}$.

Proof. See Girault and Raviart pg 182. □

3.2.2.2 G-Stability

We briefly present an overview of G -stability for two step methods. Full details can be found in [5].

Definition 3.2.4. *Let G be a 2×2 real symmetric positive definite matrix. Then, if $\vec{y} = [y^1, y^2]^T$ is a vector of functions,*

$$\|\vec{y}\|_G^2 = \sum_{i,j=1}^2 g_{ij}(y^i, y^j) = \vec{y}^T G \vec{y} \quad (3.2.17)$$

Definition 3.2.5. *A method in the form 3.1.1 or 3.1.2 is said to be G -stable if there exists real symmetric positive definite G such that the matrix*

$$\tilde{G} = \begin{bmatrix} \alpha_0\beta_0 + g_{11} & \alpha_0\beta_1 + g_{12} & \alpha_0\beta_2 \\ \alpha_1\beta_0 + g_{12} & \alpha_1\beta_1 - g_{11} + g_{22} & \alpha_1\beta_2 - g_{12} \\ \alpha_2\beta_0 & \alpha_2\beta_1 - g_{12} & \alpha_2\beta_2 - g_{22} \end{bmatrix}$$

has symmetric positive definite real part.

The utility of this definition is apparent when we set $Y^n = [y^n, y^{n+1}]$ and $\tilde{Y}^n = [y^{n-1}, y^n, y^{n+1}]$. Then,

$$\tilde{Y}_n^T \tilde{G} \tilde{Y}_n = \sum_{i,j=0}^2 (\alpha_i y^{n-1+i}, \beta_j y^{n-1+j}) + \sum_{i,j=1}^2 g_{ij}(y^{n-1+i}, y^{n-1+j}) - \sum_{i,j=1}^2 g_{ij}(y^{n+i}, y^{n+j}). \quad (3.2.18)$$

Crucially,

$$\sum_{i,j=0}^2 (\alpha_i y^{n+i}, \beta_j y^{n+j}) = \|Y^{n+1}\|_G^2 - \|Y^n\|_G^2 + \tilde{Y}_n^T \tilde{G} \tilde{Y}_n.$$

This allows us to explicitly calculate the numerical dissipation in the method. Indeed, given α_2 and β_2 such that $\alpha_2 \geq \frac{1}{2}, \beta_2 > \frac{\alpha_2}{2}$ and $\alpha_0, \alpha_1, \beta_0, \beta_1$ as defined in 3.2.2, we have

$$G = \begin{bmatrix} \lambda - \alpha_0\beta_0 & 2\lambda + \frac{1}{2}(\alpha_1\beta_2 + \alpha_2\beta_1) \\ 2\lambda + \frac{1}{2}(\alpha_1\beta_2 + \alpha_2\beta_1) & \alpha_2\beta_2 - \lambda \end{bmatrix}$$

and

$$\tilde{G} = \lambda \begin{bmatrix} 1 & -2 & 1 \\ -2 & 4 & -2 \\ 1 & -2 & 1 \end{bmatrix}$$

where

$$\lambda = \frac{1}{2}(\alpha_0\beta_2 + \alpha_2\beta_0).$$

This allows us to easily write any method in terms of an energy difference and numerical dissipation:

$$\sum_{i,j=0}^2 (\alpha_i y^{n+i}, \beta_j y^{n+j}) = \|Y^{n+1}\|_G^2 - \|Y^n\|_G^2 + \lambda \|u^{n+1} - 2u^n + u^{n-1}\|^2. \quad (3.2.19)$$

These results may be verified by direct calculation, and were first proved by Dahlquist in [11].

3.2.3 Long Time Energy Dissipation

We consider a general A -stable, second order, two step method applied to the Navier-Stokes equations. Again, we assume f is constant and divergence free, and that we have initial conditions u^{-1} and u^0 given. We additionally define

$$u_\beta^{n+1} = \sum_{i=0}^2 \beta_i u^{n-1+i}$$

and seek u^{n+1} such that

$$\frac{1}{k} \sum_{i=0}^2 \alpha_i u^{n-1+i} + u_\beta^{n+1} \cdot \nabla u_\beta^{n+1} - \nu \Delta u_\beta^{n+1} + \nabla p_\beta^{n+1} = f \quad (3.2.20)$$

$$\nabla \cdot u^{n+1} = 0.$$

Or, seek $u^{n+1} \in V$ such that for all $v \in X$

$$\frac{1}{k} \left(\sum_{i=0}^2 \alpha_i u^{n-1+i}, v \right) + (u_\beta^{n+1} \cdot \nabla u_\beta^{n+1}, v) + \nu (\nabla u_\beta^{n+1}, \nabla v) + (p_\beta^{n+1}, \nabla \cdot v) = (f, v). \quad (3.2.21)$$

By setting $u_\beta^{n+1} = v$, dividing by domain volume, and using that our method is G -stable, we have

$$\frac{1}{k|\Omega|} (\|U^{n+1}\|_G^2 - \|U^n\|_G^2 + \lambda \|u^{n+1} - 2u^n + u^{n-1}\|^2) + \frac{\nu}{\Omega} \|\nabla u_\beta^{n+1}\|^2 = (f, u_\beta^{n+1}). \quad (3.2.22)$$

Again, this is analogous to the continuous time setting with the addition of numerical dissipation.

Definition 3.2.6. For a general two step method, we define the viscous energy dissipation rate (per unit volume), ε_0 and the numerical energy dissipation rate (per unit volume) as

$$\begin{aligned}\varepsilon_0^{n+1} &= \frac{\nu}{\Omega} \|\nabla u_\beta^{n+1}\|^2 \\ \varepsilon_N^{n+1} &= \frac{1}{k|\Omega|} \lambda \|u^{n+1} - 2u^n + u^{n-1}\|^2.\end{aligned}$$

Definition 3.2.7. For a general two step one leg method, we define the velocity scales

$$\begin{aligned}U_N &= \frac{1}{N} \sum_{n=0}^{N-1} \frac{1}{|\Omega|} \|u_\beta^{n+1}\|^2 \\ U &= \limsup_{N \rightarrow \infty} U_N.\end{aligned}$$

Theorem 3.2.3. Let $\{u^n\}_{n \in \mathbb{N}} \subset X = H_0^1(\Omega)$ be the sequence of functions defined by (3.2.21). Let f be constant in time, divergence free, and zero on the boundary. Then,

$$\langle \varepsilon_0 + 2\varepsilon_N \rangle_\infty \leq \frac{U^3}{L} (2 + \mathcal{R}e^{-1})$$

Proof. This proof is, with the exception of the time discretization term, identical to 3.2.1, thus repeated details will be excluded. Apply Cauchy-Schwarz inequality (2.1.1) to the right hand side of (3.2.22):

$$\frac{1}{k|\Omega|} (\|U^{n+1}\|_G^2 - \|U^n\|_G^2 + \lambda \|u^{n+1} - 2u^n + u^{n-1}\|^2) + \frac{\nu}{\Omega} \|\nabla u_\beta^{n+1}\|^2 = \frac{1}{|\Omega|} \|f\| \|u_\beta^{n+1}\|. \quad (3.2.23)$$

Take the finite time average:

$$\begin{aligned}\frac{1}{2T|\Omega|} \|U^N\|_G^2 - \frac{1}{2T|\Omega|} \|U^0\|_G^2 + \frac{1}{N} \sum_{n=0}^{N-1} (\varepsilon_N^{n+1} + \varepsilon_0^{n+1}) \\ \leq \left(\frac{1}{N} \sum_{n=0}^{N-1} \frac{1}{|\Omega|} \|f\|^2 \right)^{1/2} \left(\frac{1}{N} \sum_{n=0}^{N-1} \frac{1}{|\Omega|} \|u_\beta^{n+1}\|^2 \right)^{1/2}.\end{aligned} \quad (3.2.24)$$

Equivalently

$$\frac{1}{2T|\Omega|} \|U^N\|_G^2 - \frac{1}{2T|\Omega|} \|U^0\|_G^2 + \langle \varepsilon_N + \varepsilon_0 \rangle_N \leq FU_N. \quad (3.2.25)$$

We now look to bound F in terms of flow variables. Take $v = f$ in (3.2.21)

$$F^2 = \frac{1}{|\Omega|} \left(\frac{1}{k} \sum_{i=0}^2 \alpha_i u^{n-1+i}, f \right) + b(u_\beta^{n+1}, u_\beta^{n+1}, f) + \frac{\nu}{|\Omega|} (\nabla u_\beta^{n+1}, \nabla f). \quad (3.2.26)$$

Again, pressure terms drop out as f is divergence free. Treating the nonlinear term as before and taking the finite time average yields

$$\begin{aligned} F^2 &= \frac{1}{|\Omega|} \frac{1}{N} \sum_{n=0}^{N-1} \left(\frac{1}{k} \sum_{i=0}^2 \alpha_i u^{n-1+i}, f \right) + \frac{1}{N} \sum_{n=0}^{N-1} \frac{1}{|\Omega|} (u_\beta^{n+1} \otimes u_\beta^{n+1}, \nabla f) \\ &\quad + \frac{1}{|\Omega|} \frac{1}{N} \sum_{n=0}^{N-1} \frac{\nu}{|\Omega|} (\nabla u_\beta^{n+1}, \nabla f) \\ &= I. + II. + III. \end{aligned} \quad (3.2.27)$$

Addressing term I., we use that $\sum_{i=0}^2 \alpha_i = 0$. (Indeed, for a general consistent k -step method, $\sum_{i=0}^k \alpha_i = 0$.) Then, we have $\alpha_0 = -(\alpha_1 + \alpha_2)$. Hence

$$\alpha_2 u^{n+1} + \alpha_1 u^n + \alpha_0 u^{n-1} = \alpha_2 u^{n+1} + (\alpha_1 + \alpha_2) u^n - (\alpha_2 u^n + (\alpha_1 + \alpha_2) u^{n-1}). \quad (3.2.28)$$

We then can rewrite I. so it is a telescoping sum:

$$\begin{aligned} I. &= \frac{1}{|\Omega|} \frac{1}{Nk} \sum_{n=0}^{N-1} (\alpha_2 u^{n+1} + (\alpha_1 + \alpha_2) u^n - (\alpha_2 u^n + (\alpha_1 + \alpha_2) u^{n-1}), f) \\ &= \frac{1}{|\Omega|} \frac{1}{Nk} (\alpha_2 u^N + (\alpha_1 + \alpha_2) u^{N-1} - (\alpha_2 u^0 + (\alpha_1 + \alpha_2) u^{-1}), f) \\ &\leq \frac{1}{T} (\alpha_2 (\|u^N\| + \|u^0\|) + (\alpha_1 + \alpha_2) (\|u^{N-1}\| + \|u^{-1}\|) \|f\|) \\ &= \mathcal{O}\left(\frac{1}{T}\right). \end{aligned} \quad (3.2.29)$$

Treatment of terms II. and III. will be unchanged. As before,

$$II. \leq \frac{F}{U_N} \frac{U_N^3}{L}$$

$$III. \leq \frac{1}{2} \frac{F}{U_N} \left(\langle \varepsilon_0 \rangle_N + \frac{UU_N^2}{L} \frac{\nu}{LU} \right).$$

Combining all terms in our estimate (3.2.27), we have

$$F^2 \leq + \frac{F}{U_N} \left(\frac{1}{2} \langle \varepsilon_0 \rangle_N + \frac{1}{2} \frac{\nu}{LU} \frac{UU_N^2}{L} + \frac{U_N^3}{L} \right). \quad (3.2.30)$$

Immediately, from (3.2.25), we have

$$\begin{aligned} & \mathcal{O} \left(\frac{1}{T} \right) + \langle \varepsilon_N + \varepsilon_0 \rangle_N \\ & \leq FU_N \leq \mathcal{O} \left(\frac{1}{T} \right) + \left(\frac{1}{2} \langle \varepsilon_0 \rangle_N + \frac{1}{2} \frac{\nu}{LU} \frac{UU_N^2}{L} + \frac{U_N^3}{L} \right). \end{aligned} \quad (3.2.31)$$

Then, by rearranging and taking $T \rightarrow \infty$ we may conclude

$$\langle 2\varepsilon_N + \varepsilon_0 \rangle_\infty \leq \left(\frac{\nu}{LU} + 2 \right) \frac{U^3}{L}. \quad (3.2.32)$$

□

3.3 Nonconstant Forcing Term

We consider the case where f is not constant, but bounded. A key difference here is the alteration of the time scale. In the case where f is constant, the timescale is the large eddy turnover time, $\frac{L}{U}$ and the scaling of the energy dissipation rate, $\frac{U^3}{L}$ can be considered:

$$\frac{U^3}{L} = \frac{U^2}{L/U} = \frac{\textit{kinetic energy}}{\textit{time}}.$$

However, when f varies in time, a new timescale is induced, which depends on the rate of change of the force:

$$\tau_f = \frac{\langle \|f\| \rangle}{\langle \|f_t\| \rangle}.$$

Then, we expect uniform in the Reynolds number,

$$\langle \varepsilon \rangle \lesssim \max \left\{ \frac{U^3}{L}, \frac{U^2}{\tau_f} \right\}.$$

In the discrete setting, we may define τ_f analogously, and we expect the same scaling. We assume that f and f_t are uniformly bounded in time, and that f is divergence free. For simplicity, we will examine this with the backward Euler time discretization, extension to a general two step method will be analogous in principal but more notationally complex.

We define U and U_N as in 3.2.2. Let $f^n = f(t^n) = f(nk)$.

Definition 3.3.1. *We define the finite and long time averages of f and the time scale induced by f as*

$$F_N = \left(\frac{1}{N} \sum_{n=0}^{N-1} \frac{1}{|\Omega|} \|f^{n+1}\|^2 \right)^{1/2}$$

$$F = \limsup_{N \rightarrow \infty} F_N$$

$$\tau_f = \frac{F}{\left(\limsup_{N \rightarrow \infty} \frac{1}{N} \sum_{n=0}^{N-1} \frac{1}{|\Omega|} \left\| \frac{f^{n+1} - f^n}{k} \right\|^2 \right)^{1/2}}.$$

As f varies in time, slight modification in the definition of length scale is required.

Definition 3.3.2. *The large length scale L is given by*

$$L = \min \left\{ |\Omega|^{1/3}, \frac{F}{\left\langle \frac{1}{|\Omega|} \|\nabla f^{n+1}\|^2 \right\rangle_\infty^{1/2}}, \frac{F}{\|\nabla f\|_{L^\infty(0,T;L^\infty(\Omega))}} \right\}.$$

Backward Euler applied to the Navier-Stokes equations with nonconstant force is as follows:

$$\begin{aligned} \frac{u^{n+1} - u^n}{k} + u^{n+1} \cdot \nabla u^{n+1} - \nu \Delta u^{n+1} + \nabla p^{n+1} &= f^{n+1} \\ \nabla \cdot u^{n+1} &= 0 \end{aligned} \quad (3.3.1)$$

or, we seek $u^{n+1} \in V$ such that $\forall v \in X$

$$\left(\frac{u^{n+1} - u^n}{k}, v \right) + (u^{n+1} \cdot \nabla u^{n+1}, v) + \nu (\nabla u^{n+1}, \nabla v) - (p^{n+1}, \nabla \cdot v) = (f^{n+1}, v). \quad (3.3.2)$$

Theorem 3.3.1. *Let $\{u^n\} \subset X = H_0^1(\Omega)$ be the sequence of functions given by (3.3.2). Let f be uniformly bounded in time, vanish on the boundary, and divergence free. Let numerical and viscous dissipation be defined as in 3.2.1. Then,*

$$\langle \varepsilon_0 + \varepsilon_N \rangle_\infty \leq \frac{U^3}{L} (2 + \mathcal{R}e^{-1}) + 2 \frac{U^2}{\tau_f}.$$

Proof. As before, we take $v = u^{n+1}$ in (3.3.2). Polarization and Cauchy-Schwarz in space and time on the right hand side yields

$$\begin{aligned} & \frac{1}{2|\Omega|T} (\|u^N\|^2 - \|u^0\|^2) + \langle 2\varepsilon_N + \varepsilon_0 \rangle_N \\ & \leq \left(\frac{1}{N} \sum_{n=0}^{N-1} \frac{1}{|\Omega|} \|f^{n+1}\|^2 \right)^{1/2} \left(\frac{1}{N} \sum_{n=0}^{N-1} \frac{1}{|\Omega|} \|u^{n+1}\|^2 \right)^{1/2} = F_N U_N. \end{aligned} \quad (3.3.3)$$

We bound F_N by taking $v = f^{n+1}$ and taking the time and space average:

$$\begin{aligned} F_N^2 &= \frac{1}{N} \sum_{n=0}^{N-1} \frac{1}{|\Omega|} \left(\frac{u^{n+1} - u^n}{k}, f^{n+1} \right) + \frac{1}{N} \sum_{n=0}^{N-1} \frac{1}{|\Omega|} b(u^{n+1}, u^{n+1}, f^{n+1}) \\ & \quad + \frac{1}{N} \sum_{n=0}^{N-1} \frac{\nu}{|\Omega|} (\nabla u^{n+1}, \nabla f^{n+1}) \\ & = I. + II. + III. \end{aligned} \quad (3.3.4)$$

Addressing each term:

$$\begin{aligned} I. &= \frac{1}{N} \sum_{n=0}^{N-1} \frac{1}{|\Omega|} \left(\frac{u^{n+1} - u^n}{k}, f^{n+1} \right) \\ &= \frac{1}{|\Omega|k} \frac{1}{N} \sum_{n=0}^{N-1} ((u^{n+1}, f^{n+1}) - (u^n, f^{n+1})) \\ &= \frac{1}{|\Omega|k} \left(\frac{1}{N} \sum_{n=0}^{N-1} ((u^n, f^n) + (u^N, f^N) - (u^0, f^0)) - \frac{1}{N} \sum_{n=0}^{N-1} (u^n, f^{n+1}) \right) \\ &= \frac{1}{|\Omega|T} ((u^N, f^N) - (u^0, f^0)) - \frac{1}{N} \sum_{n=0}^{N-1} \frac{1}{|\Omega|} \left(u^n, \frac{f^{n+1} - f^n}{k} \right) \\ &\leq \mathcal{O}\left(\frac{1}{T}\right) + \left(\frac{1}{N} \sum_{n=0}^{N-1} \frac{1}{|\Omega|} \|u^n\|^2 \right)^{1/2} \left(\frac{1}{N} \sum_{n=0}^{N-1} \frac{1}{|\Omega|} \left\| \frac{f^{n+1} - f^n}{k} \right\|^2 \right)^{1/2}. \end{aligned} \quad (3.3.5)$$

We note that

$$\begin{aligned} \left(\frac{1}{N} \sum_{n=0}^{N-1} \frac{1}{|\Omega|} \|u^n\|^2 \right)^{1/2} &= \left(\frac{\|u^N\|^2 - \|u^0\|^2}{N} + \frac{1}{N} \sum_{n=0}^{N-1} \frac{1}{|\Omega|} \|u^{n+1}\|^2 \right)^{1/2} \\ &\leq \mathcal{O} \left(\frac{1}{N^{1/2}} \right) + U_N. \end{aligned}$$

Then, continuing our bound of term I .

$$\begin{aligned} I. &\leq U_N \left(\frac{1}{N} \sum_{n=0}^{N-1} \frac{1}{|\Omega|} \left\| \frac{f^{n+1} - f^n}{k} \right\|^2 \right)^{1/2} + \mathcal{O} \left(\frac{1}{N^{1/2}} + \frac{1}{T} \right) \\ &\leq \frac{F_N}{U_N} U_N^2 \frac{\left(\frac{1}{N} \sum_{n=0}^{N-1} \frac{1}{|\Omega|} \left\| \frac{f^{n+1} - f^n}{k} \right\|^2 \right)^{1/2}}{F_N} + \mathcal{O} \left(\frac{1}{N^{1/2}} + \frac{1}{T} \right). \end{aligned} \tag{3.3.6}$$

Our bounds for terms II. and III. are virtually unchanged from previous arguments. As before, we may rewrite the nonlinear term using that u^{n+1} is divergence free:

$$\begin{aligned} II. &= \frac{1}{N} \sum_{n=0}^{N-1} \frac{1}{|\Omega|} (u^{n+1} \otimes u^{n+1}, \nabla f^{n+1}) \\ &\leq \|\nabla f\|_{L^\infty(0,T;L^\infty(\Omega))} \frac{1}{N} \sum_{n=0}^{N-1} \frac{1}{|\Omega|} \|u^{n+1}\|^2 \\ &\leq \frac{F}{L} \frac{1}{N} \sum_{n=0}^{N-1} \frac{1}{|\Omega|} \|u^{n+1}\|^2 \\ &\leq \frac{F}{L} U_N^2 \\ &= \frac{F}{U_N} \frac{U_N^3}{L}. \end{aligned}$$

Addressing term III.:

$$\begin{aligned}
III. &= \left\langle \frac{\nu}{|\Omega|} (\nabla u, \nabla f) \right\rangle_N \\
&\leq \left\langle \frac{F_N \nu}{U_N |\Omega|} \|\nabla u\|^2 \right\rangle_N^{1/2} \left\langle \frac{U_N \nu}{F_N |\Omega|} \|\nabla f\|^2 \right\rangle_N^{1/2} \\
&\leq \frac{1}{2} \frac{F_N}{U_N} \left\langle \frac{\nu}{|\Omega|} \|\nabla u\|^2 \right\rangle_N + \frac{1}{2} \frac{U_N}{F_N} \nu \left\langle \frac{1}{|\Omega|} \|\nabla f\|^2 \right\rangle_N \\
&\leq \frac{1}{2} \frac{F_N}{U_N} \left(\left\langle \frac{\nu}{|\Omega|} \|\nabla u\|^2 \right\rangle_N + \frac{U_N^2}{F_N^2} \nu \left\langle \frac{1}{|\Omega|} \|\nabla f\|^2 \right\rangle_N \right).
\end{aligned}$$

Inserting this into our bounds on F_N , we have

$$\begin{aligned}
F_N^2 &\leq \mathcal{O} \left(\frac{1}{N^{1/2}} + \frac{1}{T} \right) + \frac{F_N U_N^2}{U_N} \frac{\left(\frac{1}{N} \sum_{n=0}^{N-1} \frac{1}{|\Omega|} \left\| \frac{f^{n+1} - f^n}{k} \right\|^2 \right)^{1/2}}{F_N} + \frac{F_N}{U_N} \frac{F}{F_N} \frac{U_N^3}{L} + \\
&\quad \frac{1}{2} \frac{F_N}{U_N} \left(\left\langle \frac{\nu}{|\Omega|} \|\nabla u\|^2 \right\rangle_N + \frac{U_N^2}{F_N^2} \nu \left\langle \frac{1}{|\Omega|} \|\nabla f\|^2 \right\rangle_N \right)
\end{aligned} \tag{3.3.7}$$

or

$$\begin{aligned}
F_N U_N &\leq \mathcal{O} \left(\frac{1}{N^{1/2}} + \frac{1}{T} \right) + U_N^2 \frac{\left(\frac{1}{N} \sum_{n=0}^{N-1} \frac{1}{|\Omega|} \left\| \frac{f^{n+1} - f^n}{k} \right\|^2 \right)^{1/2}}{F_N} + \frac{F}{F_N} \frac{U_N^3}{L} + \\
&\quad \frac{1}{2} \left(\left\langle \frac{\nu}{|\Omega|} \|\nabla u\|^2 \right\rangle_N + \frac{U_N^2}{F_N^2} \nu \left\langle \frac{1}{|\Omega|} \|\nabla f\|^2 \right\rangle_N \right).
\end{aligned} \tag{3.3.8}$$

We may combine with (3.3.3), take $T \rightarrow \infty$, and rearrange terms. Note both $\mathcal{O}(\frac{1}{T})$ and $\mathcal{O}(\frac{1}{N})$ terms will drop out, and $F_N \rightarrow F, U_N \rightarrow U$.

$$\begin{aligned}
\frac{1}{2} \langle \varepsilon_N + \varepsilon_0 \rangle_\infty &\leq U^2 \frac{\left(\lim_{N \rightarrow \infty} \frac{1}{N} \sum_{n=0}^{N-1} \frac{1}{|\Omega|} \left\| \frac{f^{n+1} - f^n}{k} \right\|^2 \right)^{1/2}}{F} \\
&\quad + \frac{U^3}{L} + \frac{1}{2} \frac{\nu U^2}{F^2} \left\langle \frac{1}{|\Omega|} \|\nabla f\|^2 \right\rangle_\infty.
\end{aligned}$$

Using definition of τ_f and L :

$$\langle \varepsilon_N + \varepsilon_0 \rangle_\infty \leq 2 \frac{U^2}{\tau_f} + \frac{U^3}{L} \left(2 + \frac{\nu}{LU} \right). \quad (3.3.9)$$

□

If f is constant, we recover the result from theorem 3.2.1. If f is highly oscillatory, τ_f will be very small, and we will expect the new term to dominate.

3.4 Treatment of Nonlinear Term

We have thus far proved results for a fully implicit time discretization scheme, however the fully implicit method is expensive computationally, as we must solve a nonlinear system every timestep. In practice, this requires an iterative method (e.g. Newton's method) with a good initial guess for u^{n+1} , (e.g. $u^{n+1} \approx u^n$ or $u^{n+1} \approx 2u^n - u^{n-1}$). As fluid flow simulations stress computational resources under the best circumstances, alternative treatment of the nonlinear term is usually implemented.

In the case of backward Euler, this means replacing $u^{n+1} \cdot \nabla u^{n+1}$ with $u^* \cdot \nabla u^{n+1}$ where $u^* \approx u^{n+1}$. A common choice is $u^* = u^n$. This choice is a first order approximation to u^{n+1} and will prevent achieving higher order results with the use of time filters [29]. However, it does not require additional storage or initialization. A second order approximation to u^{n+1} is $2u^n - u^{n-1}$. This choice allows for order of higher accuracy with filters, at the cost of additional storage.

For a general two step method, a second order approximation to u_β^{n+1} is needed to maintain the order of the scheme. In practice, we replace $u_\beta^{n+1} \cdot \nabla u_\beta^{n+1}$ with

$u_{\beta^*}^{n+1} \cdot \nabla u_{\beta}^{n+1}$, where

$$u_{\beta^*}^{n+1} = \left(\frac{1}{2} + \alpha_2\right) u^n + \left(\frac{1}{2} - \alpha_2\right) u^{n-1} = u_{\beta}^{n+1} - \beta_2 (u^{n+1} - 2u^n - u^{n-1})$$

This is a second order approximation as $(u^{n+1} - 2u^n - u^{n-1}) \approx k^2 u_{tt}(t^n)$, however we do not have any a priori bound on the second time derivative of the velocity.

We now consider the effect of this linearization on the long time energy dissipation rate. By skew-symmetry, we have $b(u^n, u^{n+1}, u^{n+1}) = 0$ and $b(u_{\beta^*}^{n+1}, u_{\beta}^{n+1}, u_{\beta}^{n+1}) = 0$. Indeed, the only change to our bound occurs in the nonlinear term when bounding F . We consider the first order and second order approximations in the nonlinear term, where the results differ.

Theorem 3.4.1. *Let u^0 be given. Let f be constant, divergence free, and vanish on the boundary. Let $u^{n+1} \in X = H_0^1(\Omega)$ be generated such that for all $v \in X$,*

$$\left(\frac{u^{n+1} - u^n}{k}, v\right) + b(u^n, u^{n+1}, v) + \nu (\nabla u^{n+1}, \nabla v) + (p^{n+1}, v) = (f, v)$$

and let $\varepsilon_0, \varepsilon_N, U_N, U$ be defined as in 3.2.1. Then, independent of k ,

$$\langle \varepsilon_N + \varepsilon_0 \rangle_{\infty} \leq \frac{U^3}{L} (2 + \mathcal{R}e^{-1}).$$

Proof. Take $v = u^{n+1}$. There is no difference in our initial bound, and thus it holds

$$\mathcal{O}\left(\frac{1}{T}\right) + \left\langle \frac{1}{2} \varepsilon_N + \varepsilon_0 \right\rangle_{\infty} \leq F U_N.$$

Bounding F , the only difference is to the nonlinear term. It holds that

$$b(u^n, u^{n+1}, f) = \int_{\Omega} \nabla \cdot (u^{n+1} \otimes u^n) f \, dx,$$

thus

$$\begin{aligned}
F^2 &= \frac{1}{|\Omega|} \frac{1}{N} \sum_{n=0}^{N-1} \left(\frac{u^{n+1} - u^n}{k}, f \right) + \frac{1}{N} \sum_{n=0}^{N-1} \frac{1}{|\Omega|} (u^{n+1} \otimes u^n, \nabla f) \\
&\quad + \frac{1}{|\Omega|} \frac{1}{N} \sum_{n=0}^{N-1} \frac{\nu}{|\Omega|} (\nabla u^{n+1}, \nabla f) \\
&= I. + II. + III.
\end{aligned} \tag{3.4.1}$$

From before,

$$I. = \mathcal{O} \left(\frac{1}{T} \right) \tag{3.4.2}$$

and

$$III. \leq \frac{1}{2} \frac{F}{U_N} \left(\langle \varepsilon_0 \rangle_N + \frac{UU_N^2}{L} \frac{\nu}{LU} \right). \tag{3.4.3}$$

Finally, a minor modification is made to our bound of the nonlinear term:

$$\begin{aligned}
II. &= \frac{1}{N} \sum_{n=0}^{N-1} \frac{1}{|\Omega|} (u^{n+1} \otimes u^n, \nabla f) \\
&\leq \|\nabla f\|_{L^\infty(\Omega)} \frac{1}{N} \sum_{n=0}^{N-1} \frac{1}{|\Omega|} \|u^n\| \|u^{n+1}\| \\
&\leq \frac{F}{L} \left(\frac{1}{N} \sum_{n=0}^{N-1} \frac{1}{|\Omega|} \|u^{n+1}\|^2 \right)^{1/2} \left(\frac{1}{N} \sum_{n=0}^{N-1} \frac{1}{|\Omega|} \|u^n\|^2 \right)^{1/2} \\
&\leq \frac{F}{L} U_N \left(\frac{1}{N} \sum_{n=0}^{N-1} \frac{1}{|\Omega|} \|u^{n+1}\|^2 + \frac{\|u^0\|^2 - \|u^N\|^2}{N} \right)^{1/2} \\
&= \frac{F}{U_N} \frac{U_N^2}{L} \left(U_N^2 + \mathcal{O} \left(\frac{1}{N} \right) \right)^{1/2}.
\end{aligned} \tag{3.4.4}$$

We note that this additional term will go to zero as either $k \rightarrow 0$ or $T \rightarrow \infty$.

Recombining our estimates, rearranging as before, and taking $T \rightarrow \infty$ yields

$$\langle \varepsilon_N + \varepsilon_0 \rangle_\infty \leq \frac{U^3}{L} \left(2 + \frac{\nu}{LU} \right). \tag{3.4.5}$$

□

The key here is that the infinite time average of u^n will equal the infinite time average of u^{n+1} independent of the size of the time step. This will not hold for any other case; $u_{\beta^*}^{n+1}$ approximates u_{β}^{n+1} , but this approximation depends on the time step size and the second time derivative, and the difference will not vanish in the infinite time average.

Definition 3.4.1. *We define the following large scale, finite time averaged velocities:*

$$U_N = \left(\frac{1}{N} \sum_{n=0}^{N-1} \frac{1}{|\Omega|} \|u_{\beta}^{n+1}\|^2 \right)^{1/2}$$

and

$$U_N^* = \left(\frac{1}{N} \sum_{n=0}^{N-1} \frac{1}{|\Omega|} \|u_{\beta^*}^{n+1}\|^2 \right)^{1/2}.$$

And their infinite time averaged counterparts

$$U = \limsup_{N \rightarrow \infty} U_N$$

and

$$U^* = \limsup_{N \rightarrow \infty} U_N^*.$$

Theorem 3.4.2. *Let f be divergence free, constant in time, and vanish on the boundary. Let initial conditions u^{-1} and u^0 be given, and let $u^{n+1} \in X = H_0^1(\Omega)$ be generated such that for all $v \in X$,*

$$\left(\frac{1}{k} \sum_{i=1}^2 \alpha_i u^{n-1+i}, v \right) + b(u_{\beta^*}^{n+1}, u_{\beta}^{n+1}, v) + \nu (\nabla u_{\beta}^{n+1}, \nabla v) + (p_{\beta}^{n+1}, v) = (f, v).$$

Let $\varepsilon_0, \varepsilon_N, U_N, U$ be defined as in theorem 3.2.3. Then, we have

$$\langle 2\varepsilon_N + \varepsilon_0 \rangle_{\infty} \leq 2 \frac{U^* U^2}{L} + \frac{U^3}{L} \mathcal{R}e^{-1}.$$

Proof. Again, we see that the only change is made to the nonlinear term when bounding F . As before, we have:

$$\frac{1}{2T|\Omega|} \|U^N\|_G^2 - \frac{1}{2T|\Omega|} \|U^0\|_G^2 + \langle \varepsilon_N + \varepsilon_0 \rangle_N \leq FU_N \quad (3.4.6)$$

and

$$\begin{aligned} F^2 &= \frac{1}{|\Omega|} \frac{1}{N} \sum_{n=0}^{N-1} \left(\frac{1}{k} \sum_{i=0}^2 \alpha_i u^{n-1+i}, f \right) + \frac{1}{N} \sum_{n=0}^{N-1} \frac{1}{|\Omega|} (u_\beta^{n+1} \otimes u_{\beta^*}^{n+1}, \nabla f) \\ &\quad + \frac{1}{|\Omega|} \frac{1}{N} \sum_{n=0}^{N-1} \frac{\nu}{|\Omega|} (\nabla u_\beta^{n+1}, \nabla f) \\ &= I. + II. + III. \end{aligned} \quad (3.4.7)$$

With no modifications

$$I. = \mathcal{O} \left(\frac{1}{T} \right)$$

and

$$III. \leq \frac{F}{U_N} \left(\frac{1}{2} \langle \varepsilon_0 \rangle_N + \frac{1}{2} \frac{\nu}{LU} \frac{UU_N^2}{L} \right).$$

Bounding term II:

$$\begin{aligned} II. &= \frac{1}{N} \sum_{n=0}^{N-1} \frac{1}{|\Omega|} (u_\beta^{n+1} \otimes u_{\beta^*}^{n+1}, \nabla f) \\ &\leq \|\nabla f\|_{L^\infty(\Omega)} \frac{1}{N} \sum_{n=0}^{N-1} \frac{1}{|\Omega|} \|u_{\beta^*}^{n+1}\| \|u_\beta^{n+1}\| \\ &\leq \frac{F}{L} \left(\frac{1}{N} \sum_{n=0}^{N-1} \frac{1}{|\Omega|} \|u_\beta^{n+1}\|^2 \right)^{1/2} \left(\frac{1}{N} \sum_{n=0}^{N-1} \frac{1}{|\Omega|} \|u_{\beta^*}^{n+1}\|^2 \right)^{1/2} \\ &\leq \frac{F}{L} U_N U_N^* \\ &\leq \frac{F}{U_N} \frac{U_N^2 U_N^*}{L}. \end{aligned} \quad (3.4.8)$$

Combining our estimates, rearranging, and taking $T \rightarrow \infty$ yields

$$\langle 2\varepsilon_N + \varepsilon_0 \rangle_\infty \leq 2 \frac{U^2 U^*}{L} + \frac{\nu}{LU} \frac{U^3}{L}.$$

□

This result is independent of the size of the timestep, k . However, $U \approx U^*$ only when the time step is sufficiently small. To consider the effect of the size of the timestep, we reconsider our bound of term II .

$$\begin{aligned} II. &= \frac{1}{N} \sum_{n=0}^{N-1} \frac{1}{|\Omega|} (u_\beta^{n+1} \otimes u_{\beta^*}^{n+1}, \nabla f) \\ &= \frac{1}{N} \sum_{n=0}^{N-1} \frac{1}{|\Omega|} (u_\beta^{n+1} \otimes u_\beta^{n+1}, \nabla f) + \frac{1}{N} \sum_{n=0}^{N-1} \frac{1}{|\Omega|} (u_\beta^{n+1} \otimes (u_{\beta^*}^{n+1} - u_\beta^{n+1}), \nabla f) \\ &\leq \|\nabla f\|_{L^\infty(\Omega)} \frac{1}{N} \sum_{n=0}^{N-1} \frac{1}{|\Omega|} \|u_\beta^{n+1}\|^2 + \|\nabla f\|_{L^\infty(\Omega)} \frac{1}{N} \sum_{n=0}^{N-1} \frac{1}{|\Omega|} \|u_{\beta^*}^{n+1} - u_\beta^{n+1}\| \|u_\beta^{n+1}\| \\ &\leq \frac{F}{L} U_N^2 + \frac{F}{L} \frac{1}{N} \sum_{n=0}^{N-1} \frac{1}{|\Omega|} \beta_2 \|u^{n+1} - 2u^n + u^{n-1}\| \|u_\beta^{n+1}\|^2 \\ &\leq \frac{F}{U_N} \left(\frac{U_N^3}{L} + \beta_2 \frac{U_N^2}{L} \frac{1}{N} \sum_{n=0}^{N-1} \frac{1}{|\Omega|} \|u^{n+1} - 2u^n + u^{n-1}\|^2 \right). \end{aligned}$$

Taking N to infinity and using this in our estimate, we have

$$\langle 2\varepsilon_N + \varepsilon_0 \rangle_\infty \leq 2 \frac{U^3}{L} + \frac{\nu}{LU} \frac{U^3}{L} + \beta_2 k^2 \frac{U^2}{L} \frac{1}{N} \sum_{n=0}^{N-1} \frac{1}{|\Omega|} \left\| \frac{u^{n+1} - 2u^n + u^{n-1}}{k^2} \right\|^2. \quad (3.4.9)$$

We do not have any a priori bound on the last term, and it may grow as U increases, leading to overdissipation as the Reynolds number increases.

Remark 3.4.1. *When analyzing time discrete eddy viscosity turbulence models, the eddy viscosity is separate from the timestepping scheme. Thus, if the treatment of the nonlinear term leads to overdissipation in the NSE, it will have the same effect with eddy viscosity turbulence models.*

3.5 Numerical Experiments

In this section, we investigate numerically the effect of the time discretization scheme on the long time energy dissipation rate. Numerical tests were performed using the FEniCS software suite [54]

3.5.1 Problem Setting

The problem setting is the same used in [55]. We consider flow between offset cylinders in three dimensions. Let $r_1 = 1, r_2 = 1/10, c_1 = 1, c_2 = 0$, and $h = 1$. The domain is given by

$$\Omega = \{(x, y, z) : x^2 + y^2 \leq r_1^2, (x - c_1)^2 + (y - c_2)^2 \geq r_2^2, \text{ and } 0 \leq z \leq h\}.$$

The flow was initialized at rest, and driven by a counterclockwise rotational body

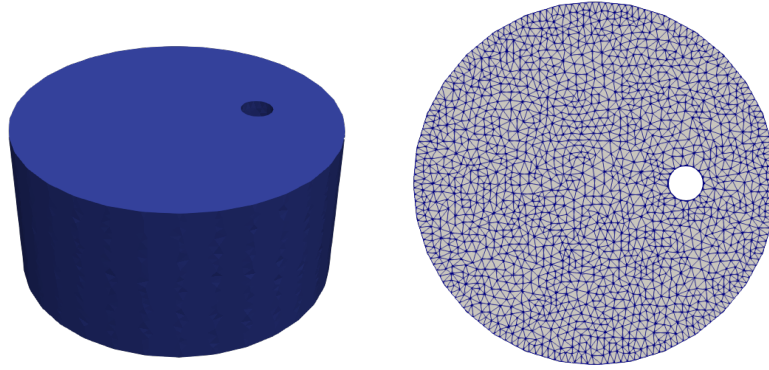


Figure 1: We consider flow between offset cylinders. The domain and a top view of the mesh are pictured.

force

$$f(x, y, z, t) = \min\{t, 1\} (-4y(1 - x^2 - y^2), 4x(1 - x^2 - y^2), 0).$$

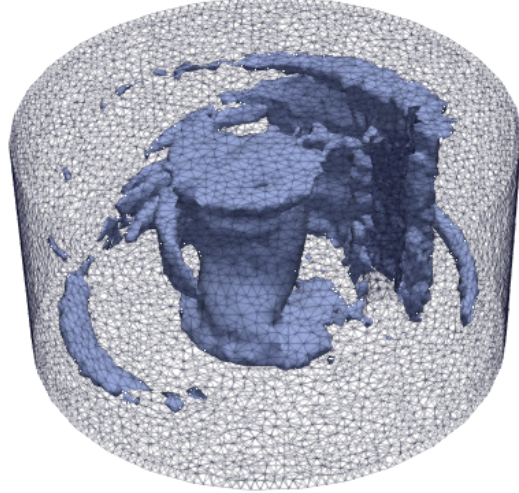


Figure 2: Q-criterion for $\nu = \frac{1}{250}$ using LIBE.

No slip boundary conditions were imposed. To vary the Reynolds number, the viscosity was varied. U is a calculated quantity, and L is fixed and equal to $|\Omega|^{1/3} = (.99\pi)^{1/3} \approx 1.4597$.

The $P^2 - P^1$ Taylor-Hood element pair was used for spacial discretization. Fully resolving the Taylor microscale was shown in [50] to be necessary for the correct scaling of the energy dissipation rate for fully developed turbulent flow.

Definition 3.5.1. *We define the Taylor microscale as*

$$\lambda_T(u) := \left(\frac{\frac{1}{15} \langle \|\nabla u\|^2 \rangle_\infty}{\langle \|u\|^2 \rangle_\infty} \right)^{-1/2}.$$

To avoid spacial discretization affecting the energy dissipation rate, we ensure that $\lambda_T(u^h) \lesssim \frac{\sqrt{30}}{2} \mathcal{R}e^{-1/2} L$ is $\mathcal{O}(1)$. In practice, we refined the mesh to ensure that

$$\lambda_T(u^h) < 4 \frac{\sqrt{30}}{2} \mathcal{R}e^{-1/2} L.$$

To ensure that calculations were efficient, the degrees of freedom were varied with the Reynolds number. Preliminary tests to determine if the mesh was sufficiently fine confirmed that mesh effects had a great effect on the total energy dissipation rate, and that the mesh width affects both ε_0 and ε_N .

3.5.2 Total Dissipation versus Reynolds Number

Here, we test two different time discretization methods. We vary the Reynolds number to test the effect of numerical dissipation on the total dissipation rate, to examine if a $\frac{U^3}{L}$ bound is seen uniformly in $\mathcal{R}e$.

3.5.2.1 Backward Euler

We tested the linearly implicit backward Euler time discretization with $u^* = u^n$. Theorem 3.4.1 suggests that the first order method with first order linearization of the convective term is the only not fully implicit method in which the time step size will not affect the total dissipation. We selected $k = .05$, which is sufficiently large that numerical dissipation is not small compared to viscous dissipation when the flow is not steady. We note that when the flow is steady, the numerical dissipation, which is a discrete approximation to the first derivative, vanishes.

The viscosity ν was varied from $\nu = \frac{1}{60}$ to $\nu = \frac{1}{1000}$, with corresponding Reynolds numbers $\mathcal{R}e \approx 100$ to $\mathcal{R}e \approx 4565$. The flow evolved from $T = 0$ to $T = 20$, and reached an approximate steady state by $T = 10$. The infinite time average of relevant quantities was approximated by the finite average between $T = 10$ and $T = 20$.

Figure 3 confirms that with the choice of $k = .05$, the numerical dissipation is not small compared to the viscous dissipation. Figure 4 shows the time evolution of the kinetic energy for the different values of ν tested.

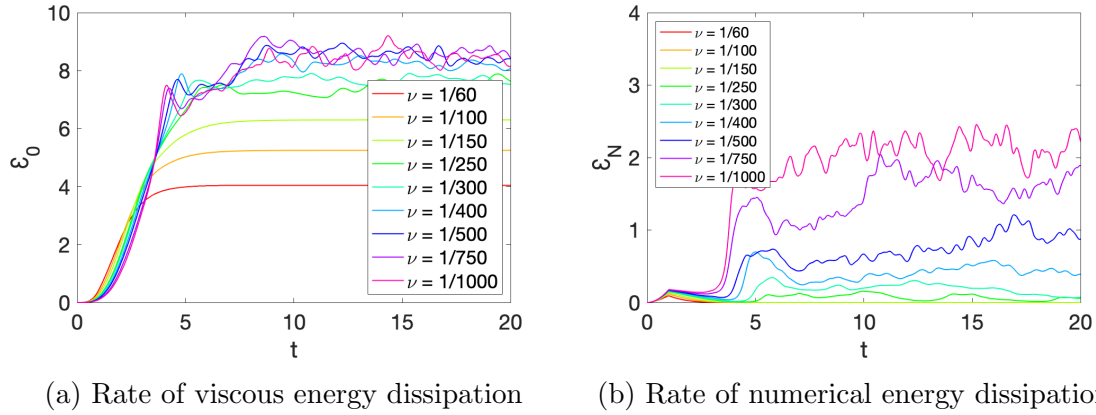


Figure 3: Using LIBE with $k = .05$, at high Reynolds numbers, the numerical dissipation rate is similar in size to the rate of viscous dissipation.

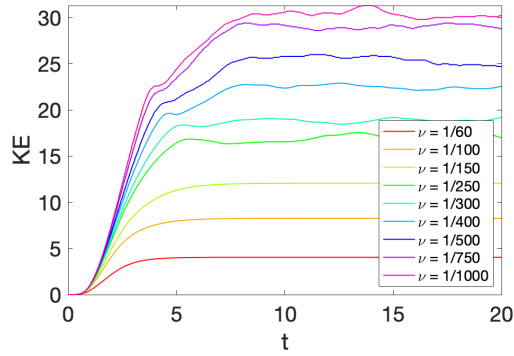


Figure 4: Using LIBE, the kinetic energy increases as ν decreases despite increased numerical dissipation.

Figure 5 shows the time averaged total dissipation versus the Reynolds number, fit to $y = a + b\mathcal{R}e^c$ with Matlab's nonlinear least squares. The initial condition given was $(a, b, c) = (2, 1, -1)$ as suggested by the analysis. Though constants are affected by the specific definition of U and L , we see the expected power of $-1.1001 \approx$

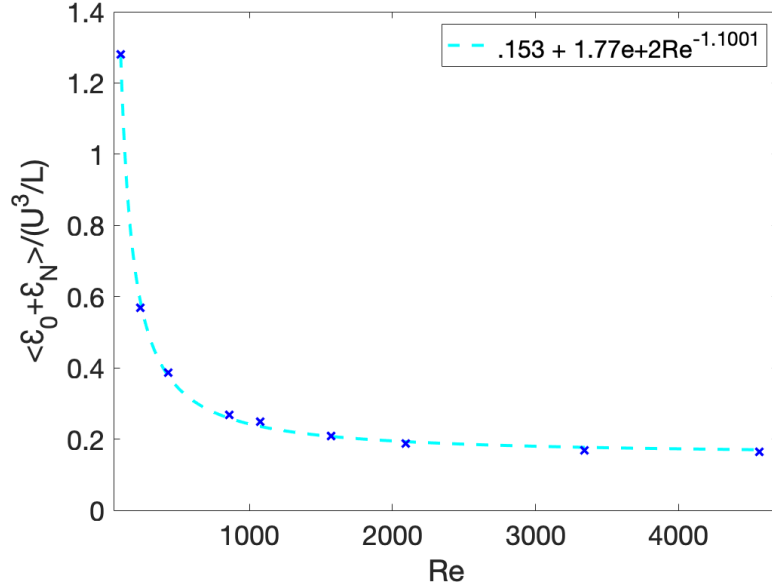


Figure 5: Using LIBE with $k = .05$, we see correct scaling of the average total dissipation rate despite the large timestep.

–1. Despite the large time step and the significant impact of numerical dissipation, correct scaling was seen.

3.5.2.2 Second Order A-stable Method

We repeated the test with the second order Backward Differentiation Formula (BDF2), an A -stable method with $\alpha_2 = \frac{3}{2}$ and $\beta_2 = 1$, and the corresponding second order approximation to u_β^{n+1} :

$$\left(\frac{3u^{n+1} - 4u^n + u^{n-1}}{2k}, v \right) + \nu (\nabla u^{n+1}, \nabla v) + b^*(2u^n - u^{n-1}, u^{n+1}, v) - (p^{n+1}, \nabla \cdot v) = (f, v). \quad (3.5.1)$$

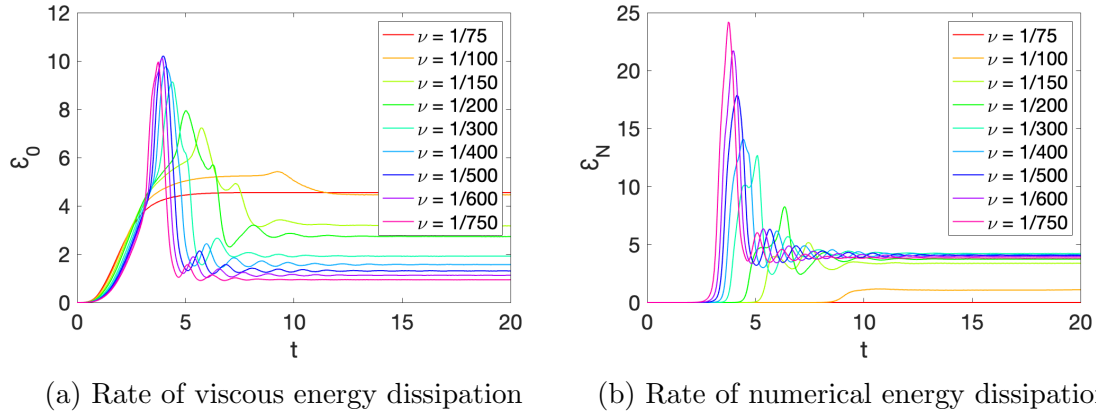


Figure 6: Using BDF2 with $k = .05$, at high Reynolds numbers, the numerical dissipation rate is much larger than the viscous dissipation rate.

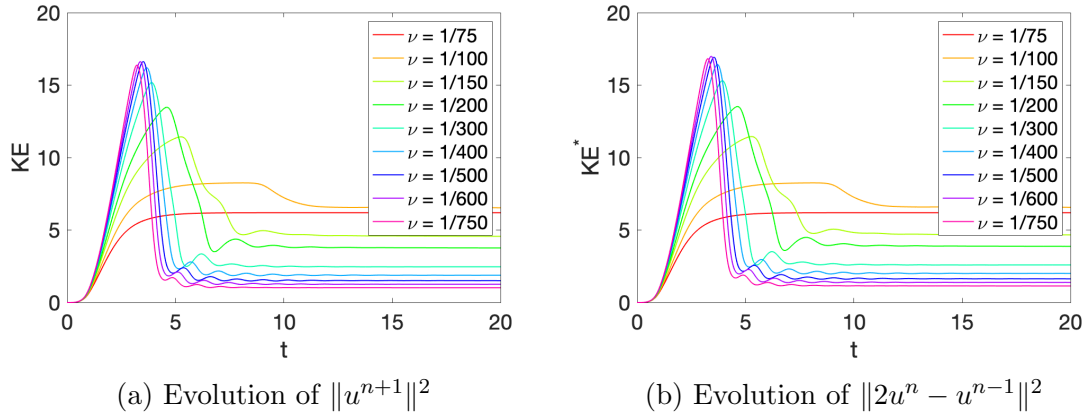


Figure 7: Using BDF2 with $k = .05$, $U \approx U^*$. Large numerical dissipation leads to decreased kinetic energy as ν decreases.

Again, $k = .05$ was the timestep size. A benefit to using higher order methods is that we expect to be able to take larger timesteps while maintaining accuracy. However, (3.4.9) indicates that too large a timestep may lead to overdissipation. Figure 6 shows that indeed, the numerical dissipation is much larger than the viscous dissipation. Though figure 7 shows that U and U^* are similar, figure 8 shows that

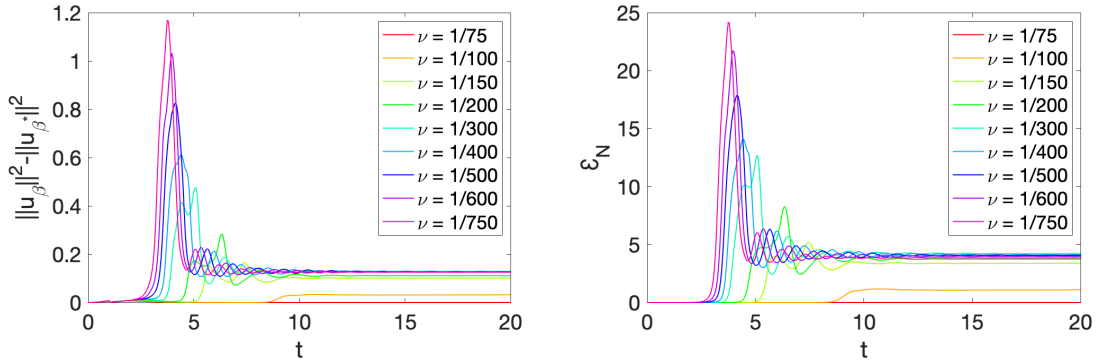


Figure 8: Numerical Dissipation in BDF2 is proportional to $(\|u^{n+1}\|^2 - \|2u^n - u^{n-1}\|^2)$.

when we have a large difference between u_{β}^{n+1} and $u_{\beta^*}^{n+1}$, the numerical dissipation is large.

Further, this spike in numerical dissipation pushes the flow to a lower Reynolds number state, i.e., U is smaller than expected. The numerical dissipation is large enough that we see overdissipation not predicted in 3.4.2.

3.5.3 Higher Order Extrapolation in Nonlinear Term

The results in section 3.5.2.2 were somewhat surprising. Numerical dissipation in the second order method was much higher than the numerical dissipation in the backward Euler method, to the point where the flow was pushed to a much lower Reynolds number compared to the backward Euler method. For example, with $\nu = \frac{1}{500}$, we saw $\mathcal{Re} \approx 2000$ with the LIBE time discretization, and $\mathcal{Re} \approx 500$ when using BDF2. This effect was also seen for flows near steady state. Table 1 shows BDF2 pushes flow to a much lower Reynolds number than LIBE.

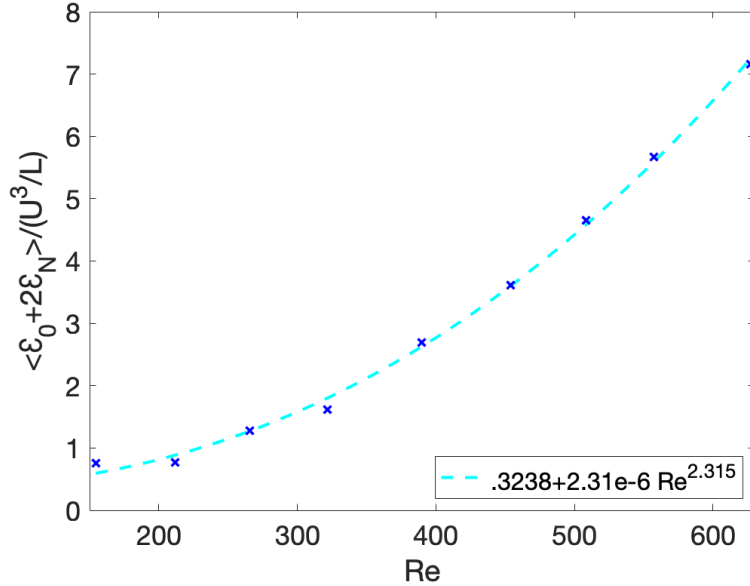


Figure 9: Using BDF2 with $k = .05$, we do not see the correct scaling of the average total dissipation rate due to the large timestep.

Analysis suggests that this must be caused by the treatment of the nonlinear term, and the extra term on the upper bound of our energy dissipation that comes from a second order approximation to u_β^{n+1} . To investigate this, we fix $\nu = \frac{1}{150}$ and $\nu = \frac{1}{250}$, and vary the timestep k . We also test using a second order approximation to u^{n+1} in the backward Euler scheme, which will be referred to as LIBE2:

$$\left(\frac{u^{n+1} - u^n}{k}, v \right) + b^*(2u^n - u^{n-1}, u^{n+1}, v) + \nu (\nabla u^{n+1}, \nabla v) + (p^{n+1}, \nabla \cdot v) = (f, v).$$

We observed similar results for LIBE2 and BDF2 (see Figure 10, Figure ??). For large time steps, we see that the numerical dissipation is large, correspondingly, the Reynolds number is low as the flow was pushed to steady state by the increased

ν	$\mathcal{R}e_{BDF2}$	$\mathcal{R}e_{LIBE}$
$\frac{1}{100}$	221.9	237.9
$\frac{1}{150}$	265.8	431.2
$\frac{1}{200}$	321.7	857.6
$\frac{1}{300}$	389.5	1077
$\frac{1}{400}$	454.1	1571
$\frac{1}{500}$	508.1	2093
$\frac{1}{750}$	626.7	3341

Table 1: Large numerical dissipation in BDF2 drives the flow to a lower Reynolds number state. The effect is amplified for small values of ν .

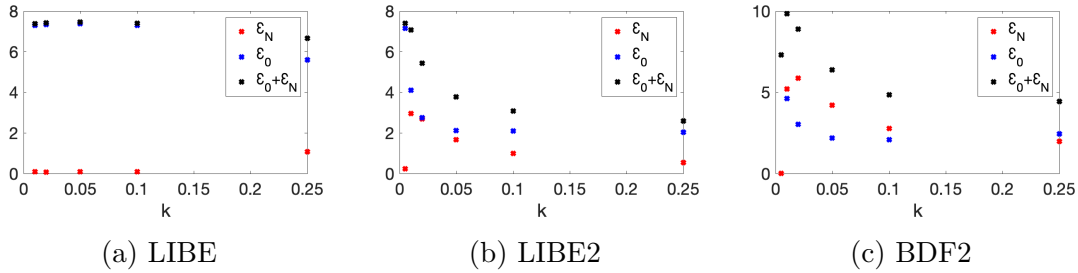


Figure 10: Average Dissipation vs k , $\nu = \frac{1}{250}$. Total dissipation is near constant for LIBE, in contrast to LIBE2 and BE.

dissipation. This appears to confirm that the second order approximation $u^{n+1} \approx 2u^n - u^{n-1}$ leads to overdissipation with large time steps. Though the numerical dissipation decreased with the timestep, even for the relatively low Reynolds number flows tested, the dissipation was still larger with LIBE2 and BDF2 than when using LIBE.

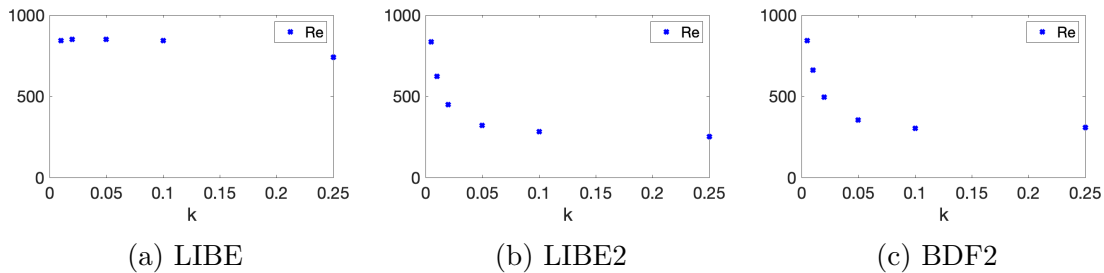


Figure 11: Re versus k , $\nu = \frac{1}{250}$. The Reynolds number is near constant for LIBE, even for large timesteps. A small timestep is required for LIBE2 and BDF2 to see the correct Reynolds number.

3.6 Conclusions

We showed that over dissipation is not expected for body force driven flow for any one or two step fully implicit one leg method, or for the LIBE method. We demonstrated numerically that we may see overdissipation in one or two step methods when higher order approximations are made in the linearization of the convective term. This preliminary work suggests multiple avenues that should be explored when analyzing energy dissipation rates, and highlights that the time discretization may have as large an effect or greater than the spacial discretization on the energy dissipation rate, with the area of greatest effect being the treatment of the nonlinear convective term.

This is particularly of interest when we consider turbulence modeling. Direct numerical simulations, which fully resolve all relevant time and length scales in the Navier-Stokes equations are unlikely to introduce numerical dissipation due to the small time step. However, flow averages are smoother, and we may expect to take

larger timesteps when modeling them. We saw numerically that overdissipation was present even at relatively low Reynolds number flows when using *BDF2*. Thus, it is very possible that a poor choice of timestepping scheme or timestep size may contribute to overdissipation in body force driven turbulence.

4.0 A New Turbulence Length Scale

4.1 Introduction

Predicting turbulent flows in practical settings means solving models intended to predict averages of solutions of the Navier-Stokes (NS) equations. Among a wide variety of approaches, summarized in Wilcox [80], eddy viscosity URANS (unsteady Reynolds Averaged NS) models are used in many applications. Many are based on the 1-equation model of Prandtl [67] and Kolmogorov [41]. This was derived in 3.1 and is given by

$$\begin{aligned} v_t + v \cdot \nabla v - \nabla \cdot ([2\nu + \nu_T] \nabla^s v) + \nabla p &= f(x, y, z), \\ \nabla \cdot v &= 0, \text{ and } \nu_T = \mu \ell \sqrt{k}, \\ k_t + v \cdot \nabla k - \nabla \cdot ([\nu + \nu_T] \nabla k) + \frac{1}{\ell} k \sqrt{k} &= \nu_T |\nabla^s v|^2. \end{aligned} \quad (4.1.1)$$

Following for example [56] and [80] p.37 eq. (3.9), v approximates a finite time window average of the Navier-Stokes velocity u

$$v(x, y, z, t) \simeq \bar{u}(x, y, z, t) = \frac{1}{\tau} \int_{t-\tau}^t u(x, y, z, t') dt'. \quad (4.1.2)$$

The fluctuation is $u' = u - \bar{u}$. Its associated turbulent kinetic energy, approximated by the k -equation solution, is $k_{true} = \frac{1}{2} \overline{|u - \bar{u}|^2}$. In (4.1.1) ν is the kinematic viscosity, p is a pressure, initial and boundary conditions for v and k will be specified, f is the body force (here $f = 0$), $\nabla^s v$ is the symmetric part of ∇v and ν_T is the eddy viscosity. Here, we will consider the model with the included $\nu \Delta k$ term, as it is commonly used

in practical numerical tests. Further consideration to inclusion versus exclusion of this term is given in chapter 5.

The Kolmogorov-Prandtl relation is $\nu_T = \mu\ell\sqrt{k}$ where μ is a calibration constant, typically 0.2 to 0.6, and often 0.55, [14] p. 114,[65]. The turbulence length-scale $\ell = \ell(x, y, z, t)$ is specified to complete the model. In current practice, ℓ varies from model to model, subregion to subregion (requiring their locations, [72]) and must be specified by the user; see [80], [70] for many examples.

This lack of a simple, effective, and universal specification of ℓ is one disadvantage of 1–equation models like (4.1.1). Another disadvantage, shared by many eddy viscosity models, is that model dissipation often exceeds energy input and leads to lower Reynolds number solutions.

Herein we analyze a specification of ℓ with greater universality and improved model dissipation

$$\ell = \min \left\{ \sqrt{2k^{1/2}\tau}, 0.41d\sqrt{\frac{d}{L}} \right\}, \text{ where} \quad (4.1.3)$$

$d =$ wall distance, $\tau =$ averaging window, $L =$ global length scale.

The main result herein, theorem 4.4.1 is that with (4.1.3) for shear flows, this over dissipation does not happen: the model’s energy dissipation rate is consistent with its energy input rate. The intent of the minimum in (4.1.3) is to select $\ell = \sqrt{2k^{1/2}\tau}$ in the flow’s interior and the new value $\ell = 0.41d\sqrt{\frac{d}{L}}$ near walls. Other realizations of this intent are possible, e.g., (4.1.5). The question of which realization of this intent best models the intermediate region is open and cannot be resolved by the volume averaged analysis herein. The traditional value of the Von Karman constant, 0.41, is retained in (4.1.3). Prandtl [66] described ℓ as “... *the diameter of the masses of fluid moving as a whole in each individual case*”. This diameter is constrained

by nearby walls leading to the classical $\ell = 0.41d$ and here $0.41d\sqrt{\frac{d}{L}}$. Prandtl also mentioned a second possibility, ”...or again, as the distance traversed by a mass of this type before it becomes blended in with neighboring masses...” This remark can be interpreted as $\ell = |u'(x, t)|\tau$, i.e., the *distance a fluctuating eddy travels in one time unit*. As $|u'| \simeq \sqrt{2}k^{1/2}$, away from walls we specify the kinematic relation

$$\ell = \sqrt{2}k(\cdot)^{1/2}\tau. \quad (4.1.4)$$

4.1.1 Justification of New Length Scale

The (dimensionally consistent) near wall $\ell = 0.41d\sqrt{\frac{d}{L}}$ is a deviation from accepted practice, so justification is necessary. Expansions in the wall normal distance following p. 283 in [65] indicate that the true turbulent kinetic energy $k_{true} = \frac{1}{2}\overline{|u - \bar{u}|^2} \rightarrow 0$ like $\mathcal{O}(d^2)$ at walls. This rate implies that k_{true} satisfies

$$k_{true} = 0 \text{ and } \nabla k_{true} \cdot n = 0 \text{ at the wall.}$$

The eddy viscosity should have a similar near wall behavior since, modulo pressure terms, $\mu\ell\sqrt{k}\nabla^s v \simeq u'u' \rightarrow 0$ at walls like $\mathcal{O}(d^2)$. If k_{true} replaces k in ν_T , then $\mu\ell\sqrt{k_{true}}\nabla^s v = \mathcal{O}(d^2)$ near walls with $\ell = 0.41d$. However, the solution to the k -equation satisfies only one boundary condition, $k = 0$ at the wall. Since the model includes the term $-\nu\Delta k$, the solution to the k equation (intended to model k_{true}) should have

$$k = 0 \text{ at the wall, and } k(d) = \mathcal{O}(d) \text{ as the wall is approached.}$$

This (incorrectly) implies $\mu\ell\sqrt{k}\nabla^s v \rightarrow 0$ at walls like $\mathcal{O}(d^{+1.5})$ when $\ell = 0.41d$. This is one reason for evaluations such as Pope [65] p. 434 Section 11.7.2 that ” ... *the*

specification $\ell = 0.41y$ is too large in the near wall region...” as well as ad hoc addition of van Driest damping. The modification $\ell = 0.41d\sqrt{\frac{d}{L}}$ in (4.1.3) ensures $\nu_T = \mathcal{O}(d^2)$ correctly in the model at points where $\nabla^s v$ is neither zero nor infinity.

The question arises of why not simply specify $\ell = \sqrt{2}k(\cdot)^{1/2}\tau$ as in [47]. The positive results in [47] were for turbulence induced by a body force with $f(x) = 0$ on $\partial\Omega$ which excludes shear flows. The physical difference in the settings (summarizing the introduction of Phillips [63]) is that in shear flows the near wall region produces small scales which dominate k_{true} , while when shear flows are excluded in [47], small scales are produced only through the nonlinearity.

4.1.2 Related work

The energy dissipation rate is a fundamental statistic of turbulence, e.g., [65], [77]. Its balance with energy input rates, $\langle \varepsilon \rangle = \mathcal{O}(\frac{U^3}{L})$, is observed in physical experiments [77]. In 1992, Doering and Constantin [21] established a direct link between phenomenology and NSE predicted energy dissipation through upper bounds consistent with the $\mathcal{O}(\frac{U^3}{L})$ rate. This work builds on [4], [32] and has developed in many important directions, e.g., [22], [32], [77], [78], [39], [79]. Remarkably, an $\mathcal{O}(\frac{U^3}{L})$ lower bound has recently been proven in [10] for stochastically forced shear flow.

Model over-dissipation, producing a lower $\mathcal{R}e$ flow, is due to the action of turbulent viscosity terms on small scales generated by breakdown of large scales through the nonlinearity or in the boundary layer. $\langle \varepsilon \rangle$ has been analyzed for some simpler models, e.g., [43], [44] (showing a dramatic difference between shear and no shear cases), and [61]. The kinematic length scale $\ell = \sqrt{2}k^{1/2}\tau$ occurred naturally in an ensemble algorithm in [JL14b] and was highly developed by Teixeira and Cheinet

[75] and [76] (see equation (7) on p. 2699), with near-wall transition to $\ell = 0.41d$ by

$$\ell = \theta(0.41d) + (1 - \theta) \left(\sqrt{2}k^{1/2}\tau \right), \text{ with } \theta = e^{-d/100}. \quad (4.1.5)$$

The global specification $\ell = \sqrt{2}k^{1/2}\tau$ was proven in [47] not to over-dissipate with shear excluded (and boundary layers negligible). This work leads to the problem considered herein to analyze shear/boundary layer induced model dissipation.

Since τ in (4.1.2), (4.1.3) is user supplied, it can be determined by the time scales required in an application or related to a time step. The latter blurs the line between URANS and time filtered large eddy simulation, [68], as noted in the abstract of [24] ”...most of the unsteady approaches ... can be regarded as a temporally filtered approach.” The time scale τ can also be regarded as a fundamental time scale of turbulence such as $\tau = k/\varepsilon$, e.g., [7]. Other natural choices of τ include $\tau \simeq \Delta/U$, $\Delta =$ an estimate of layer-width [75] and $\tau = 0.76/N$, $N =$ a selected-frequency, [15].

4.2 Shear Flow

We analyze energy dissipation caused by the boundary layer for shear flow with zero body force, building on analysis in the pioneering paper [21] and early work of Hopf [31]. Let the flow domain $\Omega = (0, L)^3$ and select ℓ -periodic boundary conditions in x, y and no-slip at $z = 0, z = L$. The wall is fixed at $z = 0$ and the wall at $z = L$

slides with velocity $(U, 0, 0)$:

<i>Boundary</i>	<i>Conditions :</i>	
moving top lid:	$v(x, y, L, t) = (U, 0, 0)$	
fixed bottom wall:	$v(x, y, 0, t) = 0$	(4.2.1)
periodic side walls:	$v(x + L, y, z, t) = v(x, y, z, t),$ $v(x, y + L, z, t) = v(x, y, z, t).$	

On this domain the wall normal distance is $d = \min\{z, L - z\}$. Since time averages of the velocity satisfy the same shear boundary conditions as the NSE solution, the correct boundary condition for $k(x, y, z, t)$ is

$$k(x, y, 0, t) = k(x, y, L, t) = 0 \text{ and } L - \text{periodicity in } x, y.$$

Since k has homogeneous boundary conditions, non-zero initial conditions must be specified; otherwise, if $k(x, y, z, 0) = 0$, then $k(x, y, z, t) \equiv 0$ thereafter.

4.2.1 Notation and preliminaries

Definition 4.2.1. *The finite and long time averages of a function $\phi(t)$ are*

$$\langle \phi \rangle_T = \frac{1}{T} \int_0^T \phi(t) dt \text{ and } \langle \phi \rangle_\infty = \limsup_{T \rightarrow \infty} \langle \phi \rangle_T.$$

These satisfy $\langle \langle \phi \rangle_\infty \rangle_\infty = \langle \phi \rangle_\infty$ and

$$\langle \phi \psi \rangle_T \leq \langle |\phi|^2 \rangle_T^{1/2} \langle |\psi|^2 \rangle_T^{1/2}, \quad \langle \phi \psi \rangle_\infty \leq \langle |\phi|^2 \rangle_\infty^{1/2} \langle |\psi|^2 \rangle_\infty^{1/2}. \quad (4.2.2)$$

A weak solution of the model momentum equation for shear flow problem satisfies the initial condition and

$$(v_t, w) + ([2\nu + \nu_T] \nabla^s v, \nabla^s w) + (v \cdot \nabla v, w) = 0 \quad (4.2.3)$$

for all test functions w , with $\nabla \cdot w = 0$, L -periodic in x and y and $w(x, y, 0, t) = 0, w(x, y, L, t) = 0$. If ϕ is a divergence free function extending the shear boundary conditions (4.2.1) into Ω , formally taking the inner product with $w = v - \phi$ and expanding gives

$$\begin{aligned} & \frac{1}{2} \frac{d}{dt} \|v\|^2 + \int_{\Omega} [2\nu + \nu_T] |\nabla^s v|^2 dx = \\ & = (v_t, \phi) + \int_{\Omega} [2\nu + \nu_T] \nabla^s v : \nabla^s \phi dx + (v \cdot \nabla v, \phi). \end{aligned}$$

Definition 4.2.2. *The total energy dissipation rate (per unit volume) is*

$$\varepsilon(v) = \frac{1}{|\Omega|} \int_{\Omega} [2\nu + \nu_T] |\nabla^s v(x, t)|^2 dx.$$

While a new ℓ gives a new model, existence of weak solutions to models of this type is treated comprehensively in [8] and [3]. Herein, we assume that a weak solution of the model (4.1.1), (4.1.3) with shear boundary conditions (4.2.1) exists, $k \geq 0$ and solutions satisfy the energy inequality

$$\begin{aligned} & \frac{1}{2} \frac{d}{dt} \|v\|^2 + \int_{\Omega} [2\nu + \nu_T] |\nabla^s v|^2 dx \leq \tag{4.2.4} \\ & (v_t, \phi) + \int_{\Omega} [2\nu + \nu_T] \nabla^s v : \nabla^s \phi dx + (v \cdot \nabla v, \phi). \end{aligned}$$

Using the energy inequality the appendix gives a proof of the following bounds.

Proposition 4.2.1. *Consider the 1-equation model (4.1.1), (4.1.3) with shear boundary conditions (4.2.1). The following are uniformly bounded in T :*

$$\begin{aligned} & \|v(T)\|^2, \int_{\Omega} k(T) dx, \int_{\Omega} \nu_T(\cdot, T) dx, \\ & \left\langle \frac{1}{L^3} \int_{\Omega} |\nabla^s v|^2 dx \right\rangle_T, \left\langle \frac{1}{L^3} \int_{\Omega} \frac{1}{l} k \sqrt{k} dx \right\rangle_T, \left\langle \frac{1}{L^3} \int_{\Omega} [2\nu + \nu_T] |\nabla^s v|^2 dx \right\rangle_T. \end{aligned}$$

Proof. In this proof of Proposition 4.2.1, C will denote any quantity uniformly bounded in time. The energy inequality and equality for v and k state

$$\begin{aligned} & \frac{1}{2} \frac{d}{dt} \|v\|^2 + \int_{\Omega} [2\nu + \nu_T] |\nabla^s v|^2 dx \leq \\ & (v_t, \phi) + \int_{\Omega} [2\nu + \nu_T] \nabla^s v : \nabla^s \phi dx + (v \cdot \nabla v, \phi), \\ & \text{and } \int_{\Omega} k_t dx + \int_{\Omega} \frac{1}{\ell} k \sqrt{k} dx = \int_{\Omega} \nu_T |\nabla^s v|^2 dx. \end{aligned}$$

Pick $\theta, 0 < \theta < 1$. Multiply the second equation by θ and add to the first. Using $\frac{d}{dt} \|\phi\|^2 = 0$ the sum becomes

$$\begin{aligned} & \frac{d}{dt} \left(\frac{1}{2} \|v\|^2 - (v, \phi) + \frac{1}{2} \|\phi\|^2 + \theta \int_{\Omega} k dx \right) + \\ & \int_{\Omega} [2\nu + (1 - \theta)\nu_T] |\nabla^s v|^2 + \theta \frac{1}{\ell} k \sqrt{k} dx \leq \tag{4.2.5} \\ & \int_{\Omega} [2\nu + \nu_T] \nabla^s v : \nabla^s \phi dx + (v \cdot \nabla v, \phi). \end{aligned}$$

For this proof choose $\beta = \frac{1}{8} \mathcal{R}e^{-1}$ (rather than $\beta = \frac{1}{8} \mathcal{R}e_{eff}^{-1}$). Consider now the three terms on the above RHS. For the last, nonlinear term, the estimate proven below is

$$(v \cdot \nabla v, \phi) \leq C + \beta \mathcal{R}e \int_{S_{\beta}} 2\nu |\nabla^s v|^2 dx \leq C + \frac{1}{8} \int_{\Omega} 2\nu |\nabla^s v|^2 dx.$$

The second term is subsumed in the LHS of 4.2.5. The first term on the RHS is bounded by the Cauchy-Schwarz-Young inequality in a standard way as

$$\int_{\Omega} 2\nu \nabla^s v : \nabla^s \phi dx \leq C + \frac{1}{8} \int_{\Omega} 2\nu |\nabla^s v|^2 dx$$

with the second term on the RHS again subsumed. The remaining term on the RHS involves ν_T . As a first step we again apply the Cauchy-Schwarz-Young inequality in a standard way and then use the direct calculation of $|\nabla^s \phi|^2$ to give

$$\begin{aligned} \int_{\Omega} \nu_T \nabla^s v \quad : \quad \nabla^s \phi dx &\leq \frac{1-\theta}{2} \int_{\Omega} \nu_T |\nabla^s v|^2 dx + \frac{1}{2(1-\theta)} \int_{\Omega} \nu_T |\nabla^s \phi|^2 dx \\ &\leq \frac{1-\theta}{2} \int_{\Omega} \nu_T |\nabla^s v|^2 dx + \frac{\mu}{2(1-\theta)} \left(\frac{U}{\beta L} \right)^2 \int_{s_{\beta}} l \sqrt{k} dx. \end{aligned}$$

Collecting these terms gives

$$\begin{aligned} \frac{d}{dt} \left(\frac{1}{2} \|v - \phi\|^2 + \theta \int_{\Omega} k dx \right) + \int_{\Omega} \left[\frac{3}{2} \nu + \frac{1-\theta}{2} \nu_T \right] |\nabla^s v|^2 + \theta \frac{1}{\ell} k \sqrt{k} dx &\leq \\ \leq C + \frac{\mu}{2(1-\theta)} \left(\frac{U}{\beta L} \right)^2 \int_{s_{\beta}} l \sqrt{k} dx. \end{aligned}$$

For the last term we apply Hölder's inequality with exponents 3 and 3/2 as follows

$$\begin{aligned} \int_{s_{\beta}} \ell \sqrt{k} dx &= \int_{s_{\beta}} \ell^{4/3} \cdot \ell^{-1/3} \sqrt{k} dx \leq \left(\int_{s_{\beta}} \ell^{-1} k^{3/2} dx \right)^{1/3} \left(\int_{s_{\beta}} (\ell^{4/3})^{3/2} dx \right)^{2/3} \\ \frac{1}{2(1-\theta)} \left(\frac{U}{\beta L} \right)^2 \int_{s_{\beta}} \mu \ell \sqrt{k} dx &\leq \frac{1}{3} \int_{\Omega} \frac{1}{\ell} k \sqrt{k} dx + \frac{2}{3} \left[\frac{1}{2(1-\theta)} \left(\frac{U}{\beta L} \right)^2 \right]^{3/2} \int_{s_{\beta}} \ell^2 dx. \end{aligned}$$

We thus have

$$\begin{aligned} &\frac{d}{dt} \left(\frac{1}{2} \|v - \phi\|^2 + \theta \int_{\Omega} k dx \right) + \\ &+ \int_{\Omega} \left[\frac{3}{2} \nu + \frac{1-\theta}{2} \nu_T \right] |\nabla^s v|^2 + \frac{\theta}{2} \frac{1}{\ell} k \sqrt{k} dx \leq C + C^* \int_{s_{\beta}} \ell^2 dx, \end{aligned} \quad (4.2.6)$$

where

$$C^* = \frac{2}{3} \left[\frac{1}{2(1-\theta)} \right]^{3/2} \left(\frac{U}{\beta L} \right)^3.$$

The result now follows by standard differential inequalities provided there is an $\alpha > 0$ with

$$\int_{\Omega} \frac{1}{\ell} k \sqrt{k} dx \geq \alpha \int_{\Omega} k dx \quad \text{and} \quad \int_{S_{\beta}} \ell^2 dx \leq C < \infty.$$

These two depend on the choice of $\ell = \min \left\{ \sqrt{2} k^{1/2} \tau, 0.41 d \sqrt{\frac{d}{L}} \right\}$. By selecting the last argument in the minimum, the condition $\int \ell^2 dx \leq C < \infty$ holds. By selecting the first term in the minimum (and noting that then $\frac{1}{\ell} k \sqrt{k} = \frac{1}{\sqrt{2}\tau} k$) the condition $\int \frac{1}{\ell} k \sqrt{k} dx \geq \alpha \int k dx$ holds. Thus the uniform bounds follows. \square

4.3 Energy dissipation in shear flows

To formulate our first main result we first present a definition of the **effective viscosity** ν_{eff} ($\geq \nu$), the **average viscosity** in the boundary layer S_{β} , and a few related quantities. These are well defined due to the uniform bounds in Proposition 2.3.

Definition 4.3.1. *The effective viscosity of solutions of (4.1.1) under (4.2.1) is*

$$\nu_{eff} := \frac{\left\langle \frac{1}{|\Omega|} \int_{\Omega} [2\nu + \nu_{turb}(\cdot)] |\nabla^s v|^2 dx \right\rangle_{\infty}}{\left\langle \frac{1}{|\Omega|} \int_{\Omega} |\nabla^s v|^2 dx \right\rangle_{\infty}}.$$

The large scale turnover time is $T^ = L/U$. The Reynolds number and effective Reynolds number are*

$$\mathcal{Re} = \frac{U L}{\nu} \quad \text{and} \quad \mathcal{Re}_{eff} = \frac{U L}{\nu_{eff}}.$$

Let $\beta = \frac{1}{8} \mathcal{Re}_{eff}^{-1}$ and denote the region S_{β} by

$$S_{\beta} = \{(x, y, z) : 0 \leq x \leq L, 0 \leq y \leq L, (1 - \beta)L < z < L\}.$$

The average viscosity, $\bar{\nu}$, in \mathcal{S}_β is denoted

$$\bar{\nu} := \left\langle \frac{1}{|\mathcal{S}_\beta|} \int_{\mathcal{S}_\beta} [2\nu + \nu_T] dx \right\rangle_\infty, \text{ where } |\mathcal{S}_\beta| = \beta L^3.$$

Generally, the ratio of the effective and average viscosity is an important statistic.

Theorem 4.3.1. *Suppose $\nu_T \geq 0$. Let v be a weak solution of*

$$v_t + v \cdot \nabla v - \nabla \cdot ([2\nu + \nu_T] \nabla^s v) + \nabla p = 0, \text{ and } \nabla \cdot v = 0$$

under (4.2.1) satisfying the energy inequality (4.2.4). Then, provided $\bar{\nu}, \nu_{eff}$ are well defined,

$$\langle \varepsilon \rangle_\infty \leq \left\{ \frac{5}{2} + 8 \frac{\bar{\nu}}{\nu_{eff}} \right\} \frac{U^3}{L}.$$

Remark 4.3.1. *The multiplicative constants $5/2, 8$ are the result of a series of inequalities in the proof. It is likely that a different proof could result in smaller values. For more general problems $\bar{\nu}$, the average viscosity in the boundary layers, should be defined to include both upper and lower layers. Due to the symmetries of this specific shear flow, the lack of a body force and Galilean invariance, it suffices to define $\bar{\nu}$ in Definition 4.3.1 as the average in the upper layer near $z = L$.*

The proof begins with the background flow from Doering and Constantin [21], $\phi(z) = [\tilde{\phi}(z), 0, 0]^T$ where

$$\tilde{\phi}(z) = \begin{cases} 0, & z \in [0, L - \beta L] \\ \frac{U}{\beta L}(z - (L - \beta L)), & z \in [L - \beta L, L] \end{cases} \quad \beta = \frac{1}{8} \mathcal{R}e_{eff}^{-1}.$$

This function $\phi(z)$ is piecewise linear, continuous, divergence free and satisfies the boundary conditions. We will need the following values of norms of ϕ .

Lemma 4.3.1. *We have $\nabla \cdot \phi = 0$ and*

$$\begin{aligned} \|\phi\|_{L^\infty(\Omega)} &= U, & \|\nabla\phi\|_{L^\infty(\Omega)} &= \frac{U}{\beta L}, \\ \|\phi\|^2 &= \frac{1}{3} U^2 \beta L^3, & \|\nabla\phi\|^2 &= \frac{U^2 L}{\beta}. \end{aligned}$$

With this choice of ϕ , time averaging the energy inequality ((4.2.4)) over $[0, T]$ and normalizing by $|\Omega| = L^3$ gives

$$\begin{aligned} & \frac{1}{2TL^3} \|v(T)\|^2 + \left\langle \frac{1}{L^3} \int_{\Omega} [2\nu + \nu_T] |\nabla^s v|^2 dx \right\rangle_T \leq & (4.3.1) \\ & \frac{1}{2TL^3} \|v(0)\|^2 + \frac{1}{TL^3} (v(T) - v(0), \phi) + \left\langle \frac{1}{L^3} (v \cdot \nabla v, \phi) \right\rangle_T + \\ & \left\langle \frac{1}{L^3} \int_{\Omega} [2\nu + \nu_T] \nabla^s v : \nabla^s \phi dx \right\rangle_T. \end{aligned}$$

Recall $\beta = \frac{1}{8} \mathcal{R}e_{eff}^{-1}$. Due to Proposition 2.3, (4.3.1) can be written as

$$\langle \varepsilon \rangle_T \leq \mathcal{O}\left(\frac{1}{T}\right) + \left\langle \frac{1}{L^3} (v \cdot \nabla v, \phi) \right\rangle_T + \left\langle \frac{1}{L^3} \int_{\Omega} [2\nu + \nu_T] \nabla^s v : \nabla^s \phi dx \right\rangle_T \quad (4.3.2)$$

The right-hand side (RHS) has two terms shared by the NSE, $(v \cdot \nabla v, \phi)$ and $\int 2\nu \nabla^s v : \nabla^s \phi dx$. The main issue is thus the third term, $\int \nu_T \nabla^s v : \nabla^s \phi dx$. Before treating that we recall the analysis of Doering and Constantine [21] and Wang [78] for the first two. For the nonlinear term $\left\langle \frac{1}{L^3} (v \cdot \nabla v, \phi) \right\rangle_T$, denoted NLT , we have

$$\begin{aligned} NLT &= \left\langle \frac{1}{L^3} (v \cdot \nabla v, \phi) \right\rangle_T = \left\langle \frac{1}{L^3} ([v - \phi] \cdot \nabla v, \phi) \right\rangle_T + \left\langle \frac{1}{L^3} (\phi \cdot \nabla v, \phi) \right\rangle_T \\ &\leq \left\langle \frac{1}{L^3} \int_{\mathcal{S}_\beta} |v - \phi| |\nabla v| |\phi| + |\phi|^2 |\nabla v| dx \right\rangle_T \\ &\leq \frac{1}{L^3} \left\langle \left\| \frac{v - \phi}{L - z} \right\|_{L^2(\mathcal{S}_\beta)} \|\nabla v\|_{L^2(\mathcal{S}_\beta)} \|(L - z)\phi\|_{L^\infty(\mathcal{S}_\beta)} + \|\phi\|_{L^\infty(\mathcal{S}_\beta)}^2 \|\nabla v\|_{L^1(\mathcal{S}_\beta)} \right\rangle_T. \end{aligned}$$

On the RHS, $\|\phi\|_{L^\infty(\mathcal{S}_\beta)}^2 = U^2$. We calculate $\|(L - z)\phi\|_{L^\infty(\mathcal{S}_\beta)} = \frac{1}{4}\beta LU$. Since $v - \phi$ vanishes on $\partial\mathcal{S}_\beta$, Hardy's inequality, the triangle inequality and a calculation imply

$$\begin{aligned} \left\| \frac{v - \phi}{L - z} \right\|_{L^2(\mathcal{S}_\beta)} &\leq 2 \|\nabla(v - \phi)\|_{L^2(\mathcal{S}_\beta)} \leq 2 \|\nabla v\|_{L^2(\mathcal{S}_\beta)} + 2 \|\nabla\phi\|_{L^2(\mathcal{S}_\beta)} \\ &\leq 2 \|\nabla v\|_{L^2(\mathcal{S}_\beta)} + 2U \sqrt{\frac{L}{\beta}}. \end{aligned}$$

Thus we have the estimate

$$NLT \leq \frac{\beta LU}{4} \frac{1}{L^3} \left\langle 2\|\nabla v\|_{L^2(\mathcal{S}_\beta)}^2 + 2U \sqrt{\frac{L}{\beta}} \|v\|_{L^2(\mathcal{S}_\beta)} \right\rangle_T + \frac{U^2}{L^3} \langle \|\nabla v\|_{L^1(\mathcal{S}_\beta)} \rangle_T. \quad (4.3.3)$$

For the last term on the RHS, Hölders inequality in space then in time implies

$$\begin{aligned} \frac{U^2}{L^3} \langle \|\nabla v\|_{L^1(\mathcal{S}_\beta)} \rangle_T &= \frac{U^2}{L^3} \left\langle \int_{\mathcal{S}_\beta} |\nabla v| \cdot 1 dx \right\rangle_T \leq \frac{U^2}{L^3} \left\langle \sqrt{\int_{\mathcal{S}_\beta} |\nabla v|^2 dx} \sqrt{\beta L^3} \right\rangle_T \\ &\leq \frac{U^2 \sqrt{\beta}}{L^{3/2}} \left\langle \sqrt{\int_{\mathcal{S}_\beta} |\nabla v|^2 dx} \right\rangle_T \leq \frac{U^2 \sqrt{\beta}}{L^{3/2}} \left\langle \int_{\mathcal{S}_\beta} |\nabla v|^2 dx \right\rangle_T^{1/2}. \end{aligned}$$

Increase the integral's domain from \mathcal{S}_β to Ω , use (as $\nabla \cdot v = 0$) $\|\nabla v\|^2 = 2\|\nabla^s v\|^2$ and $\beta = \frac{1}{8}\mathcal{R}e_{eff}^{-1}$. Rearranging and using the arithmetic-geometric inequality gives

$$\begin{aligned} \frac{U^2}{L^3} \langle \|\nabla v\|_{L^1(\mathcal{S}_\beta)} \rangle_T &\leq U^2 \sqrt{\beta} \left\langle \frac{1}{L^3} \int_{\Omega} 2|\nabla^s v|^2 dx \right\rangle_T^{1/2} \leq \\ &\leq U^2 \sqrt{\frac{2}{8} \frac{1}{LU}} \left\langle \frac{1}{L^3} \int_{\Omega} \nu_{eff} |\nabla^s v|^2 dx \right\rangle_T^{1/2} \leq \left(\frac{U^3}{L}\right)^{1/2} \frac{1}{2} \left\langle \frac{1}{L^3} \int_{\Omega} \nu_{eff} |\nabla^s v|^2 dx \right\rangle_T^{1/2} \\ &\leq \frac{1}{2} \frac{U^3}{L} + \frac{1}{8} \left\langle \frac{1}{L^3} \int_{\Omega} \nu_{eff} |\nabla^s v|^2 dx \right\rangle_T. \end{aligned}$$

Similar manipulations yield

$$\begin{aligned} \frac{1}{4}\beta LU \frac{1}{L^3} \left\langle 2U \sqrt{\frac{L}{\beta}} \|v\|_{L^2(\mathcal{S}_\beta)} \right\rangle_T &\leq \frac{1}{2}\beta LU \left\langle \frac{1}{L^3} \|\nabla v\|_{L^2(\mathcal{S}_\beta)}^2 \right\rangle_T + \frac{1}{8} \frac{U^3}{L} \\ &\leq \frac{1}{8} \left\langle \frac{1}{L^3} \nu_{eff} \|\nabla^s v\|_{L^2(\mathcal{S}_\beta)}^2 \right\rangle_T + \frac{1}{8} \frac{U^3}{L}. \end{aligned}$$

Using the last two estimates in the *NLT* upper bound (4.3.3), we obtain

$$NLT \leq 2\beta \frac{LU}{\nu_{eff}} \left\langle \frac{1}{L^3} \nu_{eff} \|\nabla^s v\|_{L^2(\mathcal{S}_\beta)}^2 \right\rangle_T + \frac{5}{8} \frac{U^3}{L}.$$

Thus,

$$\begin{aligned} \langle \varepsilon \rangle_T &\leq \mathcal{O}\left(\frac{1}{T}\right) + \frac{1}{4} \left\langle \frac{1}{L^3} \nu_{eff} \|\nabla^s v\|_{L^2(\Omega)}^2 \right\rangle_T + \frac{5}{8} \frac{U^3}{L} + \\ &\quad + \left\langle \frac{1}{L^3} \int_{\Omega} [2\nu + \nu_T] \nabla^s v : \nabla^s \phi dx \right\rangle_T. \end{aligned}$$

Consider now the last term on the RHS. Since ϕ is zero off \mathcal{S}_β ,

$$\begin{aligned} \left\langle \frac{1}{L^3} \int_{\Omega} [2\nu + \nu_T] \nabla^s v : \nabla^s \phi dx \right\rangle_T &= \left\langle \frac{1}{L^3} \int_{\mathcal{S}_\beta} [2\nu + \nu_T] \nabla^s v : \nabla^s \phi dx \right\rangle_T \\ &\leq \frac{1}{2} \langle \varepsilon \rangle_T + \frac{1}{2} \left\langle \frac{1}{L^3} \int_{\mathcal{S}_\beta} [2\nu + \nu_T] \left(\frac{U}{\beta L}\right)^2 dx \right\rangle_T \\ &\leq \frac{1}{2} \langle \varepsilon \rangle_T + \frac{1}{2} \left(\frac{U}{\beta L}\right)^2 \beta \left\langle \frac{1}{\beta L^3} \int_{\mathcal{S}_\beta} [2\nu + \nu_T] dx \right\rangle_T. \end{aligned}$$

Thus

$$\begin{aligned} \frac{1}{2} \langle \varepsilon \rangle_T &\leq \mathcal{O}\left(\frac{1}{T}\right) + \frac{1}{4} \left\langle \frac{1}{L^3} \nu_{eff} \|\nabla^s v\|_{L^2(\Omega)}^2 \right\rangle_T + \\ &\quad + \frac{5}{8} \frac{U^3}{L} + \frac{\beta}{2} \left(\frac{U}{\beta L}\right)^2 \left\langle \frac{1}{\beta L^3} \int_{\mathcal{S}_\beta} 2\nu + \nu_T dx \right\rangle_T. \end{aligned}$$

As $T \rightarrow \infty$

$$\left\langle \frac{1}{\beta L^3} \int_{\mathcal{S}_\beta} 2\nu + \nu_T dx \right\rangle_T \rightarrow \bar{\nu} \text{ and } \left\langle \frac{1}{L^3} \nu_{eff} \|\nabla^s v\|_{L^2(\Omega)}^2 \right\rangle_T \rightarrow \langle \varepsilon \rangle_\infty.$$

Thus,

$$\left(\frac{1}{2} - 2\beta \mathcal{R}e_{eff} \right) \langle \varepsilon \rangle_\infty \leq \frac{5U^3}{8L} + \frac{1}{2} \left(\frac{U}{\beta L} \right)^2 \beta \bar{\nu} \leq \left[\frac{5}{8} + \frac{1}{2\beta} \mathcal{R}e_{eff}^{-1} \frac{\bar{\nu}}{\nu_{eff}} \right] \frac{U^3}{L}.$$

The choice $\beta = \frac{1}{8} \mathcal{R}e_{eff}^{-1}$ implies $2\beta \mathcal{R}e_{eff} = 1/4$, completing the proof since

$$\langle \varepsilon \rangle_\infty \leq \frac{5U^3}{2L} + \frac{1}{2} \left(\frac{U}{\beta L} \right)^2 \beta \bar{\nu} = \left[\frac{5}{2} + 8 \frac{\bar{\nu}}{\nu_{eff}} \right] \frac{U^3}{L}.$$

4.4 Application to a 1-equation URANS model

We now apply Theorem 3.2 to (4.1.1), (4.1.3). The main work will be in estimating $\frac{\bar{\nu}}{\nu_{eff}}$.

Theorem 4.4.1. *Let v be a weak solution of (4.1.1), (4.1.3) under (4.2.1) satisfying the energy inequality (4.2.4). We have*

$$\langle \varepsilon \rangle_\infty \leq \left[5 + 32 \frac{\nu}{\nu_{eff}} + \left(\frac{0.41^2 \sqrt{2} \mu^2}{4} \right) \frac{\tau}{T^*} \right] \frac{U^3}{L}.$$

Remark. We note that $\frac{\nu}{\nu_{eff}} \leq 1$ (and possibly $\ll 1$) and for $\mu = 0.55$, $0.41^2 \sqrt{2} \mu^2 / 4 \simeq 0.017978$.

proof. The upper bound $\ell \leq 0.41d\sqrt{\frac{d}{L}}$ is used in the boundary layer region to estimate $\bar{\nu}$ as follows

$$\begin{aligned}
\bar{\nu} &= \left\langle \frac{1}{\beta L^3} \int_{\mathcal{S}_\beta} 2\nu + \nu_T dx \right\rangle_\infty \leq 2\nu + \left\langle \frac{1}{\beta L^3} \int_{\mathcal{S}_\beta} \mu \left(0.41d\sqrt{\frac{d}{L}} \right) k^{\frac{1}{2}} dx \right\rangle_\infty \\
&\leq 2\nu + 0.41\mu \frac{1}{L^{1/2}} \frac{1}{\beta L^3} \left\langle \int_{\mathcal{S}_\beta} (L-z)^{+3/2} k^{1/2} dx \right\rangle_\infty \\
&\leq 2\nu + 0.41\mu \frac{1}{L^{1/2}} \frac{1}{\beta L^3} \left\langle \sqrt{\int_{\mathcal{S}_\beta} (L-z)^3 dx} \sqrt{\int_{\mathcal{S}_\beta} k dx} \right\rangle_\infty \\
&\leq 2\nu + \frac{0.41\mu}{2} \frac{1}{L^{1/2}} \beta \left\langle \sqrt{\int_{\mathcal{S}_\beta} k dx} \right\rangle_\infty, \text{ hence} \\
\bar{\nu} &\leq 2\nu + \frac{0.41\mu}{2} L\beta \sqrt{\left\langle \frac{1}{L^3} \int_{\Omega} k dx \right\rangle_\infty}. \tag{4.4.1}
\end{aligned}$$

Next use the k -equation to estimate $\int k dx$. We have

$$\int_{\Omega} k_t dx + \int_{\Omega} \frac{1}{\ell} k \sqrt{k} dx = \int_{\Omega} \nu_T |\nabla^s v| dx. \tag{4.4.2}$$

By the choice of ℓ , $\frac{1}{\ell} k \sqrt{k}$ is bounded below by $\frac{1}{\sqrt{2\tau}} k$ because

$$\frac{1}{\ell} k \sqrt{k} = \max \left\{ \frac{1}{\sqrt{2\tau}}, \frac{\sqrt{k}}{0.41d\sqrt{\frac{d}{L}}} \right\} k \geq \frac{1}{\sqrt{2\tau}} k.$$

The long time averaging of $\int k_t dx$ is zero. Since $\frac{1}{\sqrt{2\tau}} k \leq \frac{1}{\ell} k \sqrt{k}$, we have

$$\frac{1}{\sqrt{2\tau}} \left\langle \frac{1}{|\Omega|} \int_{\Omega} k dx \right\rangle_\infty \leq \left\langle \frac{1}{|\Omega|} \int_{\Omega} \frac{1}{\ell} k \sqrt{k} dx \right\rangle_\infty = \left\langle \frac{1}{|\Omega|} \int_{\Omega} \nu_T |\nabla^s v|^2 dx \right\rangle_\infty = \langle \varepsilon \rangle_\infty.$$

Thus, $\left\langle \frac{1}{|\Omega|} \int_{\Omega} k dx \right\rangle_{\infty} \leq \sqrt{2} \tau \langle \varepsilon \rangle_{\infty}$. Using this upper estimate in (4.4.1) we obtain

$$\bar{\nu} \leq 2\nu + \frac{0.41\mu}{2} L\beta \sqrt{\left\langle \frac{1}{L^3} \int_{\Omega} k dx \right\rangle_{\infty}} \leq 2\nu + \frac{0.41\sqrt[4]{2}\mu}{2} L\beta\tau^{1/2} \sqrt{\langle \varepsilon \rangle_{\infty}}.$$

Divide by ν_{eff} , use $T^* = L/U, \beta = \frac{1}{8}\mathcal{R}e_{eff}^{-1}$ and rearrange. This gives

$$\frac{\bar{\nu}}{\nu_{eff}} \leq 2\frac{\nu}{\nu_{eff}} + \frac{0.41\sqrt[4]{2}\mu}{2} \frac{1}{8} \frac{L^{1/2}}{U^{3/2}} \sqrt{\frac{\tau}{T^*}} \sqrt{\langle \varepsilon \rangle_{\infty}}.$$

Using this estimate in Theorem 4.3.1 gives

$$\langle \varepsilon \rangle_{\infty} \leq \left[\frac{5}{2} + 16\frac{\nu}{\nu_{eff}} \right] \frac{U^3}{L} + \left[\frac{0.41\sqrt[4]{2}\mu}{2} \sqrt{\frac{\tau}{T^*}} \sqrt{\frac{U^3}{L}} \right] \sqrt{\langle \varepsilon \rangle_{\infty}}.$$

The arithmetic-geometric mean inequality then completes the proof:

$$\langle \varepsilon \rangle_{\infty} \leq \left[5 + 32\frac{\nu}{\nu_{eff}} + \frac{0.41^2\sqrt[2]{2}\mu^2}{4} \frac{\tau}{T^*} \right] \frac{U^3}{L}.$$

4.5 A Numerical Illustration

One important failure mode of eddy viscosity models is over dissipation leading to lower Reynolds number type solutions. In this scenario, as \mathcal{Re} increases, layers and internal small scales sharpen. As a result $\langle \varepsilon \rangle$ grows as \mathcal{Re} increases. Theorem 4.4.1 predicts that this does not happen. We now test this prediction by solving the model with increasing \mathcal{Re} , refining the mesh near the wall each step and calculating $\langle \varepsilon \rangle$. (We do not test if the dependence of $\langle \varepsilon \rangle$ on $\frac{\nu}{\nu_{eff}}$, τ and μ is as predicted in Theorem 4.4.1) This question of dependence of $\langle \varepsilon \rangle$ on \mathcal{Re} is the first main question in an eddy viscosity model. The results of the computations are consistent with the theoretical prediction that $\langle \varepsilon \rangle$ does not blow up as \mathcal{Re} increases. While Theorem 4.4.1 does not predict it, the test are also consistent with the typical dependence of $\langle \varepsilon \rangle$ on \mathcal{Re} for the Navier-Stokes equations. The results were obtained on a workstation with a program developed with the FEniCS software suite [54]. The code can be found on GitHub at <https://github.com/kierakean/1eqnRANS-FEM>.

4.5.1 Problem Setting

We examined the classical Taylor-Couette flow between counter-rotating cylinders for rotations well above, e.g. [69], those yielding stable patterns, [74]. The domain is given by

$$\Omega = \{(x, y, z) : r_{inner}^2 \leq x^2 + y^2 \leq r_{outer}^2, 0 \leq z \leq z_{max}\},$$

with $r_{inner} = .5, r_{outer} = 1, z_{max} = 2.2$. Figure 12. (a) depicts the domain Ω .

We imposed periodic boundary conditions in the z direction. The outer cylinder was held fixed and the flow was driven by the rotation of the inner cylinder. The

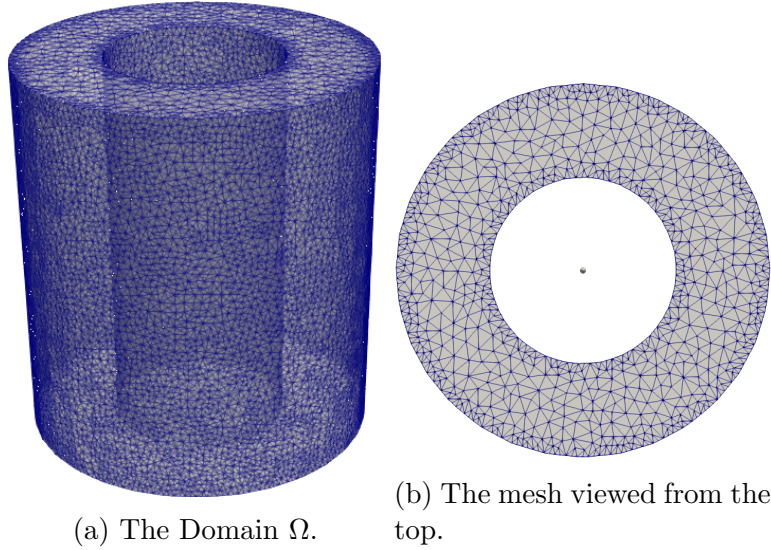


Figure 12: The unstructured mesh used in the numerical experiments.

angular velocity of the inner cylinder, ω_{inner} was smoothly increased from zero at $T = 0$ to $\omega_{inner} = 4$ at $T = 5$. Plots of flow statistics indicated that statistical equilibrium was reached around $T = 20$ so we give snapshots below at $T = 30$. We chose final time $T = 40$ and time averaged over $20 \leq t \leq 40$. The time scale was chosen to be $\tau = 0.1$.

Initialization. The model is turned on with a non-zero $k(x,5)$ at $T = 5$ when the inner cylinder has been spun up to its full angular velocity. We use a k initialization standard for turbulent flow in a square duct, Wilcox [80], given by

$$k(x, 5) = 1.5|v(x, 5)|^2 I^2, \text{ where } I = \text{turbulence intensity} \simeq 0.16\mathcal{Re}^{-1/8}.$$

The mesh. We used an unstructured mesh that was refined around the inner and outer boundaries, as can be seen from the top of the mesh in Figure 12 (b). We did preliminary tests at Reynolds number $\mathcal{Re} = 1000$ by refining the mesh until $\langle \varepsilon \rangle$

was unchanged on three successive refinements. These parameters yielded a Taylor number of

$$Ta := \frac{\omega^2 r_{inner} (r_{outer} - r_{inner})^3}{\nu^2} = 10^6.$$

We then did all reported tests on the coarsest mesh that produced the same value of $\langle \varepsilon \rangle$.

Tests were run with varying Reynolds numbers by varying the viscosity ν from 3×10^{-3} to 5×10^{-4} ($Ta \simeq 10^{10}$ to 2.5×10^{17}). Persistent vortices, marked by the Q-criterion, are plotted for two Reynolds numbers in Figure 13.

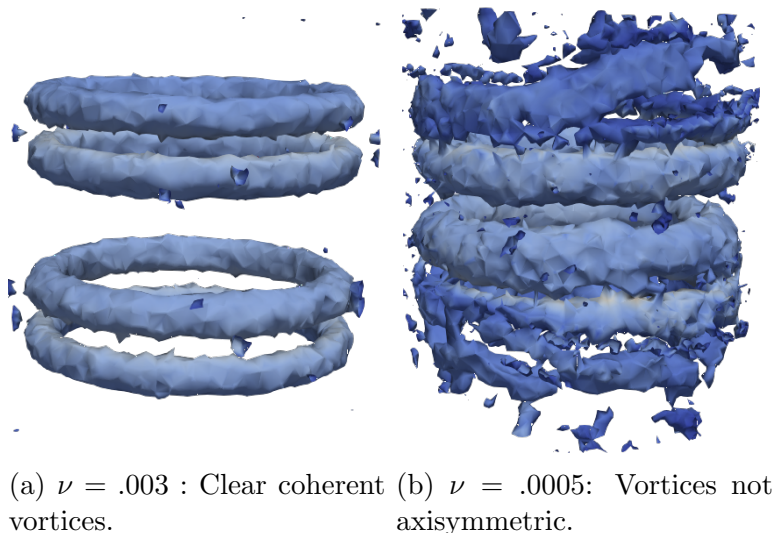


Figure 13: Q-criterion at $T = 30$.

We used the $P^2 - P^1$ Taylor-Hood element pair. The velocity space, X_h and pressure space, Q_h had 948,000 and 44,600 degrees of freedom, respectively. We used the time stepping scheme backward Euler plus time filter from [30] for the momentum and continuity equation. The added time filter increased accuracy and reduced numerical dissipation making the calculated $\langle \varepsilon \rangle$ more accurate. We used Backward Euler for the k equation. This choice smoothed the $k(x, t)$ evolution and

reduced solver issues. We took $\Delta t = 1e - 2$ and ran the simulation from $T = 0$ to $T = 40$.

4.5.2 Energy Dissipation Rate

In Figure 14 $\varepsilon(t)$ is plotted as a function of time. The jump at $T = 5$ corresponds to when the k equation (and thus the turbulent viscosity) is turned on.

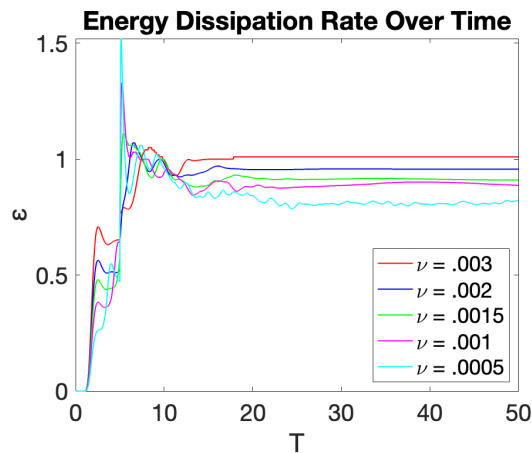


Figure 14: The energy dissipation rate over time.

To find the dependence on the Reynolds number, we plotted $\frac{\langle \varepsilon \rangle}{U^3}$ as a function of Reynolds number, and fit to $y = a + b\mathcal{R}e^c$ using Matlab's nonlinear least squares tool. The initial guess chosen for the (iterative) solver was $y = .05 + 5\mathcal{R}e^{-1}$.

Figure 15 shows that the long time average of the energy dissipation rate for the model scales like a constant plus the inverse of the Reynolds number, $\langle \varepsilon \rangle \simeq (0.05 + 4.8\mathcal{R}e^{-1}) \frac{U^3}{L}$, consistent with our analysis.

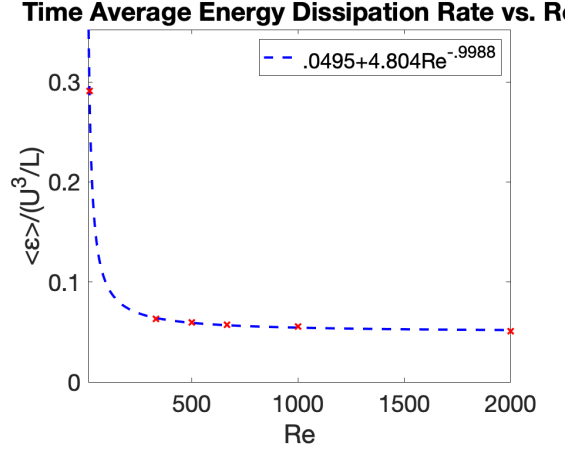


Figure 15: The energy dissipation rate over time.

4.6 Conclusions and open problems

The work herein was motivated by the idea that models more closely reflecting the global kinetic energy balance in turbulence can be simpler and require fewer calibration parameters for accuracy. One important aspect of kinetic energy balance is the averaged energy dissipation rate, $\langle \varepsilon \rangle$, in turbulence models matching averaged energy input rates, $\frac{U^3}{L}$, as they do for the NSE. For 4.1.1 this matching, related to models not over dissipating solutions, depends on the choice of the turbulence length scale ℓ , the decision to include or exclude the term $-\nu \Delta k$ in the k -equation and (in numerics) numerical dissipation in the methods used.

For the turbulence length scale, away from walls we used the simple and universal kinematic specification $\ell = \sqrt{2}k^{1/2}\tau$. Near walls it is necessary to match the near wall behavior of ν_T to that of the Reynolds stress $-\overline{u'u'}$. Including the term $-\nu \Delta k$, matching requires near wall behavior $\ell = \mathcal{O}(d^{3/2})$. With this matching, model energy

dissipation rates do match input rates, as desired for accuracy. For implementation, $\ell = \min \left\{ \sqrt{2}k^{1/2}\tau, 0.41d\sqrt{\frac{d}{L}} \right\}$ retains the issue of specifying the wall distance but it does not require pre-determining fluid sub-regions.

The 1–equation model studied has been used in many numerical codes, yet open problems abound. The important analytic problems of existence and positivity of k , while open for the new length scale, seem within reach given the advances in theory presented in Chacon-Rebollo and Lewandowski [8].

The model parameters used in our tests were $\mu = 0.55$ and von Karman constant 0.41. These values are classical for $\ell = 0.41d$. Recalibration may be necessary. The numerical illustration found that with these parameter values $\langle \varepsilon \rangle \simeq (0.05 + 4.8\mathcal{R}e^{-1}) \frac{U^3}{L}$. The $\mathcal{R}e \rightarrow \infty$ limiting value 0.05 includes numerical dissipation and grid effects. It is slightly smaller than the best estimate for the NSE of 0.088 of Doering and Constantine [21].

5.0 Conditioning of Super-Muckenhoupt Degenerate Elliptic Boundary Value Problems

5.1 Introduction

The question of inclusion or exclusion of $-\nu\Delta k$ is debated. It is linked potentially to the specification of ℓ , possible ill-posedness of the continuum model and corresponding ill conditioning of the spacial numerical discretization, and may heavily effect near wall behavior of the model, and correspondingly dissipation rates. In theory, this term is often omitted, in numerical tests solver failure may be seen when this term is excluded. However, precise study of the effect of exclusion remains for the most part completely open. Motivated by this question, in this chapter we examine the effect of the exclusion on the condition number through the analysis of the degenerate elliptic problem

$$-\nabla \cdot (d^2 \nabla k) = f \tag{5.1.1}$$

a linearized, simplified version of the term

$$-\nabla \cdot (\nu_T \nabla k)$$

where d is the wall normal distance

$$d(x) = \inf_{y \in \partial\Omega} |x - y|.$$

Section recalls the derivation of the k -equation given in section 2.3.2 to show the exclusion of $-\nu\Delta k$ is the correct choice to correctly capture near wall asymptotics. Section 5.3 briefly touches on existing theory of degenerate elliptic boundary value

problems. Estimates on condition number are proved in section 5.5, as well as brief discussion of the effect of additional lower order terms. Finally, 5.6 discusses regularization strategies applied to the Super-Muckenhoupt degenerate elliptic boundary value problem, which may be extended to the full k -equation.

5.2 The k -Equation

We recall the 1-equation turbulence model of Prandtl and Kolmogorov, where v approximates an average of the Navier-Stokes velocity, and k approximates the turbulent kinetic energy. The turbulent viscosity is given by $\nu_T = \mu\ell\sqrt{k}$, where ℓ is a chosen length scale.

$$\begin{aligned} v_t + v \cdot \nabla v - \nabla \cdot ([2\nu + \nu_T(\cdot)]\nabla^s v) + \nabla p &= f(x) \\ \nabla \cdot v &= 0 \end{aligned} \tag{5.2.1}$$

$$k_t + v \cdot \nabla k - \nabla \cdot (\nu_T(\cdot)\nabla k) + \frac{1}{\ell}k\sqrt{k} = \nu_T(\cdot)|\nabla^s v|^2.$$

We recall the derivation of the k -equation. In particular, prior to any simplifications, we have

$$\overline{u'_t u'} + \overline{u \cdot \nabla u u} - (\bar{u} \cdot \nabla \bar{u} \bar{u} + \nabla \cdot (\bar{u} \otimes \bar{u}) \bar{u}) - \nu \overline{\Delta u' u'} + \overline{\nabla p' u'} = 0. \tag{5.2.2}$$

We then consider the near wall behavior of each term. As u goes to zero at the wall, \bar{u} and u' . Each term in this equation goes to zero at the walls. Expanding terms and substituting the definition of k , and modeling the terms arising from the nonlinear term, we have:

$$k_t + v \cdot \nabla k - \nabla \cdot (\nu_T \nabla k) - \nu \overline{\Delta u' u'} = \nu_T |\nabla^s v|^2. \tag{5.2.3}$$

We recall ν_T models Reynold's stresses and goes to zero at the wall. In fact, all terms will go to zero at the wall, preserving what is true for the exact equation. This only changes when we consider the expansion

$$-\nu \overline{\Delta u' u'} = -\nu \Delta k + \nu \overline{|\nabla u'|^2}.$$

Individually, the terms on the right hand side do not vanish at the wall. The sum will vanish as the left hand side goes to zero at the wall. Thus to preserve accurate behavior of the model, we should model $-\nu \overline{\Delta u' u'}$ with terms that go to zero at the wall, either by subtractive cancellation or by terms that are individually $\mathcal{O}(d)$.

Prandtl and Kolmogorov model ε' as $\frac{k^{3/2}}{\ell}$. With common choice of length scales, $\ell = \sqrt{2k\tau}$ or $\ell = .41d$, this term will vanish at the wall. However, $\nu \Delta k$ will not, so there is no chance of subtractive cancellation.

Remark 5.2.1. *The length scale given in Chapter 4*

$$\ell = \min \left\{ \sqrt{2k\tau}, .41d \sqrt{\frac{d}{L}} \right\}$$

is based on the assumption that $k = \mathcal{O}(d)$. In this case, we may include $\nu \Delta k$ as $\frac{k^{3/2}}{\ell} = \mathcal{O}(1)$, and there is a chance of subtractive cancellation.

The term $\nu \Delta k$ in the interior of the domain is generally very small compared to other terms. However, at the wall, it is the only term that is nonzero, and is thus both dominant and leads to incorrect near wall asymptotics of the model. Thus, exclusion of this term is the correct choice for model accuracy.

Remark 5.2.2. *In practice, the turbulent viscosity is often lagged. Thus, we treat ν_T , which models Reynolds stresses, as a general $\mathcal{O}(d^2)$ term. We consider the kinematic length scale, $\ell = \sqrt{2k\tau}$ to arrive at a simplified model*

$$k_t + v \cdot \nabla k - \nabla \cdot (d^2 \nabla k) + \frac{1}{\mu\sqrt{2\tau}} k = \nu_T |\nabla^s v|^2 \quad (5.2.4)$$

$$k|_{\partial\Omega} = 0$$

and the degenerate elliptic counterpart

$$-\nabla \cdot (d^2 \nabla k) + \frac{1}{\mu\sqrt{2\tau}} k = \nu_T |\nabla^s v|^2 \quad (5.2.5)$$

$$k|_{\partial\Omega} = 0.$$

5.3 General Degenerate Elliptic Boundary Value Problems

Degenerate elliptic and semielliptic partial differential equations have many applications for which existence and uniqueness of solutions have been studied, see [62],[52]. However, the nature of solutions is related specifically to the individual problem, and broad application is not necessarily possible. Chapter 6 of [27] explores a perturbed problem in a similar form as (5.3.2), however conditions on exponents exclude the specific problem we look to study in 5.1.

Motivated by (5.2.4), we consider the following elliptic boundary value problem:

$$-\nabla \cdot (a(x)\nabla u(x)) + \text{Lower Order Terms} = f(x) \quad x \in \Omega \quad (5.3.1)$$

$$u = 0 \quad x \in \partial\Omega$$

This is degenerate when $a(x) = 0$ at some point in $\bar{\Omega}$. Commonly studied are equations degenerating at a point occur when angular symmetry is used for dimension reduction.

Herein, we consider the case of degenerate equations where $a(x)|_{\partial\Omega} = 0$. In particular, the following PDE:

$$-\nabla \cdot ([d^\alpha(x) + a_0]\nabla u(x)) + a_1 u = f(x)u|_{\partial\Omega} = 0 \quad (5.3.2)$$

with weak form

$$\int_{\Omega} ([d^\alpha(x) + a_0]\nabla u \nabla v) + a_1 uv \, dx = \int_{\Omega} f v \, dx. \quad (5.3.3)$$

Analysis of (5.3.2) with $a_1, a_2 = 0$ is complete in the case where $\alpha < 1$. In this case, d^α is a Muckenhoupt weight [23], and the PDE will satisfy a nonuniform ellipticity condition (see [58]). Theory is complete in the continuous setting. Additionally, [59] contains complete numerical analysis of the Muckenhoupt weighted elliptic problems. The super-Muckenhoupt case is where $\alpha \geq 1$. In this case, the continuum problem is ill-posed, as there is no way to make sense of the boundary condition.

Remark 5.3.1. *The boundary condition cannot be imposed in any meaningful way for (5.1.1). We may easily construct a sequence u_i such that $u_i|_{\partial\Omega} = 0$, u_i approaches a nonzero constant and*

$$\int_{\Omega} |d\nabla u_i|^2 \, dx \rightarrow 0.$$

That is, we can determine a solution at best up to a constant, but the problem is ill posed as we cannot meaningfully set boundary values.

We also examine the effect of the inclusion of the lower order term, i.e. considering $a_1 > 0$. We show that the addition of the lower order term leads to equivalent scaling of condition numbers as the nondegenerate case, with or without lower order terms.

5.4 Notation and Preliminaries

In this section, we define notation and state assumptions about our finite element space. Let Ω be a convex polyhedral subset of \mathbb{R}^N . Let \mathcal{T}_h be a regular triangulation of Ω and let h be the minimum meshwidth. We assume there exists some $C < \infty$ such that $\forall T \in \mathcal{T}_h, \text{diam}(T) < Ch$.

Let $X^h \subset H_0^1(\Omega)$ be a finite dimensional subspace, such that for $u \in X^h, u|_T$ is continuous for all $T \in \mathcal{T}_h$. Let $\{\varphi_i\}_{i=1}^m$ be a basis for this space.

Remark 5.4.1. *The dimension of the finite element space, m , will scale like h^{-N} .*

Define

$$a(u, v) = \int_{\Omega} [d^\alpha + a_0] \nabla u \nabla v \, dx + \int_{\Omega} a_1 uv \, dx.$$

This bilinear form is continuous and symmetric. However, it is degenerate in the continuous setting when $a_1 = 0$. We will define the finite element stiffness matrix associated with $a(\cdot, \cdot)$:

$$\mathbb{A}_{ij} = a_\alpha(\varphi_j, \varphi_i).$$

Let $\vec{v} = [v_1, v_2, \dots, v_m]^T, \vec{u} = [u_1, u_2, \dots, u_m]^T$ and $u, v \in X^h$ such that $u = \sum_{i=1}^m u_i \varphi_i, v = \sum_{i=1}^m v_i \varphi_i$. Then

$$\vec{v}^T \mathbb{A}_\alpha \vec{u} = a(u, v)$$

Remark 5.4.2. *All norms are equivalent in finite dimensions, however the equivalence may depend on mesh width and spacial dimension. In particular, the relationship between the $|\cdot|_{l^2}$ norm of the vector of coefficients and the $\|\cdot\|_{L^2(\Omega)}$ norm of the function is given by*

$$|u|_{l^2}^2 \approx C_\Omega h^{-N} \|u\|_{L^2(\Omega)}^2.$$

We will consider the condition number in the 2-norm. Define

$$\kappa = \frac{\lambda_{max}}{\lambda_{min}}$$

Where $\lambda_{max}, \lambda_{min}$ are the maximum and minimum eigenvalues of the stiffness matrix \mathbb{A} respectively. If \mathbb{A} is nonsymmetric, this is the spectral condition number, which is a lower bound for the true condition number

$$\kappa = \|\mathbb{A}\| \|\mathbb{A}^{-1}\|.$$

Further, as \mathbb{A} is symmetric, maximum and minimum eigenvalues can be calculated as the maximum and minimum of the Rayleigh quotient:

$$\lambda_{min} = \min_{u \in \mathbb{R}^m, u \neq 0} \frac{\vec{u}^T \mathbb{A}_\alpha \vec{u}}{\vec{u}^T \vec{u}} = \min_{u \in X^h, u \neq 0} \frac{a_\alpha(u, u)}{C_\Omega h^{-N} \|u\|^2} \quad (5.4.1)$$

$$\lambda_{max} = \max_{u \in \mathbb{R}^m, u \neq 0} \frac{\vec{u}^T \mathbb{A}_\alpha \vec{u}}{\vec{u}^T \vec{u}} = \max_{u \in X^h, u \neq 0} \frac{a_\alpha(u, u)}{C_\Omega h^{-N} \|u\|^2}. \quad (5.4.2)$$

5.5 Condition Number Estimates

In this section, we prove a standard Hardy Inequality for completeness, and extend the result to weights not in the Muckenhoupt class. We then use this analysis to estimate condition numbers of the linear system associated with (5.3.2).

5.5.1 Muckenhoupt Case

For clarity and concision, the following theorem and proof is offered in one dimension. Extending to higher dimensions is directly analogous. Standard techniques also allow extension to general convex domains.

Theorem 5.5.1. *Let $\Omega = [0, L] \subset \mathbb{R}$, and let $\beta < 1$. Then, there exists a constant, $C(\beta, L)$ such that for all $u \in H_0^1(\Omega)$,*

$$\int_{\Omega} |u|^2 dx \leq C(\beta, L) \int_{\Omega} d^{\beta} |u'(x)|^2 dx.$$

Proof. Let $x \in \Omega$. Then, $d(x) = \min x, L - x$.

Now, let $u \in H_0^1(\Omega)$.

$$\begin{aligned} |u(x)| &= |u(x) - u(0)| = \left| \int_0^x u'(t) dt \right| \\ &= |u(L) - u(x)| = \left| \int_x^L u'(t) dt \right|. \end{aligned}$$

Then, by properties of absolute value and Cauchy-Schwarz

$$\begin{aligned} |u(x)|^2 &= \left| \int_0^x u'(t) dt \right|^2 \\ &\leq \left(\int_0^x |u'(t)| dt \right)^2 \\ &= \left(\int_0^x |u'(t)| t^{\beta/2} t^{-\beta/2} dt \right)^2 \\ &\leq \int_0^x |u'(t)|^2 t^{\beta} dt \int_0^x t^{-\beta} dt. \end{aligned}$$

A similar chain of inequalities and a change of variables will show

$$|u(x)|^2 \leq \int_0^{L-x} |u'(t)|^2 s^{\beta} ds \int_0^{L-x} s^{-\beta} dt.$$

If $x < \frac{L}{2}$, we use the first inequality and $d = t$, if $x > \frac{L}{2}$ we use the second and $d = s$. In either case, we may then extend our integral to the entire domain, preserving the inequality as all quantities are positive.

$$|u(x)|^2 \leq \int_0^L |u'(t)|^2 d^\beta dt \int_0^L t^{-\beta} dt.$$

We set

$$\tilde{C}(\beta, L) = \int_0^L t^{-\beta} dt$$

and note that this is finite as $\beta < 1$.

Now, we can integrate again over the entire domain. Let $C(\beta, L) = \tilde{C}(\beta, L)L$

$$\begin{aligned} \int_{\Omega} |u(x)|^2 dx &\leq \tilde{C}(\beta, L) \int_0^L \left(\int_0^L |u'(t)|^2 d^\beta dt \right) dx \\ &\leq C(\beta, L) \int_0^L |\nabla u(x)|^2 d^\beta dx. \end{aligned}$$

□

Remark 5.5.1. *In future sections, we will suppress the dependence on L as we consider a fixed domain, and write the constant $C_\beta = C(\beta, L)$.*

5.5.2 Non-Muckenhoupt weights

We now consider the case in which $\alpha \geq 1$.

We begin by dividing the domain into a near wall region and an interior region. Let $\mathcal{T}_b \subset \mathcal{T}_h$ be all elements in the mesh that are on the boundary. Let \mathcal{T}_i be all remaining interior elements. Correspondingly, $\Omega_b = \bigcup_{T \in \mathcal{T}_b} T$, $\Omega_i = \bigcup_{T \in \mathcal{T}_i} T$. We note that for $x \in \Omega_i$, $d(x) \geq h$.

Proposition 5.5.1. *If $T \in \mathcal{T}_b$,*

$$\int_T |\nabla u(x)|^2 d^\beta x$$

is a norm.

Proof. Scaling and sub-additivity are clear. Suppose

$$\int_T (d^{\beta/2} |\nabla u(x)|)^2 dx = 0.$$

Then, $d^{\beta/2} |\nabla u(x)| = 0$ on T . Except on a set of measure zero, $d > 0$, thus $|\nabla u| = 0$ on T . As $u|_T$ is a continuous polynomial and $u = 0$ at at least one point as u is on the boundary, $u = 0$ on T . \square

Remark 5.5.2. *As u is continuous on Ω , in particular Ω_b ,*

$$\int_{\Omega_b} |\nabla u(x)|^2 d^\beta x$$

and

$$\int_{\Omega} |\nabla u(x)|^2 d^\beta x$$

are norms for all β . However, this does not hold on Ω_i as $\nabla u = 0$ does not imply $u = 0$ on interior elements.

Theorem 5.5.2. *Let $u \in X^h$. Let $\beta < 1, \alpha \geq \beta$. Then, there exists $C < \infty$ which depends on $\beta, |\Omega|$, and mesh regularity such that*

$$\int_{\Omega} |u|^2 dx \leq Ch^{\beta-\alpha} \int_{\Omega} d^\alpha |\nabla u|^2 dx.$$

Proof. We split the domain into boundary and interior region:

$$\begin{aligned}
\|u\|^2 &\leq C_\beta \int_{\Omega} |\nabla u(x)|^2 d^\beta dx \\
&= C_\beta \left(\int_{\Omega_b} |\nabla u(x)|^2 d^\beta dx + \int_{\Omega_i} |\nabla u(x)|^2 d^\beta dx \right) \\
&\leq C_\beta \left(\int_{\Omega_b} |\nabla u(x)|^2 d^\beta dx + \int_{\Omega_i} |\nabla u(x)|^2 \frac{d^{\alpha-\beta}}{h^{\alpha-\beta}} d^\beta dx \right) \\
&\leq C_\beta \left(\int_{\Omega_b} |\nabla u(x)|^2 d^\beta dx + h^{\beta-\alpha} \int_{\Omega_i} |\nabla u(x)|^2 d^\alpha dx \right).
\end{aligned} \tag{5.5.1}$$

Next, we examine Ω_b . We look element by element. A change of variables ($\hat{x} = \frac{x}{h}$) gives us:

$$\begin{aligned}
\int_T |\nabla u(x)|^2 d^\beta dx &= \int_{\hat{T}} |h^{-1} \hat{\nabla} \hat{u}(\hat{x})|^2 (h\hat{d})^\beta h^{-N} d\hat{x} \\
&= h^{\beta-2} h^{-N} \int_{\hat{T}} |\hat{\nabla} \hat{u}(\hat{x})|^2 \hat{d}^\beta d\hat{x}.
\end{aligned} \tag{5.5.2}$$

By norm equivalence, we have $\int_{\hat{T}} |\hat{\nabla} \hat{u}(\hat{x})|^2 \hat{d}^\beta d\hat{x} \leq C_T \int_{\hat{T}} |\hat{\nabla} \hat{u}(\hat{x})|^2 \hat{d}^\alpha d\hat{x}$, where C_T does not depend on h .

Then

$$\begin{aligned}
h^{\beta-2} h^{-N} \int_{\hat{T}} |\hat{\nabla} \hat{u}(\hat{x})|^2 \hat{d}^\beta d\hat{x} &\leq C_T h^{\beta-2} h^{-N} \int_{\hat{T}} |\hat{\nabla} \hat{u}(\hat{x})|^2 \hat{d}^\alpha d\hat{x} \\
&= C_T h^{\beta-2} h^{2-\alpha} h^{-N} \int_{\hat{T}} |h^{-1} \hat{\nabla} \hat{u}(\hat{x})|^2 (h\hat{d})^\alpha d\hat{x} \\
&= C_T h^{\beta-\alpha} \int_T |\nabla u(x)|^2 d^\alpha dx.
\end{aligned} \tag{5.5.3}$$

Or, overall

$$\int_T |\nabla u(x)|^2 d^\beta dx \leq C_T h^{\beta-\alpha} \int_T |\nabla u(x)|^2 d^\alpha dx. \tag{5.5.4}$$

Then, let $C_{\mathcal{T}} = \max_{T \in \mathcal{T}_b} C_T$

$$\begin{aligned}
\int_{\Omega_b} |\nabla u(x)|^2 d^\beta dx &= \sum_{T \in \mathcal{T}_b} \int_T |\nabla u(x)|^2 d^\beta dx \\
&\leq \sum_{T \in \mathcal{T}_b} C_T h^{\beta-\alpha} \int_T |\nabla u(x)|^2 d^\alpha dx \\
&\leq C_{\mathcal{T}} h^{\beta-\alpha} \int_{\Omega_b} |\nabla u(x)|^2 d^\alpha dx.
\end{aligned} \tag{5.5.5}$$

Now, we recombine with our previous estimate.

$$\begin{aligned}
\|u\|^2 &\leq C_\beta \left(\int_{\Omega_b} |\nabla u(x)|^2 d^\beta dx + \int_{\Omega_i} |\nabla u(x)|^2 d^\beta dx \right) \\
&\leq C_\beta h^{\beta-\alpha} \left(C_{\mathcal{T}} \int_{\Omega_b} |\nabla u(x)|^2 d^\alpha dx + \int_{\Omega_i} |\nabla u(x)|^2 d^\alpha dx \right) \\
&= C_\beta C_{\mathcal{T}} h^{\beta-\alpha} \int_{\Omega} |\nabla u(x)|^2 d^\alpha dx.
\end{aligned} \tag{5.5.6}$$

□

5.5.3 Condition Number

We look to estimate the maximum and minimum eigenvalues of \mathbb{A}_α and their dependence on h, α and N .

Let $u \in X^h$. Apply theorem 5.5.2 and remark 2.1.4 to bound $a(u, u)$ below

$$\begin{aligned}
a(u, u) &= \int_{\Omega} [d^\alpha + a_0] |\nabla u|^2 dx + \int_{\Omega} a_1 |u|^2 dx \\
&= \int_{\Omega} d^\alpha |\nabla u|^2 dx + a_0 \|\nabla u\|^2 + a_1 \|u\|^2 \\
&\geq (Ch^{\alpha-\beta} + a_0 C_P + a_1) \|u\|^2.
\end{aligned} \tag{5.5.7}$$

Then, immediately we have $\forall u \in X^h$,

$$\frac{a(u, u)}{C_\Omega h^{-N} \|u\|^2} \geq \frac{Ch^{\alpha-\beta} + a_0 C_P + a_1}{C_\Omega h^{-N}}.$$

Thus, by 5.4.1,

$$\lambda_{min} \geq \frac{Ch^{\alpha-\beta} + a_0C_P + a_1}{C_\Omega h^{-N}}$$

We recall that $\alpha \geq \beta$ so the exponent of h in the numerator is positive. If both a_0 and $a_1 = 0$, we we have $\lambda_{min} = \mathcal{O}(h^{N+\alpha-\beta})$. However, if we either include lower order terms or if the equation is nondegenerate, their contribution will dominate the numerator as $h \rightarrow 0$ and we see $\lambda_{min} = \mathcal{O}(h^N)$.

It is equally simple to bound $a(u, u)$ above. By a standard inverse inequality,

$$\|\nabla u\|^2 \leq C_{inv}h^{-2}\|u\|^2.$$

Let $d_{max} = \max_{x \in \Omega} d(x)$. Thus:

$$\begin{aligned} a(u, u) &= \int_{\Omega} [d^\alpha + a_0] |\nabla u|^2 dx + \int_{\Omega} a_1 |u|^2 dx \\ &= (a_0 + d_{max}) \|\nabla u\|^2 + a_1 \|u\|^2 \\ &\leq ((a_0 + d_{max})C_{inv}h^{-2} + a_1) \|u\|^2 \end{aligned} \tag{5.5.8}$$

We then have

$$\frac{a(u, u)}{C_\Omega h^{-N} \|u\|^2} \leq \frac{(a_0 + d_{max})C_{inv}h^{-2} + a_1}{C_\Omega h^{-N}}$$

and by 5.4.2

$$\lambda_{max} \leq \frac{(a_0 + d_{max})C_{inv}h^{-2} + a_1}{C_\Omega h^{-N}}.$$

As $h \rightarrow 0$, the numerator is dominated by $(a_0 + d_{max})C_{inv}h^{-2}$ regardless of inclusion or exclusion of lower order terms and whether or not the problem is degenerate. Then, we have $\lambda_{max} = \mathcal{O}(h^{N-2})$.

Putting the two estimates together, we have

$$\kappa = \frac{\lambda_{max}}{\lambda_{min}} = \frac{(a_0 + d_{max})C_{inv}h^{-2} + a_1}{Ch^{\alpha-\beta} + a_0C_P + a_1}.$$

5.5.4 Numerical Tests

Here, we look to numerically investigate the sharpness of our estimates of eigenvalues and condition number. Tests were performed using FEniCS software suite [54]. The domain chosen was a unit circle in two dimensions. Tests on the effects of the degeneracy at the boundary were performed varying α while fixing $a_0 = a_1 = 0$. To test the effects of lower order terms, $\alpha = 2$ was fixed and tests were performed with $a_0 = 0, 1$ and $a_1 = 0, 1$. In all tests, we used Lagrange basis functions with polynomial degree = 1.

5.5.4.1 Effects of Degeneracy at the Boundary

Section 5.5.3 predicts that the minimum eigenvalue will scale like $\mathcal{O}(h^{N+\alpha-\beta})$ for $\beta \leq \alpha$, $\beta < 1$. We test $\alpha = 0, .5, 1, 2$, and 3. For $\alpha < 1$, we expect scaling like $\mathcal{O}(h^N)$, for $\alpha \geq 1$ we select $\beta = 1 - \varepsilon$ and expect $\mathcal{O}(h^{\alpha+N-1})$. We expect the maximum eigenvalue to scale like $\mathcal{O}(h^{N-2})$ regardless of α .

In our tests, we take $N = 2$. Expected scaling of the minimum eigenvalue for $\alpha = 0, \alpha = .5$ is $\mathcal{O}(h^2)$, we see $\mathcal{O}(h^{1.976})$ and $\mathcal{O}(h^{2.025})$ respectively, i.e. scaling is as predicted. For $\alpha = 1$, we expect scaling like $\mathcal{O}(h^{2+\varepsilon})$ and see $\mathcal{O}(h^{2.237})$, slightly worse than expected but not catastrophically so. We expect scaling of $\mathcal{O}(h^{3+\varepsilon})$ and $\mathcal{O}(h^{4+\varepsilon})$ for $\alpha = 2, 3$ respectively. The actual scaling, $\mathcal{O}(h^{3.044})$ and $\mathcal{O}(h^{3.998})$ reflects the predicted results.

5.5.4.2 Effects of lower order terms

Tests were performed with $a_0 = 0, 1$ and $a_1 = 0, 1$. The predicted behavior is that it will minimum eigenvalue scale like $\mathcal{O}(h^2)$ in all tests except when lower order terms

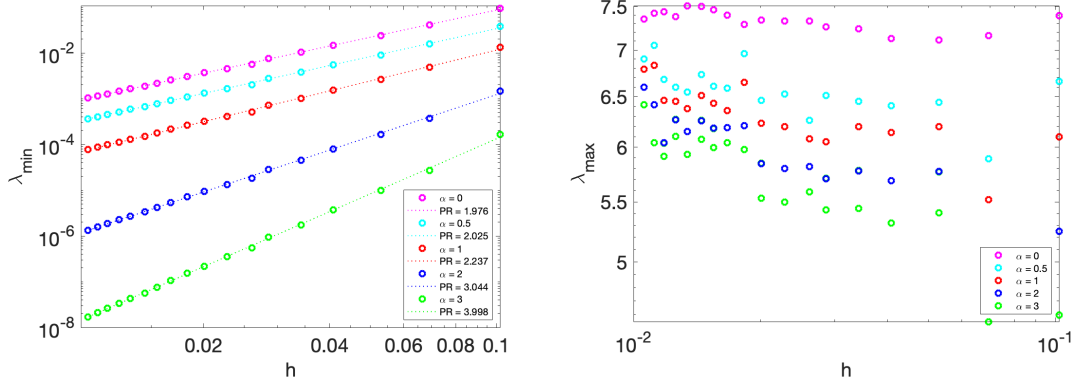


Figure 16: Minimum eigenvalue scales like $h^{N-1+\alpha}$ for $\alpha \geq 1$, h^{N-1} for $\alpha < 1$. Maximum eigenvalue scales like h^{N-2}

are excluded and the equation is degenerate. The observed behavior was as expected. When $a_0 \neq 0$, the equation was not degenerate and as expected, the eigenvalues like $\mathcal{O}(h^2)$, regardless of the addition of lower order terms. We also confirmed that the addition of lower order terms did ameliorate the degeneracy at the boundary, that is for $a_0 = 0, a_1 = 1$ we saw the expected $\mathcal{O}(h^2)$ behavior of the minimum eigenvalue. Echoing the previous test, the degenerate equation with no lower order terms scaled like $\mathcal{O}(h^3)$. In both cases, maximum eigenvalue is virtually independent of h .

5.6 Regularization

There are many applications where it is necessary to solve ill posed problems, or ill conditioned problems with noisy data, hence there exist a wide range of regularization strategies as well as methods for selecting regularization parameters, see [42],[40],[53].

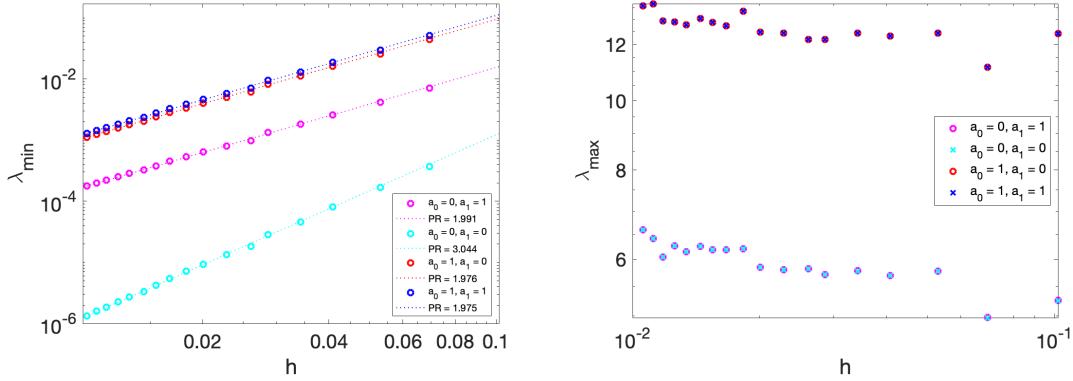


Figure 17: Minimum and maximum eigenvalues varying a_0, a_1 agree with theory: lower order terms alleviate ill conditioning

We will consider these regularization strategies applied to our simplified degenerate elliptic problem, 5.3.2. In particular, though our matrix is ill conditioned, it is positive and invertible, and we do not need to consider strategies designed to handle problems that are not.

Though our data may have minimal noise compared to data collected with imprecise instruments, the right hand side vector is not exact, and the accuracy may depend on mesh size, quadrature scheme, and smoothness of the function. Exact estimates for how many digits are accurate are problem dependant. We also have an estimate for the condition number of the linear system that is dependent on mesh width. This will allow us to consider regularization strategies that may be extended to the full k -equation in place of the $\nu\Delta k$ term.

The key here is that these regularization strategies are based on estimates of problem noise, and are implemented to improve conditioning of the linear system and increase accuracy in the computed solution. In contrast, ν is a physical parameter

that dictates the behavior of the flow but has no effect or relation to the noise in the data. Thus, using it as a regularization parameter is absurd.

5.6.1 Regularization for General Ill-Posed Problems

We will present for completeness two basic error estimates. Here, we assume that \mathbb{A} is a symmetric positive definite matrices, and we will consider the l^2 operator norm:

$$\|\mathbb{A}\| = \max_{\vec{x} \in \mathbb{R}^n \setminus \{0\}} \frac{\|\mathbb{A}\vec{x}\|_2}{\|\vec{x}\|_2}.$$

We recall that

$$\rho(\mathbb{A}) \leq \|\mathbb{A}\|_2,$$

and that if \mathbb{A} is normal, this becomes an equality.

We seek \vec{x}_{true} such that

$$\mathbb{A}\vec{x}_{true} = \vec{b}_{true}. \tag{5.6.1}$$

However, we also assume that we do not know \vec{b}_{true} . That is, we have \vec{b} such that $\|\vec{b} - \vec{b}_{true}\| = \mathcal{O}(\text{noise})$. We then will solve

$$\mathbb{A}\vec{x} = \vec{b} \tag{5.6.2}$$

and we seek to minimize

$$\|\vec{x}_{true} - \vec{x}\|.$$

First, we present two simple lemmas

Lemma 5.6.1. *Let \mathbb{A} a be symmetric positive definite and $\mu > 0$. Then,*

$$\|(\mathbb{A} + \mu\mathbb{I})^{-1}\| \leq \frac{1}{\mu}.$$

Proof. The eigenvalues of $(\mathbb{A} + \mu\mathbb{I})^{-1}$ are given by $\frac{1}{\lambda_i + \mu}$ where λ_i is an eigenvalue of \mathbb{A} . As $\lambda_i > 0$, each eigenvalue of $(\mathbb{A} + \mu\mathbb{I})^{-1}$ is bounded by $\frac{1}{\mu}$.

As $(\mathbb{A} + \mu\mathbb{I})^{-1}$ is symmetric positive definite, the norm is bounded by $\frac{1}{\mu}$ \square

Lemma 5.6.2. *Let \mathbb{A} be symmetric positive definite. Then for any μ ,*

$$\|(\mathbb{A} + \mu\mathbb{I})^{-1}\mathbb{A}\| \leq 1.$$

Proof. First, the eigenvalues of $(\mathbb{A} + \mu\mathbb{I})^{-1}\mathbb{A}$ are given by

$$\frac{\lambda_i}{\lambda_i + \mu},$$

where λ_i is an eigenvalue of \mathbb{A} . Next, as $(\mathbb{A} + \mu\mathbb{I})^{-1}\mathbb{A}$ is symmetric positive definite (it is more clear that $[(\mathbb{A} + \mu\mathbb{I})^{-1}\mathbb{A}]^{-1} = \mathbb{A}^{-1}(\mathbb{A} + \mu\mathbb{I})$ is symmetric positive definite, a symmetric positive definite matrix will have a symmetric positive definite inverse).

As all eigenvalues are clearly bounded above by 1, so is the ℓ^2 norm of the matrix. \square

Then, we have the following simple error estimates

Theorem 5.6.1. *Let \vec{x} solve $\mathbb{A}\vec{x} = \vec{b}$ and let \vec{x}_{true} solve $\mathbb{A}\vec{x}_{true} = \vec{b}_{true}$. Then,*

$$\frac{\|\vec{x}_{true} - \vec{x}\|}{\|\vec{x}\|} \leq \|\mathbb{A}\| \|\mathbb{A}^{-1}\| \frac{\|\vec{b}_{true} - \vec{b}\|}{\|\vec{b}_{true}\|}.$$

Proof. Subtract (5.6.2) from (5.6.1)

$$\mathbb{A}(\vec{x}_{true} - \vec{x}) = \vec{b}_{true} - \vec{b},$$

\mathbb{A} is invertible.

$$\vec{x}_{true} - \vec{x} = \mathbb{A}^{-1}(\vec{b}_{true} - \vec{b}).$$

Matrix norms are sub-multiplicative. Thus, we have

$$\|\mathbb{A}^{-1}(\vec{b}_{true} - \vec{b})\| \leq \|\mathbb{A}^{-1}\| \|\vec{b}_{true} - \vec{b}\|$$

and

$$\|\mathbb{A}\vec{x}_{true}\| \leq \|\mathbb{A}\| \|\vec{x}_{true}\|.$$

Thus, dividing by $\|\vec{b}_{true}\| = \|\mathbb{A}\vec{x}_{true}\|$, using sub-multiplicativity, and rearranging, we have

$$\frac{\|\vec{x}_{true} - \vec{x}\|}{\|\vec{x}\|} \leq \|\mathbb{A}\| \|\mathbb{A}^{-1}\| \frac{\|\vec{b}_{true} - \vec{b}\|}{\|\vec{b}_{true}\|}.$$

□

Theorem 5.6.2. *Let \vec{x} solve $(\mathbb{A} + \mu\mathbb{I})\vec{x} = \vec{b}$ and let \vec{x}_{true} solve $\mathbb{A}\vec{x}_{true} = \vec{b}_{true}$. Then,*

$$\|\vec{x}_{true} - \vec{x}\| \leq \frac{1}{\mu} \|\vec{b}_{true} - \vec{b}\| + c \|\mathbb{A}^{-1}\| \mu.$$

Proof. We have

$$(\mathbb{A} + \mu\mathbb{I})(\vec{x}_{true} - \vec{x}) = \vec{b}_{true} - \vec{b} + \mu\vec{x}_{true}.$$

$\mathbb{A} + \mu\mathbb{I}$ is invertible.

$$\vec{x}_{true} - \vec{x} = (\mathbb{A} + \mu\mathbb{I})^{-1}(\vec{b}_{true} - \vec{b}) + (\mathbb{A} + \mu\mathbb{I})^{-1}\mu\vec{x}_{true}$$

Taking the norm of both sides and using sub-multiplicativity on the first term, we have

$$\|\vec{x}_{true} - \vec{x}\| = \|(\mathbb{A} + \mu\mathbb{I})^{-1}\| \|\vec{b}_{true} - \vec{b}\| + \|(\mathbb{A} + \mu\mathbb{I})^{-1}\mu\vec{x}_{true}\|.$$

As \mathbb{A} and $\mu\mathbb{I}$ are symmetric positive definite, we have $\frac{1}{\lambda} = \|(\mu\mathbb{I})^{-1}\| \leq \|(\mathbb{A} + \mu\mathbb{I})^{-1}\|$:

$$\|\vec{x}_{true} - \vec{x}\| = \frac{1}{\lambda} \|\vec{b}_{true} - \vec{b}\| + \|(\mathbb{A} + \mu\mathbb{I})^{-1}\mu\vec{x}_{true}\|.$$

For the second term, we use that $\vec{x}_{true} \in \mathcal{R}(\mathbb{A})$, i.e. there exists some $\vec{y} = \mathbb{A}^{-1}\vec{x}_{true}$. Then, using lemma 5.6.2

$$\|(\mathbb{A} + \mu\mathbb{I})^{-1}\mu\vec{x}_{true}\| = \mu\|(\mathbb{A} + \mu\mathbb{I})^{-1}\mathbb{A}\mathbb{A}^{-1}\vec{x}_{true}\| \leq \mu\|\mathbb{A}\vec{x}_{true}\|\|(\mathbb{A} + \mu\mathbb{I})^{-1}\mathbb{A}\| \leq c\|\mathbb{A}^{-1}\|.$$

This gives us

$$\|\vec{x}_{true} - \vec{x}\| \leq \frac{1}{\mu}\|\vec{b}_{true} - \vec{b}\| + c\mu\|\mathbb{A}^{-1}\|.$$

For a result in terms of relative errors, use $\|\vec{y}\| \leq \|\mathbb{A}^{-1}\|\|\vec{x}_{true}\|$, $\|\mathbb{A}\|\|\vec{x}_{true}\|$, and use as before that

$$\frac{1}{\|\mathbb{A}\|\|\vec{x}_{true}\|} \leq \frac{1}{\|\mathbb{A}\vec{x}_{true}\|} = \frac{1}{\|\vec{b}_{true}\|}.$$

This leads immediately to

$$\frac{\|\vec{x}_{true} - \vec{x}\|}{\|\vec{x}_{true}\|} \leq \frac{\|\mathbb{A}\|}{\mu} \frac{\|\vec{b}_{true} - \vec{b}\|}{\|\vec{b}_{true}\|} + \mu\|\mathbb{A}^{-1}\|.$$

□

The preceding theorems offer insight into the choice of regularization. Without regularization, we have

$$\text{Relative Error} \leq \kappa(\mathbb{A}) \text{Relative Noise}$$

or

$$\text{Error} \leq \|\mathbb{A}^{-1}\| \text{Noise}.$$

With regularization, we chose μ such that $\mu \approx \mathcal{O}\left((\text{Noise})^{1/2}\right)$

$$\text{Error} \leq \mathcal{O}\left(\|\mathbb{A}^{-1}\| \text{Noise}^{1/2}\right).$$

Thus, for very ill posed problems, it is necessary to add regularization, as all data inherently contains some noise, even if at the level of machine precision. We

note that with minor modifications, $\mu\mathbb{I}$ may be replaced with an easily invertible matrix \mathbb{S} with $\|\mathbb{S}\| \approx \mu$. With no information about problem structure, the choice $\mu\mathbb{I}$ is logical, more information about the particular structure of \mathbb{A} may lead us to a different choice. Further, in terms of implementation, adding $\mu\mathbb{M}$ where \mathbb{M} is the finite element mass matrix, or $\mu\mathbb{S}$ where \mathbb{S} is the finite element stiffness matrix may be the simplest option, where μ is chosen as before.

5.6.2 Regularization for Degenerate Elliptic Boundary Value Problems

Applying standard regularization techniques to the ill-posed, super Muckenhoupt degenerate elliptic boundary value problem is relatively straightforward.

We have seen that adding a lower order term improves the condition number, resulting in scaling that is equivalent to the nondegenerate problem as $h \rightarrow 0$. Estimating the noise is heavily problem dependent, and the dependence of the condition number on the mesh width has been thoroughly examined in this chapter. The simplest method is to consider the perturbed problem

$$-\nabla \cdot (d^2 \nabla k) + \mu k = f.$$

We recall the scaling of the norm (or largest eigenvalue) of the finite element mass matrix is $\mathcal{O}(h^N)$, thus μ can be selected to minimize error based on estimates of noise and mesh width as well as the spacial dimension.

We also may perturb the problem as

$$-\nabla \cdot (d^2 \nabla k) - \mu \Delta k = f,$$

where the scaling of the finite element mass matrix is like $\mathcal{O}(h^{N-2})$. Again, the scaling of μ is selected to minimize the error best given the spacial dimension and

estimates of noise and mesh width. The selection of $\mu = \nu$ does not take this into account. Improved solver performance may be expected due to additional regularization, however there is no guarantee that ν is of the correct size to also minimize errors.

Remark 5.6.1. *Noise is estimated from problem data, model accuracy, and mesh width. Heuristics exist for this estimation.*

$\|\mathbb{A}^{-1}\| = \frac{1}{\lambda_{min}} \approx h^{N-1+\alpha}$. Then, for use in the k -equation, μ may be chosen to be approximately $(\mathcal{O}(\text{Noise}) h^{N+1})^{1/2}$ to minimize error.

5.7 Conclusion

We proved a simple estimate on the condition number of the stiffness matrix of a simplified, linearized problem and showed numerically that we observe the predicted scaling. We also discuss regularization options to address the ill conditioning of the linear system, which may be extended to improve solver performance in the full k -equation. Recalling the motivation of the k -equation and its derivation, propose regularization independent of physical parameters. We also note that we expect the lower order terms from the time derivative and the modelled dissipation of turbulent kinetic energy to also provide regularization that should ameliorate the ill effects of the boundary degeneracy.

While leaving open the question of existence of solutions, we show that due to the inclusion of lower order terms, the inclusion or exclusion of the term $\nu \Delta k$ does not affect the spectral conditioning of the linear system, independent of the near wall behavior of ν_T . Then, if the problem is ill-posed, it is not reflected in this condition

number.

6.0 Conclusions and Open Problems

From aeronautics to climate models, from extracting oil from the ground to the flow of coolant in nuclear reactors, there are a wide range of applications where accurate fluid flow simulations offer great benefit to human life. However, fully resolving complex flows remains computationally infeasible for many important applications, and models that seek to resolve this are faced with myriad issues as well. This dissertation seeks to address a few key practical difficulties faced while simulating these flows. These problems, individually and together, open new research directions to explore as we strive towards the elusive goal of time accurate predictions of high Reynolds number flows.

Chapter 3 demonstrates numerically that some treatment of the nonlinear convective term in conjunction with a large timestep may lead to dramatic overdissipation in body force driven flow. We recall that we must decrease the time step as the Reynolds number increases to fully resolve the smallest eddies; it is unclear the relation between the time step size restriction for second order methods is more restrictive than the condition to fully resolve small eddies.

However, we also consider eddy viscosity turbulence models, e.g. chapter 4, which model averages of the flow. These averages evolve more smoothly in time and we may expect to be able to take larger time steps, particularly with higher order methods. However, the eddy viscosity model is independent of the treatment of the nonlinear term. It is possible that additional dissipation caused by the choice of linearization of the convective term would adversely affect the total dissipation rate, leading to overdissipation unrelated to the choice of eddy viscosity model.

As we have identified a potential problem in simulations of body force driven

flow, it is important to consider remedies. Time filters to raise the order of a scheme or decrease numerical dissipation have been studied in [20], [73], and used in section 4.5. Investigating the effectiveness of such filters in controlling numerical dissipation and recovering the correct scaling of the energy dissipation rate is an open problem.

Further, time adaptivity to control numerical dissipation by controlling the ratio of numerical to viscous dissipation was introduced in [6], and could potentially increase accuracy and efficiency while preventing overdissipation in the long time average. Figure 8 indicates that controlling $\|u_\beta^{n+1}\|^2 - \|u_{\beta^*}^{n+1}\|^2$ may control the added dissipation due to the higher order approximation in the nonlinear term. Analyzing the long time energy dissipation rate for such adaptive timestepping methods remains an important issue in addressing efficiency and accuracy in fluid flow calculations. Lastly, [50] offers a calculable quantity to ensure that the mesh will not effect the scaling of the energy dissipation rate. Developing an analogous result for the time discretization would be valuable.

In body force driven flow, U depends on the dissipation and force, and cannot be prescribed directly, in contrast to some boundary driven flows. Crucially, we saw that this leads to two velocity scales defined by the timestepping scheme for second order linearly implicit treatment of the nonlinearity. The difference in U and U^* , which correlated with overdissipation, may not be present in such boundary driven flow (e.g. chapter 4). There, the definition of U is independent of the energy dissipation rate or time discretization scheme. This overdissipation was not seen in the numerical tests in 4.5, however, the timestep was small and a time filter to control numerical dissipation was used. In practice, many important applications are boundary driven, hence continuing this analysis to the case where the fluid is driven by boundary conditions and not a body force is of great interest. Careful analysis and numerical testing of the effect of numerical dissipation and in particular

the treatment of the nonlinear term in these applications is important.

Chapter 4 analyzes a new turbulence length scale that leverages true near wall asymptotics to ensure the correct energy dissipation rate. Correcting near wall asymptotics of ν_T directly can be seen in [37], where the near wall behavior of ν_T is enforced to be $\mathcal{O}(d^2)$, a choice that guarantees the model will not overdissipate. These promising results indicate that turbulence models based on strong mathematical foundations that respect the true behavior may lead to more accurate simulations of fluid flows, in particular in the consideration of the energy dissipation rate.

In particular, extensions to ensemble algorithms is one of great interest. These algorithms, in addition to extending predictability horizons in the calculation of the mean flow offer an estimate for turbulent kinetic energy with the kinetic energy in the ensemble fluctuations. This choice of k will be $\mathcal{O}(d^2)$ automatically, making it a natural choice for eddy viscosity turbulence models. This allows for length scales that avoid the occasionally expensive calculation of near wall distance. This is explored in [34], [33].

Artificial compressibility was combined with ensembles in [25], where an increase in speed was seen in the ensemble calculations. Using this method for increased efficiency in calculations to approximations to k has not yet been explored. [19] presents analysis of energy dissipation rate for flows with grad-div stabilization. Extending this analysis to penalty type methods and penalty ensembles remains open as well. This extension aligns conceptually with the principle of discovering models that are efficient, simple, and accurate to the true behavior of the modeled equations.

Chapter 5.2 discusses an simplification of the k -equation which is ill-posed in the continuous case. We explore the ill-conditioning caused by this in k -equation when the $\nu\Delta k$ term is omitted. Analysis of the condition number suggests that the time dependant elliptic problem will not be ill conditioned. Further exploration of causes

of solver failure with the exclusion of the term may be considered. Regardless, we present a basic strategy for regularization of the ill conditioned linear systems arising from the simplified version of the k -equation. We suggest that this regularization strategy, based on problem data not on physical parameters, may offer the same benefit as the addition of the viscous term while respecting the near wall behavior. Numerical exploration of the near wall behavior of the calculated k with the exclusion and inclusion of the regularization terms should be performed, and considered for multiple choices of turbulence length scales.

Bibliography

- [1] BAIOCCHI, C., AND CROUZEIX, M. On the equivalence of A-stability and G-stability. *Applied Numerical Mathematics* 5, 1 (1989), 19–22.
- [2] BOUSSINESQ, J. Essai sur la théorie des eaux courantes. *Mémoires Présentés Par Divers Savants à l'Académie Sci.* 23 (1877).
- [3] BULÍČEK, M., AND MÁLEK, J. Large data analysis for Kolmogorov's two-equation model of turbulence. *Nonlinear Analysis: Real World Applications* 50 (Nov 2016).
- [4] BUSSE, F. The optimum theory of turbulence. 77–121.
- [5] BUTCHER, J. C. Thirty years of G-stability. *BIT* 46, 3 (Sep 2006), 479–489.
- [6] CAPUANO, F., SANDERSE, B., DE ANGELIS, E., AND COPPOLA, G. A minimum-dissipation time-integration strategy for large-eddy simulation of incompressible turbulent flows. In *AIMETA 2017 Proceedings of the XXIII Conference of the Italian Association of Theoretical and Applied Mechanics* (Sept. 2017), pp. 2311–2323.
- [7] C.G. SPEZIALE, R. A., AND ANDERSON, E. A new mixing length formulation for the eddy-diffusivity closure. *AIAA J.* 30 (1992).
- [8] CHACON REBOLLO, T., AND LEWANDOWSKI, R. *Mathematical and numerical foundations of turbulence models and applications*, 2014 ed. Modeling and simulation in science, engineering & technology. Birkhauser Boston, Secaucus, NJ, June 2014.
- [9] CHORIN, A. J., AND MARSDEN, J. E. *A mathematical introduction to fluid mechanics*, 3 ed. Texts in Applied Mathematics. Springer, New York, NY, June 2000.
- [10] CHOW, Y. T., AND PAKZAD, A. On the zeroth law of turbulence for the stochastically forced Navier-Stokes equations. *Discrete and Continuous Dynamical Systems - B* 27, 9 (2022), 5181–5203.

- [11] DAHLQUIST, G. On the relation of G-stability to other stability concepts for linear multistep methods.
- [12] DAHLQUIST, G. On accuracy and unconditional stability of linear multistep methods for second order differential equations. *BIT* 18, 2 (jun 1978), 133–136.
- [13] DAHLQUIST, G. On one-leg multistep methods. *SIAM Journal on Numerical Analysis* 20, 6 (1983), 1130–1138.
- [14] DAVIDSON, P. *Turbulence*, 2 ed. Oxford University Press, London, England, July 2015.
- [15] DEARDORFF, J. Clear and cloud-capped mixed layers, their numerical simulation, structure and growth and parameterisation. In *Seminar on the Treatment of the Boundary Layer in Numerical Weather Prediction, 6-10 September 1976* (Shinfield Park, Reading, 1976), ECMWF, ECMWF, pp. 234–284.
- [16] DECARIA, V. Variable stepsize, variable order methods for partial differential equations. Sep 2019.
- [17] DECARIA, V., GUZEL, A., LAYTON, W., AND LI, Y. A variable stepsize, variable order family of low complexity. *SIAM Journal on Scientific Computing* 43, 3 (2021), A2130–A2160.
- [18] DECARIA, V., ILIESCU, T., LAYTON, W., MCLAUGHLIN, M., AND SCHNEIER, M. An artificial compression reduced order model. *SIAM Journal on Numerical Analysis* 58, 1 (2020), 565–589.
- [19] DECARIA, V., LAYTON, W., PAKZAD, A., RONG, Y., SAHIN, N., AND ZHAO, H. On the determination of the grad-div criterion. *Journal of Mathematical Analysis and Applications* 467, 2 (2018), 1032–1037.
- [20] DECARIA, V., LAYTON, W., AND ZHAO, H. A time-accurate, adaptive discretization for fluid flow problems. arXiv, 2018.

- [21] DOERING, C. R., AND CONSTANTIN, P. Energy dissipation in shear driven turbulence. *Phys. Rev. Lett.* 69 (Sep 1992), 1648–1651.
- [22] DOERING, C. R., AND FOIAS, C. Energy dissipation in body-forced turbulence. *Journal of Fluid Mechanics* 467 (2002), 289–306.
- [23] DYDA, B., IHNATSYEVA, L., LEHRBÄCK, J., TUOMINEN, H., AND VÄHÄKANGAS, A. V. Muckenhoupt A_p -properties of distance functions and applications to Hardy-Sobolev -type inequalities. arXiv, 2017.
- [24] FADAI-GHOTBI, A., FRIESS, C., MANCEAU, R., GATSKI, T. B., AND BORÉE, J. Temporal filtering: A consistent formalism for seamless hybrid RANS–LES modeling in inhomogeneous turbulence. *International Journal of Heat and Fluid Flow* 31, 3 (2010), 378–389. Sixth International Symposium on Turbulence and Shear Flow Phenomena.
- [25] FIORDILINO, J. A., AND MCCLAUGHLIN, M. An artificial compressibility ensemble timestepping algorithm for flow problems. arXiv, 2017.
- [26] FURBO, E. Evaluation of RANS turbulence models for flow problems with significant impact of boundary layers. Master’s thesis, Uppsala Universitet, 2010.
- [27] GHERGU, M., AND RADULESCU, V. *Nonlinear PDEs*, 2012 ed. Springer Monographs in Mathematics. Springer, Berlin, Germany, Nov. 2013.
- [28] GIRAULT, V., AND RAVIART, P.-A. *Finite element approximation of the Navier-stokes equations*. Springer, 1979.
- [29] GUZEL, A., AND LAYTON, W. Analysis of the effect of time filters on the implicit method: increased accuracy and improved stability. arXiv, 2017.
- [30] GUZEL, A., AND LAYTON, W. Time filters increase accuracy of the fully implicit method. *BIT Numerical Mathematics* 58 (Feb 2018).
- [31] HOPF, E. On nonlinear partial differential equations.

- [32] HOWARD, L. N. Bounds on flow quantities. *Annual Review of Fluid Mechanics* 4, 1 (1972), 473–494.
- [33] JIANG, N. A higher order ensemble simulation algorithm for fluid flows. *J. Sci. Comput.* 64, 1 (Jul 2015), 264–288.
- [34] JIANG, N., AND LAYTON, W. Numerical analysis of two ensemble eddy viscosity numerical regularizations of fluid motion. *Numerical Methods for Partial Differential Equations* 31, 3 (2015), 630–651.
- [35] JIANG, N., AND LAYTON, W. Algorithms and models for turbulence not at statistical equilibrium. *Computers Mathematics with Applications* 71, 11 (2016), 2352–2372. Proceedings of the conference on Advances in Scientific Computing and Applied Mathematics. A special issue in honor of Max Gunzburger’s 70th birthday.
- [36] JIANG, N., LAYTON, W., MCLAUGHLIN, M., RONG, Y., AND ZHAO, H. On the foundations of eddy viscosity models of turbulence. *Fluids* 5, 4 (Sep 2020), 167.
- [37] KEAN, K., LAYTON, W., AND SCHNEIER, M. Clipping over dissipation in turbulence models. *arXiv 2109.12107* (2021).
- [38] KEAN, K., AND SCHNEIER, M. Error analysis of supremizer pressure recovery for POD based reduced order models of the time-dependent Navier-Stokes equations. *SIAM J. Numer. Anal.* 58 (2020), 2235–2264.
- [39] KERSWELL, R. Variational bounds on shear-driven turbulence and turbulent Boussinesq convection. *Physica D: Nonlinear Phenomena* 100, 3 (1997), 355–376.
- [40] KILMER, M. E., AND O’LEARY., D. P. Choosing regularization parameters in iterative methods for ill-posed problems. *SIAM Journal on Matrix Analysis and Applications* 22, 4 (2001), 1204–1221.
- [41] KOLMOGOROV, A. N. Equations of turbulent motion in an incompressible fluid. *Dokl. Akad. Nauk SSSR* 30 (1942), 299–303.

- [42] LAYTON, W. Lecture notes on Tikhonov regularization.
- [43] LAYTON, W. Energy dissipation bounds for heat flows for a model in large eddy simulation. *Mathematical and Computer Modelling* 35, 13 (2002), 1445–1451.
- [44] LAYTON, W. Energy dissipation in the Smagorinsky model of turbulence. *Applied Mathematics Letters* 59 (2016), 56–59.
- [45] LAYTON, W. Lecture notes on the numerical analysis of incompressible, viscous flows, 2016.
- [46] LAYTON, W., AND MCCLAUGHLIN, M. Doubly-adaptive artificial compression methods for incompressible flow. *Journal of Numerical Mathematics* 28, 3 (2020), 175–192.
- [47] LAYTON, W., AND MCCLAUGHLIN, M. On URANS congruity with time averaging: Analytical laws suggest improved models. In *Mathematical Analysis With Applications* (Cham, 2020), S. Pinelas, A. Kim, and V. Vlasov, Eds., Springer International Publishing, pp. 85–108.
- [48] LAYTON, W., PEI, W., QIN, Y., AND TRENCHIA, C. Analysis of the variable step method of Dahlquist, Liniger and Nevanlinna for fluid flow.
- [49] LAYTON, W., PEI, W., AND TRENCHIA, C. Refactorization of a variable step, unconditionally stable method of Dahlquist, Liniger and Nevanlinna. *Applied Mathematics Letters* 125 (2022), 107789.
- [50] LAYTON, W., AND SCHNEIER, M. Diagnostics for eddy viscosity models of turbulence including data-driven/neural network based parameterizations. *Results in Applied Mathematics* 8 (2020), 100099. Special Issue on Recent Advances in Computational Mathematics and Applications.
- [51] LAYTON, W. J. The 1877 Boussinesq conjecture : Turbulent fluctuations are dissipative on the mean flows.

- [52] LE, V. K., AND SCHMITT, K. On boundary value problems for degenerate quasilinear elliptic equations and inequalities. *Journal of Differential Equations* 144, 1 (1998), 170–218.
- [53] LENZEN, F., AND SCHERZER, O. Tikhonov type regularization methods: History and recent progress. *Proceeding Eccomas 2004* (01 2004).
- [54] LOGG, A., MARDAL, K., AND WELLS, G. *Automated solution of differential equations by the finite element method: The FEniCS book*, vol. 84. Springer Science & Business Media, 2012.
- [55] MCLAUGHLIN, M. Fast, adaptive algorithms for flow problems. Jun 2020.
- [56] MOHAMMADI, B., AND PIRONNEAU, O. Analysis of the k-epsilon turbulence model.
- [57] MOHEBUJJAMAN, M., REBHOLZ, L. G., XIE, X., AND ILIESCU, T. Energy balance and mass conservation in reduced order models of fluid flows. *Journal of Computational Physics* 346 (2017), 262–277.
- [58] MURTHY, M. K., AND STAMPACCHIA, G. Boundary value problems for some degenerate-elliptic operators. *Annali di Matematica Pura ed Applicata* 80 (1968), 1–122.
- [59] NOCHETTO, R., OTAROLA, E., AND SALGADO, A. Piecewise polynomial interpolation in muckenhoupt weighted sobolev spaces and applications. *Numerische Mathematik* 132 (01 2016).
- [60] OVERHOLT, M., AND POPE, S. Direct numerical simulation of a statistically stationary, turbulent reacting flow. *Combustion Theory and Modelling* 3, 2 (Jun 1999), 371–408.
- [61] PAKZAD, A. Damping functions correct over-dissipation of the Smagorinsky model. *Mathematical Methods in the Applied Sciences* 40 (Aug 2016).

- [62] PASSASEO, D. Some concentration phenomena in degenerate semilinear elliptic problems. *Nonlinear Analysis: Theory, Methods Applications* 24, 7 (1995), 1011–1025.
- [63] PHILLIPS, O. Shear flow turbulence. *Annual Review of Fluid Mechanics* 1 (1969), 245–264.
- [64] PIRRÒ, D., AND QUADRIO, M. Direct numerical simulation of turbulent Taylor–Couette flow. *European Journal of Mechanics - B/Fluids* 27, 5 (2008), 552–566.
- [65] POPE, S. *Turbulent Flows*. Cambridge Univ. Press, 2000.
- [66] PRANDTL, L. On fully developed turbulence. *Proceedings of the 2nd International Congress of Applied Mechanics* (1926), 62–74.
- [67] PRANDTL, L. "Über ein neues formelsystem für die ausgebildete turbulenz. *Nachr. Akad. Wiss. Göttingen* (1945), 6–16.
- [68] PRUETT, C. Temporal large-eddy simulation: theory and implementation. *Theoretical and Computational Fluid Dynamics*. 22 (May 2008), 275–304.
- [69] S. GROSSMANN, D. LOHSE, C. S. High–Reynolds number Taylor–Couette turbulence. *Annual Review of Fluid Mechanics* 48 (2016), 53–80.
- [70] S. KUNDU, M. K., AND GHOSHAL, K. Reinvestigation on mixing length in an open channel turbulent flow. *Acta Geophysica V* (2017).
- [71] SPALART, P. Reflections on RANS modelling. In *Progress in Hybrid RANS-LES Modelling* (Berlin, Heidelberg, 2010), S.-H. Peng, P. Doerffer, and W. Haase, Eds., Springer Berlin Heidelberg, pp. 7–24.
- [72] SPALART, P. R. Philosophies and fallacies in turbulence modeling. *Progress in Aerospace Sciences* 74 (2015), 1–15.

- [73] TAKHIROV, A., TRENCH, C., AND WATERS, J. Second-order efficient nonlinear filter stabilization for high reynolds number flows. *Numerical Methods for Partial Differential Equations* (12 2021).
- [74] TAYLOR, G. Stability of a viscous liquid contained between two rotating cylinders. *Phil. Trans. R. Soc. A* 343 (1923), 223–289.
- [75] TEIXEIRA, J., AND CHEINET, S. A new mixing length formulation for the eddy-diffusivity closure. *Laboratory Memorandum Report NRL/MR/7532-01-7244* (May 2001).
- [76] TEIXEIRA, J., AND CHEINET, S. A simple mixing length formulation for the eddy-diffusivity parameterization of dry convection. *Boundary-Layer Meteorology* 110 (May 2004), 435–453.
- [77] VASSILICOS, J. C. Dissipation in turbulent flows. *Annual Review of Fluid Mechanics* 47, 1 (2015), 95–114.
- [78] WANG, X. Time averaged energy dissipation rate for shear driven flows in R^n . *Physica D: Nonlinear Phenomena* 99, 4 (1997), 555–563.
- [79] WANG, X. Effect of tangential derivative in the boundary layer on time averaged energy dissipation rate. *Physica D: Nonlinear Phenomena* 144, 1 (2000), 142–153.
- [80] WILCOX, D. *Turbulence Modeling for CFD*, 3 ed. DCW Industries, Jan 2006.
- [81] XIAO, H., AND CINNELLA, P. Quantification of model uncertainty in RANS simulations: A review. *Progress in Aerospace Sciences* 108 (2019), 1–31.
- [82] XIE, X., KEAN, K., AND XU, S. A doubly adaptive penalty method for the Navier Stokes equations. arXiv, 2022.